Organization Results Research Report

July 2005

RI 00.059
OR06.002

Performance and Serviceability of HPS Girders, MO224 Lafayette County

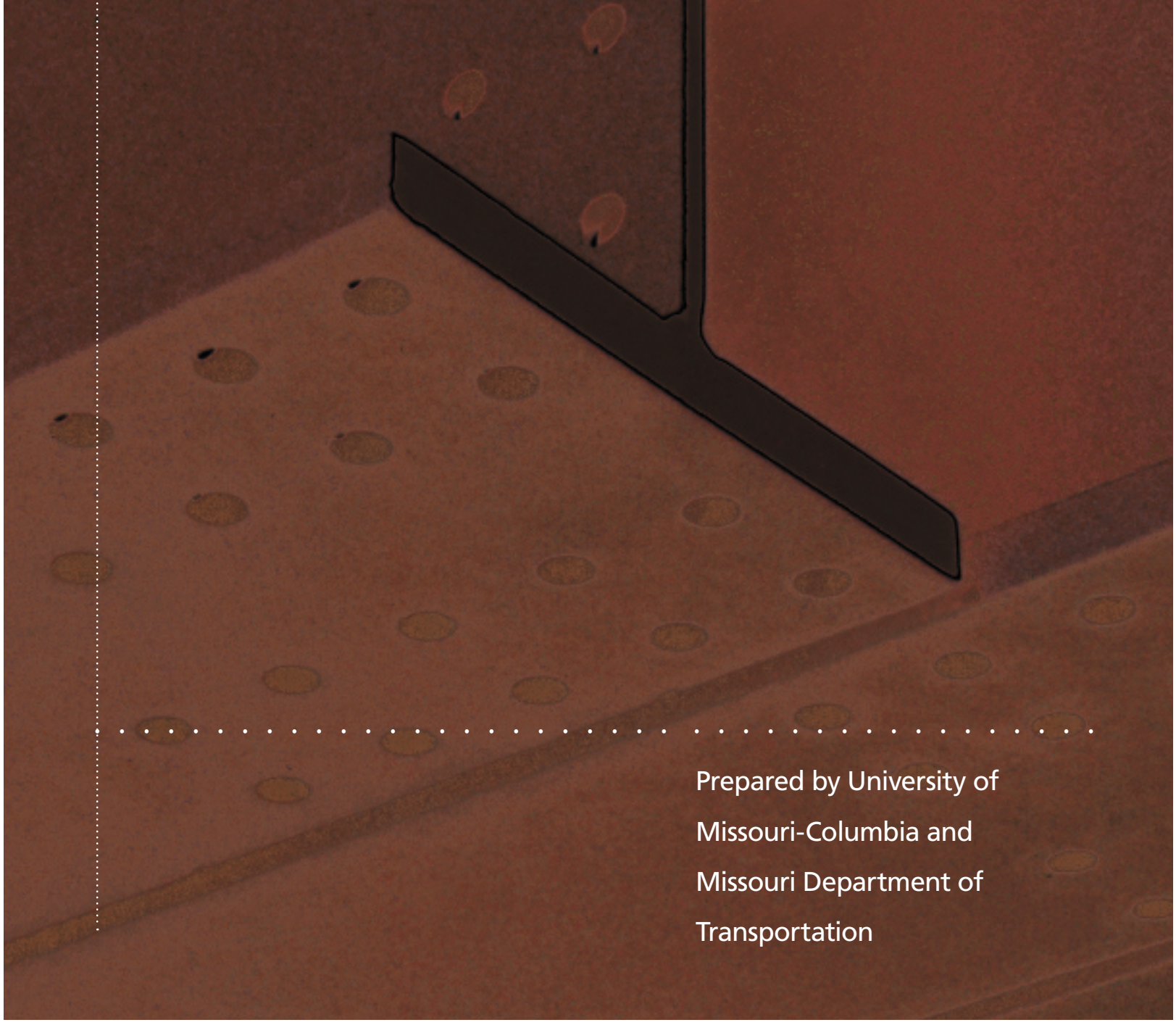

Prepared by University of Missouri-Columbia and Missouri Department of Transportation

TECHNICAL REPORT DOCUMENTATION PAGE

1. Report No. OR06-002	2. Government Accession No.	3. Recipient's Catalog No.
4. Title and Subtitle PERFORMANCE AND SERVICEABILITY OF HPS GIRDERS, MO 224, LAFAYETTE COUNTY		5. Report Date August, 2005 6. Performing Organization Code UMC
7. Author(s) Michael G. Barker		8. Performing Organization Report No. OR06-002 / RI00-059
9. Performing Organization Name and Address University of Missouri - Columbia		10. Work Unit No. 11. Contract or Grant No.
12. Sponsoring Agency Name and Address Missouri Department of Transportation Research, Development and Technology P. O. Box 270-Jefferson City, MO 65102		13. Type of Report and Period Covered Final Report 14. Sponsoring Agency Code MoDOT
15. Supplementary Notes The investigation was conducted in cooperation with the U. S. Department of Transportation, Federal Highway Administration.		

16. Abstract

The Missouri Department of Transportation (MoDOT) built the state's first High Performance Steel (HPS) Bridge in 2002. MoDOT Bridge A6101 uses HPS70W in the design of the 138 ft – 138 ft two-span, five girder bridge. Design calculations show that using HPS only in the highly stressed regions (hybrid design) led to a superstructure steel weight savings of nearly 17% and an estimated cost savings of approximately 11% compared to a conventional 50ksi bridge. The University of Missouri-Columbia worked with MoDOT to instrument, field test, analyze, and evaluate the performance of the completed Bridge A6101. The tests concentrated on strength and serviceability behavior of the structure. The serviceability field testing of Bridge A6101 confirms that MoDOT uses conservative deflection criteria. The maximum measured deflections for an equivalent HS20 loading match closely to the AASHTO method of estimating deflections. The MoDOT approach significantly over-estimates the measured deflections. The conservative serviceability procedures used by some states, such as MoDOT, will cause many HPS designs to be controlled by deflection, such as A6101 was, instead of strength parameters, which negates the benefit of using higher strength materials. The strength performance testing involved comparing design capacities to equivalent experimental design capacities. For design, the minimum design capacity is an HS23.8 truck loading whereas the critical experimental design capacity is an HS26.2. Thus, this bridge does exhibit additional capacity over the design prediction. Although design predictions seem to be conservative for interior girders, they may be unconservative for exterior girders.

Like in many progressive states, the future of HPS is promising in Missouri. HPS70W is a superior steel that can lead to more economical bridges than conventional 50ksi designs. HPS can produce significant savings, especially when used in hybrid designs with 50W or HPS50W. However, the conservative serviceability procedures used by some states, such as MoDOT, will cause many HPS designs to be controlled by deflection, such as A6101 was, instead of strength parameters, which negates the benefit of using higher strength materials.

17. Key Words Bridge Field Testing, Serviceability Deflections, Performance Testing		18. Distribution Statement No restrictions. This document is available to the public through National Technical Information Center, Springfield, Virginia 22161	
19. Security Classification (of this report) Unclassified	20. Security Classification (of this page) Unclassified	21. No. of Pages 130	22. Price

Form DOT F 1700.7 (06/98)

Final Report

RI00-059

PERFORMANCE AND SERVICEABILITY OF HPS GIRDERS, MO 224, LAFAYETTE COUNTY

Prepared for the
Missouri Department of Transportation
Research Development & Technology

By:
Michael G. Barker, PE
University of Wyoming
formerly of the
University of Missouri-Columbia

August 2005

The opinions, findings and conclusions expressed in this report are those of the principal investigator and the Missouri Department of Transportation. They are not necessarily those of the U.S. Department of Transportation or the Federal Highway Administration. This report does not constitute a standard, specification or regulation.

ACKNOWLEDGEMENTS

The author wishes to recognize the graduate students that worked on this project: Justin M. Davis and Everett R. Oesch. Special thanks are due to C.H. Cassil who worked on this project after his tenure at the University of Missouri-Columbia ended abruptly and controversially. His excellent technical support and commitment to the research, even though he was not compensated, was greatly appreciated. We can all take a lesson from his character and dedication.

EXECUTIVE SUMMARY

The Missouri Department of Transportation (MoDOT) built the state's first High Performance Steel (HPS) Bridge in 2002 as part of the Federal Highway Administration's Innovative Bridge Research and Construction (IBRC) program. MoDOT Bridge A6101 uses HPS70W in the design of the 138 ft – 138 ft two-span, five girder bridge. Design calculations show that using HPS only in the highly stressed regions (hybrid design) led to a superstructure steel weight savings of nearly 17% and an estimated cost savings of approximately 11% compared to a conventional 50ksi bridge.

The University of Missouri-Columbia worked with MoDOT to instrument, field test, analyze, and evaluate the performance of the completed Bridge A6101. The tests concentrated on strength and serviceability behavior of the structure. This bridge was also modeled by the University of West Virginia using ABAQUS Finite Element Software.

One objective of this research was to examine deflection serviceability limits. The pressing matter is that MoDOT uses more conservative deflection criteria than AASHTO. This conservative approach is best evident when comparing the deflection distribution factors and allowable deflections. For Bridge A6101, MoDOT predicts a deflection 49% higher than AASHTO while allowing 20% less deflection. Bridge A6101 meets the AASHTO deflection criteria but not the MoDOT. In effect, the bridge would need to possess 87% more stiffness than an AASHTO design to meet current MoDOT deflection criteria.

The serviceability field testing of Bridge A6101 confirms the conservative MoDOT deflection criteria. The maximum measured deflections for an equivalent HS20 loading match closely to the AASHTO method of estimating deflections. The MoDOT approach significantly over-estimates the measured deflections. The research also addresses acceleration and vibration characteristics of the bridge.

The other objective of this research was to perform field testing to confirm strength performance. The work involved comparing design capacities to equivalent experimental design capacities. For design, the minimum design capacity is an HS23.8 truck loading controlled by the positive moment region of an interior girder. The critical experimental design capacity is an HS26.2 controlled by the positive moment region of an exterior girder. Thus, this bridge does exhibit additional capacity over the design prediction. While the experimental results show that the design procedures are conservative for interior girders, they also show that the procedures may be unconservative for exterior girders. The experimental results were confirmed with finite element analyses.

Like in many progressive states, the future of HPS is promising in Missouri. HPS70W is a superior steel with higher yield strength, improved weldability, greater levels of toughness, and improved weathering resistance that can lead to more economical bridges than conventional 50ksi designs. HPS can produce significant savings, especially when used in hybrid designs with 50W or HPS50W. However, the conservative serviceability procedures used by some states, such as MoDOT, will cause many HPS designs to be controlled by deflection, such as A6101 was, instead of strength parameters, which negates the benefit of using higher strength materials.

TABLE OF CONTENTS

LIST OF FIGURES IX

LIST OF TABLES XI

CHAPTER 1 – INTRODUCTION 1
1.1 Project Background 1
1.2 Strength Testing Objectives 2
1.3 Serviceability Testing Objectives 2
1.3 Organization 3

CHAPTER 2 – DESIGN OF BRIDGE A6101 5
2.1 Introduction 5
2.2 General Information 5
2.3 SIMON Bridge Design Program 7
2.4 Hybrid HPS Girder Design 7
2.4.1 Design Assumptions 7
2.4.2 Strength Design 9
2.4.3 AASHTO Design Deflection 10
2.4.4 MoDOT Design Deflection 11
2.5 Homogeneous 50 ksi Girder Design 12
2.5.1 Strength Design 13
2.5.2 Design Deflection 14
2.6 Conclusions 14
2.6.1 Strength Design Conclusions 15
2.6.2 Deflection Conclusions 15
2.6.3 Material Cost Conclusions 16
2.6.4 Design Conclusions 17

CHAPTER 3 - STRENGTH FIELD TESTING OF BRIDGE A6101 19
3.1 Introduction 19
3.2 Testing Equipment 19
3.2.1 Data Acquisition Vehicle 19
3.2.2 Portable Man Lift 20
3.2.3 Load Truck 21
3.2.4 Strain Measurements 22
3.3 Field Test Loading Profiles 25
3.4 Field Test Data Collection Plans 31
3.4.1 Test Plan VI (Abandoned) 32
3.4.2 Test Plan II (Performed) 34
3.5 Field Test Data Reduction 36
3.5.1 Experimental Stress Profiles 36
3.5.2 Girder Total Experimental Moment, M_T 39
3.5.3 Experimental Section Modulus, S_E 41

3.6 Experimental and Design Load Capacities 41
3.6.1 AASHTO LFD Design Capacity 43
3.6.2 Experimental Capacity 45
3.6.3 Performance Comparison 46
3.7 Data, Stresses and Maximum Bridge Response 49
3.8 FEM Stress Comparisons 54
3.9 Moments 55
3.9.1 Sample Calculation: Maximum Positive Interior Moment (Girder 4) 56
3.9.2 Experimental Moment Results 58
3.10 Rating Factors 60
3.10.1 Sample Calculation: Maximum Positive Interior Rating Factor (Girder 4) 60
3.10.2 Design and Experimental Rating Factor Results 68
3.11 Summary 70

CHAPTER 4 – SERVICEABILITY FIELD TESTING OF BRIDGE A6101 72
4.1 Serviceability Background Information 72
4.1.1 AASHTO Deflection Criteria 73
4.1.2 MoDOT Deflection Criteria 75
4.1.3 Comparison to Other State's Deflection Criteria 76
4.1.4 Ontario Bridge Code 76
4.1.5 Effect of Serviceability Criteria on HPS Bridges 79
4.2 Serviceability Field Testing Procedures 80
4.2.1 Loading System 81
4.2.2 Data Acquisition System 82
4.2.2.1 String Pots 82
4.2.2.2 Laser Deflection Device 84
4.2.2.3 Accelerometers 86
4.3 Serviceability Field Conditions 87
4.4 Deflection Testing Procedure 88
4.5 Acceleration Testing Procedure 89
4.6 Serviceability Measurement Equipment Performance 91
4.6.1 String Pot Performance 92
4.6.2 Laser Deflection Device Performance 93
4.6.3 Accelerometer Performance 95
4.7 Abaqus Finite Element Model 97
4.8 Measured Deflection Results 100
4.8.1 Conversion of Field Test Load Truck Deflection to HS20 Deflection ... 100
4.8.2 Load Combinations 102
4.8.3 AASHTO Measured Girder Deflections 104
4.8.4 MoDOT Measured Girder Deflections 106

4.9 Natural Frequency Results 108
4.9.1 Ontario Equation Harmonic Frequency 108
4.9.2 Natural Frequency by Fast Fourier Transform 110
4.9.3 Resonant Frequency Comparison 113
4.9.4 Second Harmonic Frequency 114
4.9.5 Ontario Bridge Code Allowable Deflection 115
4.10 Serviceability Results Summary 118

CHAPTER 5 – SUMMARY AND CONCLUSIONS 120
5.1 Missouri HPS Bridge A6101 120
5.2 Strength Performance Conclusions 120
5.2.1 Critical Experimental Bridge Capacity 121
5.2.2 Bridge Strength Performance 122
5.2.3 Strength Summary 123
5.3 Serviceability Performance Conclusions 123
5.3.1 Comparison of MoDOT, AASHTO, and Ontario Serviceability Criteria124
5.3.2 Comparison of Measured and Predicted Deflection Values 125
5.3.3 Serviceability Field Testing Summary 127
5.4 Closing Remarks 128

REFERENCES 129

LIST OF FIGURES

Figure 1.1 – Bridge A6101in Lexington, Missouri 3

Figure 2.1 – General Layout and Dimensions of Bridge A6101 6
Figure 2.2 – Side View of Bridge A6101 6
Figure 2.3 – Design Dimensions of Bridge A6101 Hybrid HPS Girder 9
Figure 2.4 – Bridge A6101 Exterior Girder..... 10
Figure 2.5 – Design Dimensions of Hypothetical Homogeneous 50 ksi Girder 13

Figure 3.1 - University of Missouri Data Acquisition Vehicle..... 20
Figure 3.2 - Genie Z-45/25J Articulated Boom 21
Figure 3.3 - University of Missouri's Load Truck with Weights 22
Figure 3.4 - Weighing Pads 22
Figure 3.5 - Weldable Strain Gage 23
Figure 3.6 - Data Acquisition Box 24
Figure 3.7 - Hookups on outside of RV for Data Acquisition Boxes 25
Figure 3.8 - Positioning of Load Truck for Testing Runs..... 26
Figure 3.9 - Experimental Load Truck Weight..... 26
Figure 3.10 - String along bridge and deck marking 27
Figure 3.11 - Truck during testing and equipment below the bridge..... 27
Figure 3.12 - Data from Gage P1-1 (Smoothed)..... 28
Figure 3.13(a): Maximum load positions for Girder 1 (Load Cases 1 & 4) 29
Figure 3.13(b) - Maximum load positions for Girder 2 (Load Cases 1 & 4,
Load Cases 2 & 6)..... 29
Figure 3.13(c): Maximum load positions for Girder 3 (Load Cases 3 & 8,
Load Cases 5 & 10)..... 30
Figure 3.13(d) - Maximum load positions for Girder 4 (Load Cases 9 & 12
Load Cases 7 & 11)..... 30
Figure 3.13(e) - Maximum load positions for Girder 5 (Load Cases 9 & 12)..... 31
Figure 3.14 - Strain Gage Placement (Test Plan VI) 33
Figure 3.15 - Strain Gage Cross Section..... 34
Figure 3.17 - Stress profiles along Girder 4 in the maximum positive moment region ... 38
Figure 3.18 - Total Moment..... 39
Figure 3.19 - HS20 Load Truck..... 42
Figure 3.20 (a) - Raw Data (Not Smoothed) (Gage P1-1)..... 49
Figure 3.20 (b): Raw Data (Smoothed) (Gage P1-1)..... 50
Figure 3.21 - Load position for Influence Line Diagram..... 64
Figure 3.22 - Statical Moment Diagram along Span 65

Figure 4.1 – Ontario Bridge Code Allowable Deflection Chart (Ontario, 1983) 77
Figure 4.2 – 1st and 2nd Resonant Frequency Mode Shapes for Two-Span Beam (Billing, 1979) 79
Figure 4.3 – Side View of Backhoe 81
Figure 4.4 – String Pot Placement (Girders 1 – 5) 83
Figure 4.5 – Close-up of String Pot on Ground 83
Figure 4.6 – Laser Deflection Device Setup (Girder 2 only) 85
Figure 4.7 – Laser Mounted on Tripod 85
Figure 4.8 – Laser Deflection Device in Position on Girder 2 86
Figure 4.9 – Accelerometer Placement (Girders 2 and 3) 87
Figure 4.10 – Measured Dimensions of Girder Cross Sections 88
Figure 4.11 – Front Tires of Backhoe Bouncing on Surface of Bridge 90
Figure 4.12 – Backhoe Testing Wheel Weights 91
Figure 4.13 – String Pot Measurements for Load Test Run 3 92
Figure 4.14 – Laser Deflection Device Measurements for Load Run 3 94
Figure 4.15 – Girder 2 Accelerometer Data for Backhoe Run 6 (smoothed twice) 96
Figure 4.16 – Abaqus FEM Predicted Deflections 98
Figure 4.17 – Measured and FEM Predicted Deflection Comparison 99
Figure 4.18 – User Defined Load Truck Axle Weights 102
Figure 4.19 – Comparison of AASHTO, MoDOT Girder 1 Critical Loading 103
Figure 4.20 – Acceleration Data Used for University of Missouri Origin and Excel FFT's 111
Figure 4.21 – Origin FFT Resonant Frequencies 112
Figure 4.22 – Excel FFT Resonant Frequencies 112
Figure 4.23 – Ontario Bridge Code Allowable Deflections for f = 1.869 Hz 115

LIST OF TABLES

Table 2.1 – Non-Composite Dead Load Estimation 8
Table 2.2 – Comparison of AASHTO and MoDOT Deflection Criteria for Bridge A6101 16
Table 2.3 – Weight and Material Cost of Homogeneous 50 ksi and Hybrid 50/70 Girders 17

Table 3.1: Maximum Run Combinations 51
Table 3.2 – Girder Stresses When Truck at Maximum Positive Position 52
Table 3.3 – Girder Stresses When Truck at Maximum Negative Position 53
Table 3.4 - Stress Comparison between West Virginia FEM and Missouri Measured Stresses 54
Table 3.5 - Maximum Positive Stresses for Individual Girders from Particular Maximum Loading 55
Table 3.6 – Maximum Stresses Caused from Load Case 9+12(Positive Section) 56
Table 3.7 - Moment Summary 59
Table 3.8 - Maximum Positive and Maximum Negative Rating Factors 68
Table 3.9 - Maximum Positive Rating Factors and Adjustment Factors 69
Table 3.10 - Maximum Negative Rating Factors and Adjustment Factors 70

Table 4.1 – Modal Frequency Factors for Two-Span Beam (Billing, 1979) 78
Table 4.2 – Maximum Deflection of Girder 2 Measured by Laser Deflection Device 95
Table 4.3 – Abaqus FEM Maximum Predicted Deflections for All Girders 97
Table 4.4 – Girder 2 Deflection Comparison 99
Table 4.5 – Possible Load Combinations for Bridge A6101 104
Table 4.6 – AASHTO Measured Total Live Load Deflections 105
Table 4.7 – AASHTO Measured, Design Live Load Deflection Comparison 105
Table 4.8 – MoDOT Measured Total Live Load Deflection 107
Table 4.9 – MoDOT Measured, Design Live Load Deflection Comparison 107
Table 4.10 – Calculation of Negative Composite Moment of Inertia 109
Table 4.11 – Base Frequency Calculation using Ontario Bridge Code Equation 109
Table 4.12 – Bridge A6101 First Resonant Frequency Comparison 113
Table 4.13 – Bridge A6101 Second Harmonic Frequency Comparison 114
Table 4.14 – Ontario Bridge Code Allowable Deflection of Bridge A6101 (f = 1.869 Hz) 116
Table 4.15 – Comparison of MoDOT, AASHTO, Ontario Deflection Criteria 117

Table 5.1 Design and Experimental Rating Factors 122
Table 5.2 Deflection Results for AASHTO and MoDOT 127

CHAPTER 1 – INTRODUCTION

1.1 PROJECT BACKGROUND

The Missouri Department of Transportation (MoDOT) built the state's first High Performance Steel (HPS) Bridge in 2002 as part of the Federal Highway Administration's Innovative Bridge Research and Construction (IBRC) program. MoDOT Bridge A6101 uses HPS70W in the design of the 138 ft – 138 ft two-span, five girder bridge. Design calculations show that using HPS only in the highly stressed regions (hybrid design) led to a superstructure steel weight savings of nearly 17% and a cost savings of approximately 11% compared to a conventional 50W bridge using typical steel costs (Davis, 2003).

The University of Missouri-Columbia worked with MoDOT and West Virginia University to instrument, field test, analyze, and evaluate the performance of the completed Bridge A6101. The tests concentrated on strength and serviceability behavior of the structure. This bridge was also modeled by the University of West Virginia using ABAQUS Finite Element Software and a comparison between the FEM stresses and the actual stresses are examined (Wu, 2003). The objectives of the field testing are to evaluate the strength and serviceability performance of the hybrid HPS Bridge A6101.

Like in many progressive states, the future of HPS is promising in Missouri. HPS70W is a superior steel with higher yield strength, improved weldability, greater levels of toughness, and improved weathering resistance that can lead to more economical bridges than conventional 50W designs. HPS can produce significant savings, especially when used in hybrid designs with 50W or HPS50W.

However, using HPS means less steel material and, therefore, live load deflections increase over conventional 50W bridges. Missouri enforces deflection criteria (MoDOT, 2002) that are significantly more restrictive than those in AASHTO (1996). In fact, Bridge A6101 does not meet the MoDOT criteria and a design exception to Missouri standards was required to accept the design for the bridge. Bridge A6101 does meet AASHTO deflection criteria.

1.2 STRENGTH TESTING OBJECTIVES

The objectives of the strength testing of Bridge A6101 are to compare actual response of known loads to design theory. This is accomplished through monitoring stresses when the bridge is subjected to calibrated loading. The stress results are modified to represent the design loading and compared to design theory. It is common knowledge that actual bridge response can vary significantly from design predictions. Past research (Barker, et al., 1999) has developed procedures to qualify and quantify factors that represent the difference between design practice and bridge response. These field test procedures are applied to evaluate the strength performance of HPS Bridge A6101.

1.3 SERVICEABILITY TESTING OBJECTIVES

The objectives of the serviceability testing are to evaluate measured deflections, accelerations, and natural frequencies to values estimated in the design of Bridge A6101. In particular, MoDOT's current live load criteria is compared to AASHTO design criteria and measured deflections. The focus of this report will be to compare the deflection and acceleration findings of the field test to the differing expectations of the MoDOT (2002) and AASHTO (1996) codes. The findings will also be compared to the Ontario Highway

Bridge Design Code (1983), and also a Finite Element Model performed by West Virginia University (Wu, 2003).

Figure 1.1 – Bridge A6101in Lexington, Missouri

1.2 ORGANIZATION

This report is divided into three main categories. The first is the design of HPS Bridge A6101 and design and cost comparisons to conventional 50ksi steel bridges in Chapter 2. Chapter 2 also discusses the strength and serviceability concerns in bridge design.

Chapter 3 presents the strength performance of Bridge A6101 compared to design theory. The chapter illustrates the testing of the bridge, the data collected, the data reduction to turn raw data into meaningful engineering results, and finally the experimental capacity results.

Chapter 4 presents the serviceability field testing of Bridge A6101. The testing, data collection, analysis procedures employed and the bridge response are developed and presented. The experimental behavior of Bridge A6101 is compared to design provisions.

Chapter 5 summarizes this research and presents conclusions.

CHAPTER 2 – DESIGN OF BRIDGE A6101

2.1 INTRODUCTION

Bridge A6101 was designed as a hybrid girder bridge with HPS70W used in the flanges where stresses are large. The bridge was designed according to AASHTO (1996) Load Factor Design (LFD) procedures.

2.2 GENERAL INFORMATION

Bridge A6101 is a two span continuous bridge that carries Route 224 over the newly constructed section of Highway 13 in Lafayette County, Missouri. The bridge was designed using metric dimensions, but, for this report, the dimensions have been converted to the English system, as the AASHTO code and MoDOT currently use English dimensions. The bridge is symmetric, and the span lengths are 137.8 ft. A6101 is 42.06 ft wide overall with a roadway width of 39.37 ft. There are five girders spaced at 8.96 ft with a skew of 17.08° with lateral cross bracing placed at about every 23 ft. The deck is 8.5 in thick, and has a haunch of 2.5 in from the top of the web. The bridge is composite in the positive moment regions, but noncomposite over the interior pier. The general layout of Bridge A6101 can be seen in Figure 2.1. A side view of the bridge is shown in Figure 2.2.

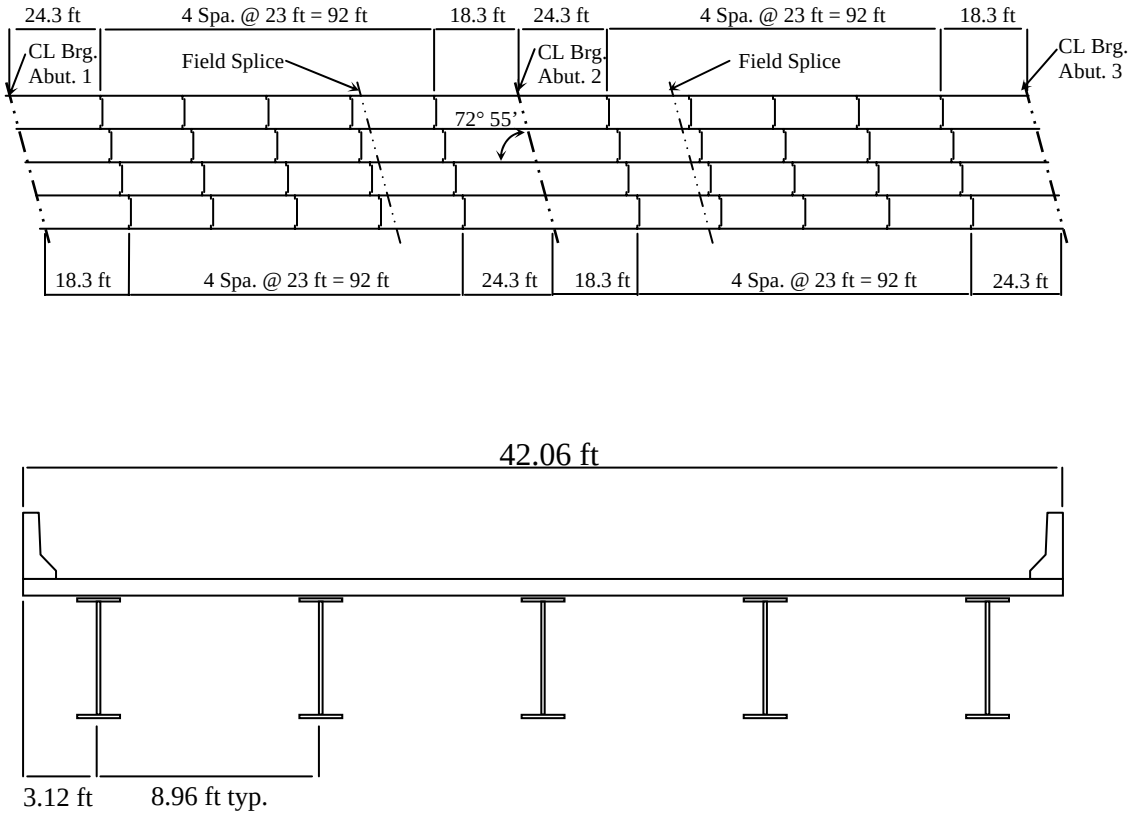

5 Girders @ 8.96 ft Spacing

Figure 2.1 – General Layout and Dimensions of Bridge A6101

Figure 2.2 – Side View of Bridge A6101

2.3 SIMON BRIDGE DESIGN PROGRAM

MoDOT designed Bridge A6101 using SIMON (AISC, 1996), a software program that is popular with many state agencies. SIMON takes initial dimensions input by the designer, and checks the design against the AASHTO code. The program can be used to optimize the design. SIMON also estimates the live load deflection in the girder using the AASHTO provisions. However, it does not let deflection control the design. If the live load deflection is greater than allowed, a warning is printed and the strength design continues.

2.4 HYBRID HPS GIRDER DESIGN

Because of the increased strength of HPS, it is possible to design a girder with less cross sectional area than in a conventional 50 ksi girder. However, since the HPS is more expensive to produce than the 50 ksi steel, it is not necessarily cost effective to build an entire girder out of HPS. Instead, studies have shown (Barker, 2000) that using HPS only in high stress areas (hybrid design) can be cost effective. For Bridge A6101, this means the bottom flange in the composite positive moment region and for both flanges in the non-composite negative moment region.

2.4.1 Design Assumptions

The AASHTO LFD method is used for the girder designs. The following are the inputs for distribution and loading used in the SIMON design program. For Bridge A6101 the moment distribution factor for an interior girder is

$$S / 5.5 = 8.96 / 5.5 = 1.629 \text{ wheel lines per girder}$$

and for an exterior girder

S / (4 + S / 4) = 8.96 / (4 + 8.96 / 4) = 1.436 wheel lines per girder

The non-composite dead load is estimated from the slab, diaphragms, haunching, stiffeners, and splices. The steel girder weight is also non-composite dead load, but it is calculated and included in the design automatically by SIMON. The estimated non-composite dead load for Bridge A6101 is broken down in Table 2.1.

Table 2.1 – Non-Composite Dead Load Estimation

	Distributed Load (lb/ft)	
	Interior Girder	Exterior Girder
Slab	970	822
Diaphragms	18	9
Haunch	23	26
Stiffeners	4	4
Splices	6	6
Bolts	1	1
Total N.C. Dead Load	1022	868

The composite dead load includes the weight of the barrier curbs and a future wearing surface. The composite dead loads are divided evenly among all five girders, giving each girder on Bridge A6101 a 436 lb/ft loading.

The effective structural slab depth is the total slab thickness minus a sacrificial one inch of expendable surface for a value of 7.66 in (MoDOT 3.30.1.5, 2002). The effective composite slab width is the minimum of

1. ¼ Span Length = 137.8 / 4 = 34.35 ft
2. Girder Spacing = 8.96 ft
3. 12 * effective slab thickness = 12 * 7.66 = 91.9 in

Therefore, an effective width of 91.9 in is used for interior girders, and 83 in for exterior girders.

2.4.2 Strength Design

Using these values for loading and distribution, a SIMON design was conducted for an interior girder and an exterior girder. The interior girder controlled the strength design, so for ease of construction all girders use the same plate sizes. The SIMON girder design for Bridge A6101 is illustrated in Figure 2.3. As stated earlier, the design was metric, so the English units are not round numbers. Figure 2.4 displays an exterior girder of Bridge A6101.

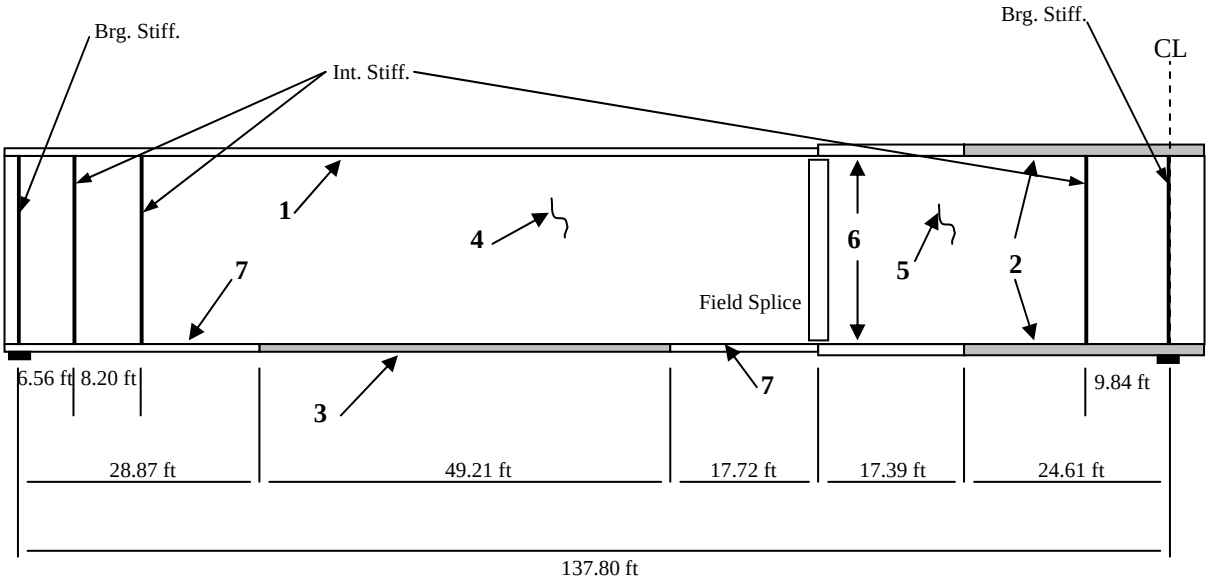

1. 12.598 x 0.787 in (50 ksi) Based on Non-Composite LTB
2. 20.472 x 1.26 in (HPS70W) Based on Bending Stresses
3. 16.535 x 0.787 in (HPS70W) Based on Bending Stresses
4. 59.055 x 0.4724 in (50 ksi) Based on Shear
5. 59.055 x 0.5512 in (50 ksi) Based on Shear
6. 20.472 x 1.26 in (50ksi) Match Size of 2
7. 16.535 x 0.787 in (50 ksi) Match Size of 3 (option to use HPS)

Figure 2.3 – Design Dimensions of Bridge A6101 Hybrid HPS Girder

SIMON also calculates the weight of the girder, which is 28.87 tons for one hybrid HPS girder, of which only 6.5 tons is HPS70W. Therefore, the total weight of

steel used for girders in Bridge A6101 is 144.35 tons, with 32.5 tons of that weight being HPS70W.

Figure 2.4 – Bridge A6101 Exterior Girder

2.4.3 AASHTO Design Deflection

In addition to checking the strength requirements of the bridge, SIMON also predicts the maximum live load deflection of the girder. This estimated deflection is based on the AASHTO equal deflection distribution factor, which is discussed in Chapter 4. For Bridge A6101, there are three 12 ft traffic lanes, which means that an intensity reduction factor of 0.9 is used. Therefore, the AASHTO live load deflection distribution factor for Bridge A6101 is calculated using Equation 4.1 as

$$D.F. = (3*2*0.9) / 5 = 1.08 \text{ wheel lines per girder}$$

SIMON multiplies the deflection caused by one wheel line with this distribution factor to estimate the total girder deflection. For Bridge A6101, SIMON estimates a live load deflection of 1.540 in for an interior girder, and 1.565 in for an exterior girder (Davis, 2003). The exterior girder deflection is slightly larger because the effective width of concrete is smaller. Therefore, the AASHTO live load deflection criteria for a bridge without pedestrian traffic is satisfied by:

1.565 in < L/800 = 2.067 in Bridge Deflection OK

2.4.4 MoDOT Design Deflection

The MoDOT live load deflection distribution factor is more conservative than the AASHTO code, as discussed in Chapter 4. For MoDOT's factor, lanes are assumed to be only 10 ft wide. This results in A6101 having four 10 ft traffic lanes. (While the bridge roadway is just less than 40 ft wide, it was designed with metric units, so the 12 m roadway has four 3 m traffic lanes.) The moment distribution factor for an interior girder on Bridge A6101 equals the girder spacing divided by 5.5, which is 1.629. So, using Equation 4.2, the MoDOT deflection distribution factor for an interior girder is

D.F. = [1.629 + (4*2) / 5] / 2 = 1.615 wheel lines per girder

To find the deflection estimated by this distribution factor, the deflection calculated by SIMON is divided by the AASHTO distribution factor, and then multiplied by the MoDOT distribution factor. So the design deflection that would be used by MoDOT for Bridge A6101 is

1.540 in / 1.08 * 1.615 = 2.302 in

For an exterior girder, the moment distribution factor is 1.436, so the deflection distribution factor is

D.F. = [1.436 + (4*2) / 5] / 2 = 1.518 wheel lines per girder

Consequently, the exterior girder is predicted to deflect

1.565 in / 1.08 * 1.518 = 2.20 in.

Not only is MoDOT's estimated deflection larger than AASHTO's, but Missouri applies a stricter deflection limit of L/1000 to all composite bridges. Thus, Bridge A6101 does not meet the Missouri deflection criteria:

2.302 in > L/1000 = 1.654 in Bridge Deflection NOT OK

This means that for the deflection to satisfy the MoDOT deflection criteria, the girders would need to be redesigned larger, which would increase the stiffness and thereby decrease the deflection. However, the larger section would produce a bridge stronger than strength criteria dictate, thereby negating any cost savings from using HPS. Adding material to increase the stiffness would increase bridge costs due solely to the conservative MoDOT deflection criteria. Consequently, although this is a MoDOT bridge that does not meet MoDOT's deflection criteria, MoDOT (2000) waived the deflection limits on this particular bridge so that their current serviceability criteria could be examined.

2.5 HOMOGENEOUS 50 KSI GIRDER DESIGN

To examine the cost savings of the hybrid HPS girder bridge, a second hypothetical design was completed using conventional 50 ksi steel in a homogeneous girder design (Davis, 2003). As with the hybrid design, SIMON was used to maximize the efficiency of the design, and the same design assumptions were used. A comparison of steel weight and girder costs can be used to examine the benefits of using hybrid HPS girders.

2.5.1 Strength Design

Once again, an interior and exterior girder design was completed using SIMON, and the interior girder controlled the design. The resulting hypothetical girder is similar to the hybrid girder in that the web is the same size and the widths of the flanges are the same size. However, the flanges of the homogeneous 50 ksi girder must be thicker than the hybrid girder in order to meet design specifications. The plate sizes that would be used in a homogenous 50 ksi girder are illustrated in Figure 2.5.

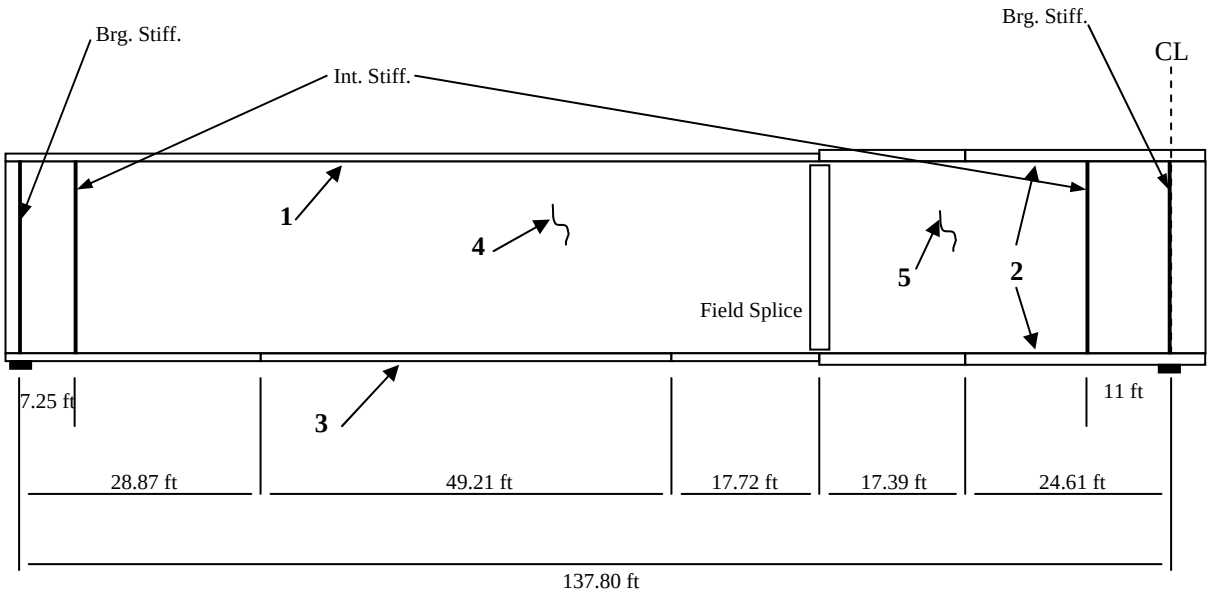

1. 12.598 x 0.787 in (50 ksi)
2. 20.472 x 1.875 in (50 ksi)
3. 16.535 x 1.1875 in (50 ksi)
4. 59.06 x 0.4724 in (50 ksi)
5. 59.06 x 0.5512 in (50 ksi)

Figure 2.5 – Design Dimensions of Hypothetical Homogeneous 50 ksi Girder

The weight of each girder is found to be 34.66 tons, giving a total weight of 173.31 tons of 50 ksi steel used for the girders.

2.5.2 Design Deflection

SIMON predicts that the interior hypothetical 50 ksi girder will have a live load deflection of 1.205 in. Again, this is using the AASHTO distribution factor which remains 1.08. The MoDOT deflection distribution factor also remains 1.615 for an interior girder. Thus, the MoDOT deflection for an interior girder of the homogeneous 50 ksi design is

1.205 in / 1.08 * 1.615 = 1.802 in

While the AASHTO deflection criteria is met as

1.205 in < L / 800 = 2.067 in Bridge Deflection OK

The MoDOT deflection criteria are still not met even with the larger cross section.

1.802 in > L / 1000 = 1.654 in Bridge Deflection NOT OK

This shows deflection in a MoDOT design actually controls even the homogenous 50 ksi girder. The girder would need to be redesigned larger to increase stiffness. This, of course, would result in a more expensive bridge as a direct consequence of the conservative MoDOT deflection criteria.

2.6 CONCLUSIONS

Several conclusions can be made from comparing the design of the hybrid HPS girder and the equivalent homogeneous 50 ksi girder, as well as comparing the deflection criteria used by MoDOT and AASHTO. Using SIMON, both strength and deflection characteristics can be compared, as well as cost of material. Advantages and disadvantages of using a hybrid HPS design can then be examined.

2.6.1 Strength Design Conclusions

Both the hybrid HPS and the homogeneous 50 ksi girder were designed for the same loading, so the ultimate strength of both are close to being equal. The comparison of performance ratios along the length of the girder shows that both girders are optimal designs (Davis, 2003). However, the hybrid HPS bridge requires 17% less steel. By placing HPS70W only in high stress areas, the girder weight is reduced significantly from a homogenous 50 ksi girder.

2.6.2 Deflection Conclusions

One objective of this research is to examine deflection limit design. The pressing matter in examining the deflection of the hybrid HPS girder is that MoDOT uses more conservative deflection criteria than AASHTO. This conservative approach is best evident when comparing the deflection distribution factors and allowable deflections of an interior girder, as shown in Table 2.2 for Bridge A6101. Compared to AASHTO, MoDOT uses narrower lanes, which for A6101 means an additional lane, does not use a load intensity reduction factor, and averages in the moment distribution factor with the uniform deflection distribution. The table shows that for Bridge A6101, MoDOT predicts a deflection 49% higher than AASHTO while allowing 20% less deflection. Bridge A6101 meets the AASHTO deflection criteria but not the MoDOT. In effect, the bridge would need to possess 87% more (1.61/1.08 * 2.07/1.65) stiffness than an AASHTO design to meet current MoDOT deflection criteria. For Bridge A6101 to be built as it was, MoDOT needed to implement a design exception from the Misouri bridge standards. Chapter 4 addresses the MoDOT and AASHTO deflection criteria as it applies to the field testing of Bridge A6101.

Table 2.2 – Comparison of AASHTO and MoDOT Deflection Criteria for Bridge A6101

	AASHTO	MoDOT
Lane Width (ft)	12	10
# of Lanes	3	4
Load Intensity Factor	0.9	1
S/5.5	-	1.63
Distribution Factor	**1.08**	**1.61**
Allowable Deflection	L / 800	L / 1000
Allowable Deflection (in)	**2.07**	**1.65**

Due to the larger girder, a hypothetical homogeneous 50 ksi girder deflects about 20% less than the hybrid HPS girder. However, both girders meet the AASHTO deflection criteria, but both do not meet MoDOT deflection criteria. This means that both designs would need to be changed to a larger girder to increase stiffness for MoDOT criteria to be met. In fact, because stiffness is based on inertia of the girders and not by yield strength, both girders would have to be the same size to meet deflection requirements in Missouri. Thus, there would be no benefit in using HPS in the girders.

2.6.3 Material Cost Conclusions

HPS70W costs about 1.3 times (in 2002) the price of 50 ksi steel (MoDOT, 2000). The hybrid girder total weight savings from the homogeneous girder design, however, makes the hybrid HPS bridge more economical. The breakdown of the estimated cost for material for the 50 ksi girder and the hybrid girder is shown in Table 2.3.

Table 2.3 – Weight and Material Cost of Homogeneous 50 ksi and Hybrid 50/70 Girders

	50 ksi Weight (tons/girder)	50 ksi Cost ($/girder)	HPS70W Weight (tons/girder)	HPS70W Cost ($/girder)	**Total Weight (tons/girder)**	**Total Cost ($/girder)**
Homogeneous 50 ksi	34.66	83184	0	0	**34.66**	**$83,184.00**
Hybrid 50/70	22.37	53688	6.5	20280	**28.87**	**$73,968.00**

Assumed In-Place Unit Cost		
50 ksi	2400	$/ton
HPS70W	3120	$/ton

The table illustrates the main benefit of using a hybrid HPS girder design. By using as little of the expensive material as possible, the weight and cost of the entire structure is lowered. For Bridge A6101, 5.79 tons and $9,200 are saved per girder, which for the entire bridge equals about 29 tons and $46,000. The hybrid design reduces the amount of material roughly 17% and the cost by 11%. While this is not an overwhelming amount, a large cost savings can be realized if HPS can be utilized in a similar way in more bridges.

2.6.4 Design Conclusions

This chapter has shown that using a hybrid HPS design can be an economical solution for bridge construction. The hybrid girder is lighter and less expensive than a homogeneous 50 ksi girder. The only drawback of using HPS is that the smaller girders allow more deflection, which does not impact the design or savings as long as deflections do not control. Designs that use AASHTO deflection criteria do not seem to be problematic. However, this can be a problem in states with more conservative deflection criteria such as Missouri. The conservative methods used by MoDOT will cause many

hybrid HPS designs to be controlled by deflection, such as A6101, instead of strength parameters, which negates the benefit of using higher strength materials.

CHAPTER 3 - STRENGTH FIELD TESTING OF BRIDGE A6101

3.1 INTRODUCTION

Bridge A6101 was tested using the University of Missouri – Columbia's Field Test system and personnel. The equipment was developed to be mobile, versatile, and reliable (Barker, et al., 1999). The goal in the development of this equipment was to reduce the cost, time and effort required to field test bridges. The objective was to develop a system that could test a bridge in a matter of a couple of days rather than weeks. A modular "plug-and-play" system was developed to allow quick instrumentation, testing, and clean up of a bridge test. With this time frame and associated costs, load-rating bridges becomes economically appealing.

Following will be a description of the field test system and the controlled loading program for Bridge A6101 (Oesch, 2003). The process of collecting data and reducing it to a useable form is presented. Finally, the field test experimental capacity equations are presented and related to design capacity prediction equations developed for use in the performance study.

3.2 TESTING EQUIPMENT

3.2.1 Data Acquisition Vehicle

The command center for the field test system is the data acquisition vehicle. The command center provides transportation and living quarters for the testing team as well as a protected and air-conditioned housing for data acquisition computers and hardware. A photograph of the vehicle is shown in Figure 3.1.

Figure 3.1 - University of Missouri Data Acquisition Vehicle

The RV was refurbished to meet the requirements that come with field-testing. The rear workspace houses a data acquisition rack for 95 low level (strain) channels and 25 high level (deflection) channels. The data acquisition CPU, the communications receiver and an oscilloscope can also be found in the data acquisition rack. Other equipment found in the rear data acquisition vehicle are the monitor for the data acquisition CPU, a data reduction computer, uninterruptible power supplies, a printer, and a communications system. Power is supplied to the data acquisition vehicle by a 4 KW on board generator as well as a 12 KW exterior generator that could be hooked into the system to meet the demands of a large-scale field test. A detailed description of the data acquisition vehicle can be found in McDaniel (1998).

3.2.2 Portable Man Lift

Due to the height of the bridge, scaffolding or a hanging catwalk system was not suitable for installing equipment on the girders underneath the bridge. Thus, a Genie Z-45/25J four-wheel drive articulated boom was rented allowing two team members to

move around and work up under the bridge. A photo of the boom lift is shown in Figure 3.2.

Figure 3.2 - Genie Z-45/25J Articulated Boom

The boom has a steel platform able to lift up to 500 pounds and allows ample space for two workers and equipment. The articulated boom can reach a vertical working height of 51 ft and a horizontal reach of 24 ft. The boom proved to be helpful when installing instrumentation and equipment.

3.2.3 Load Truck

The goal of field-testing is to accurately measure the response of the bridge to known loads. The University of Missouri – Columbia's Field Test Team performs this task by using its calibrated load truck. The load truck is a 1984 Freightliner truck, seen in Figure 3.3, equipped with an M-21-8 Jiffy lift Classic Lift Eagle boom. Steel blocks, each with an average weight of 1500 pounds, are used to apply axle loads. After the truck is loaded, the wheel loads are determined using four weighing pads, as seen in Figure 3.4.

Figure 3.3 - University of Missouri's Load Truck with Weights

Figure 3.4 - Weighing Pads

3.2.4 Strain Measurements

The strains introduced in the bridge due to the calibrated loading were measured using weldable strain gages. Weldable gages are ideal in that they can be attached to the

girder surface with little surface preparation. A picture of a weldable strain gage is shown in Figure 3.5.

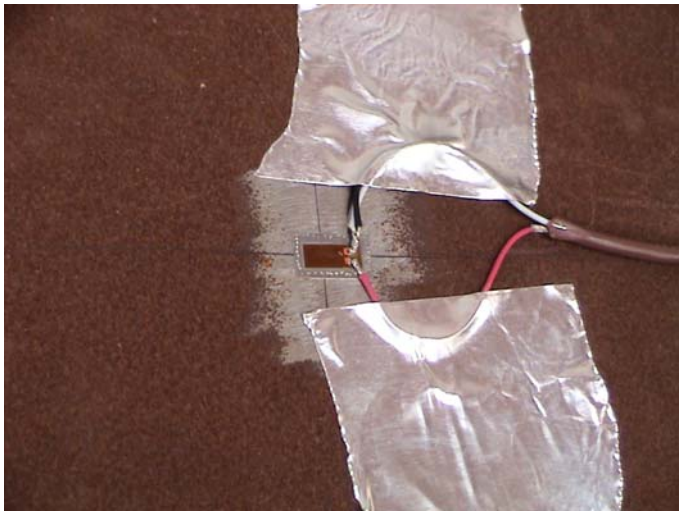

Figure 3.5 - Weldable Strain Gage

The strain gages were connected to data acquisition boxes containing power and completion circuits. The goal of these boxes is to transfer data from the sensors to the data acquisition system located in the RV. They have the capability of monitoring as many as 19 strain gages for each box at one time. A picture of a completely wired data acquisition box is shown in Figure 3.6.

During the test of Bridge A6101, only 2 boxes were necessary to obtain the number of channels monitored. One box was placed on the center pier (for negative moment readings) while the other was mounted to one of the cross frames near the maximum positive moment region.

From each data acquisition box, the data is transferred to the RV through 27 pairs of foil shielded Alpha brand type 6022C cables. At the RV, the cables are hooked into military Amphenol connectors on the side of the RV that lead into the data acquisition

equipment. There are also extra power outlets on the outside of the vehicle to run power up to the data acquisition boxes. A picture of the side of the RV is shown in Figure 3.7. Inside the RV, the data is collected from the strain gages by a LabView (1997) Program that can quickly be converted into Excel spreadsheets.

Figure 3.6 - Data Acquisition Box

Figure 3.7 - Hookups on outside of RV for Data Acquisition Boxes

3.3 FIELD TEST LOADING PROFILES

Previous research (Barker, et al., 1999) has shown that static loading can be adequately modeled by driving the test truck over the bridge at a slow crawl speed. It was found that driving the truck at a crawl speed resulted in the same maximum response as did static placement. A set of lateral truck runs were selected so that individual girders were maximized using design criteria and superposition of data. The lateral position of the truck was measured from the northern guardrail. Bridge A6101 was wide enough for 12 lateral test runs. Dots were painted at quarter points along the bridge and a string was run along the bridge to show the truck operator where to keep his left wheels. The positioning of the test runs are shown in Figure 3.8. The experimental wheel loads are shown in Figure 3.9 and a picture of the string run along the bridge deck markings is shown in Figure 3.10. Figure 3.11 shows the truck crossing the bridge during testing.

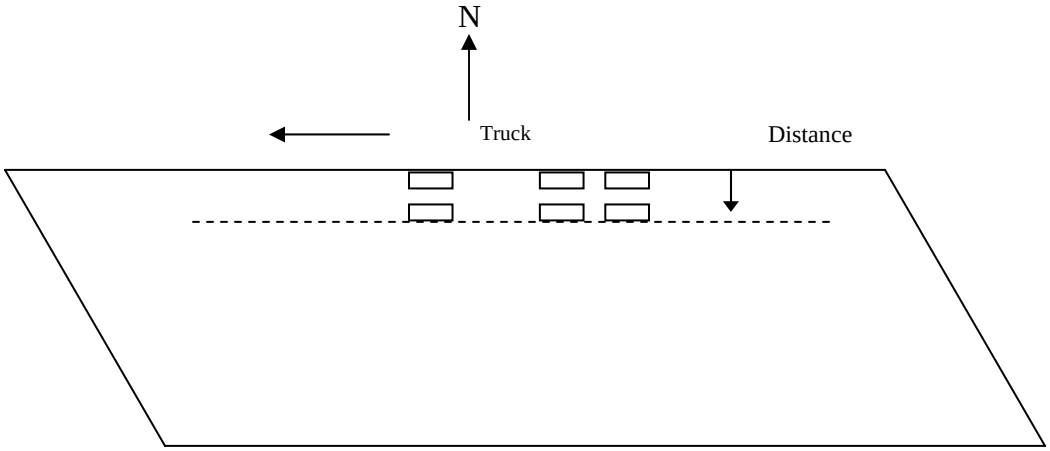

Run	Distance of Outside Edge of Driver Side Tire from Bottom Inside Face of North Parapet
1	8'-0"
2	11'-8 3/4"
3	16'-8 1/4"
4	18'-0"
5	20'-8 1/4"
6	21'-8 3/4"
7	25'-7 3/4"
8	26'-8 1/4"
9	29'-4 1/2"
10	30'-8 1/4"
11	35'-7 3/4"
12	Face of S. Parapet

Figure 3.8 - Positioning of Load Truck for Testing Runs

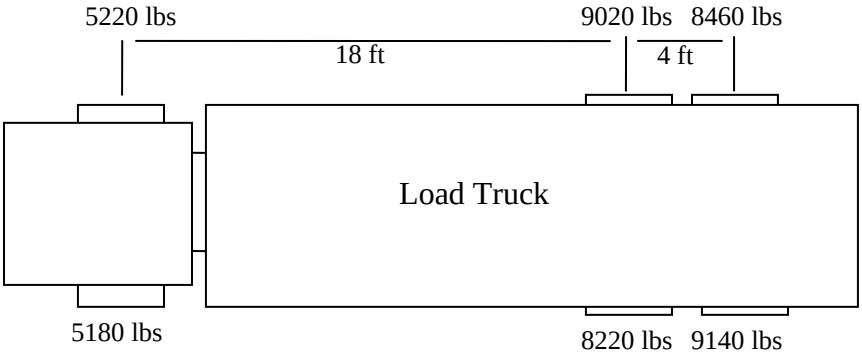

Figure 3.9 - Experimental Load Truck Weight

Figure 3.10 - String along bridge and deck marking

Figure 3.11 - Truck during testing and equipment below the bridge

The truck was driven at crawl speed across the bridge forward and then backed up at the same crawl speed on the same line to show redundancy and closure in the data. An example of the data is shown in Figure 3.12. This data is from a gage on the bottom flange of the north girder in the positive section (P1-1) during Run 1.

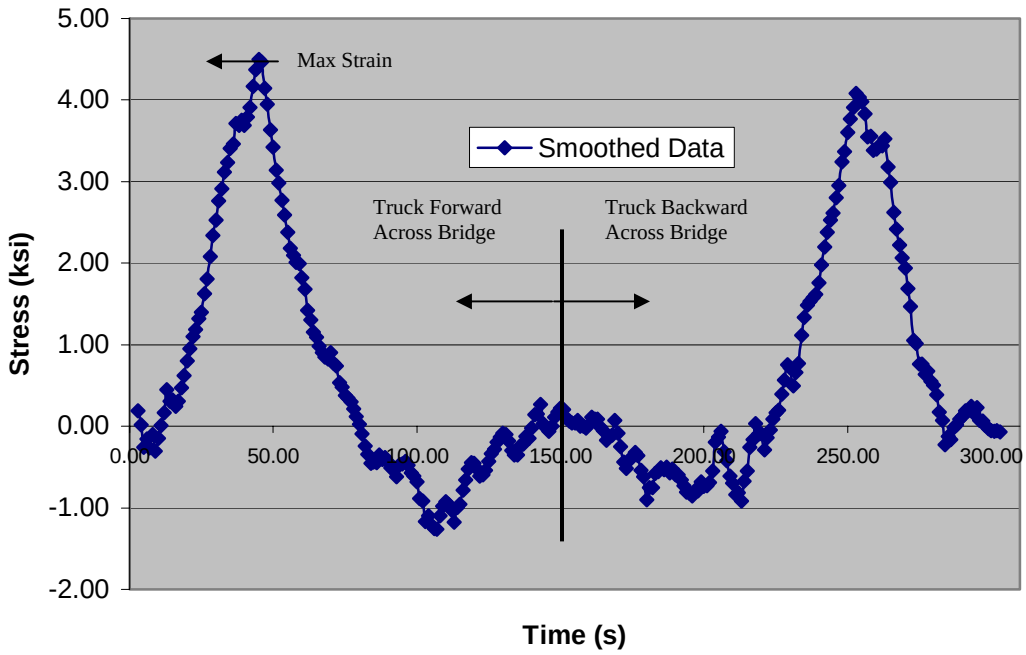

Figure 3.12 - Data from Gage P1-1 (Smoothed)

To determine the maximum measured stress that a girder would obtain according to design procedures, the method of load superposition was used. The method involves superimposing two test runs next to each other (4 ft. between centerline of wheels) on the bridge. For example, the maximum load cases for Girder 3 could either be the combination of Run 3 and 8 <u>or</u> the combination of Run 5 and 10 as shown in Figure 3.13(c). The load combinations for all girders are shown in Figures 3.13(a)-(e).

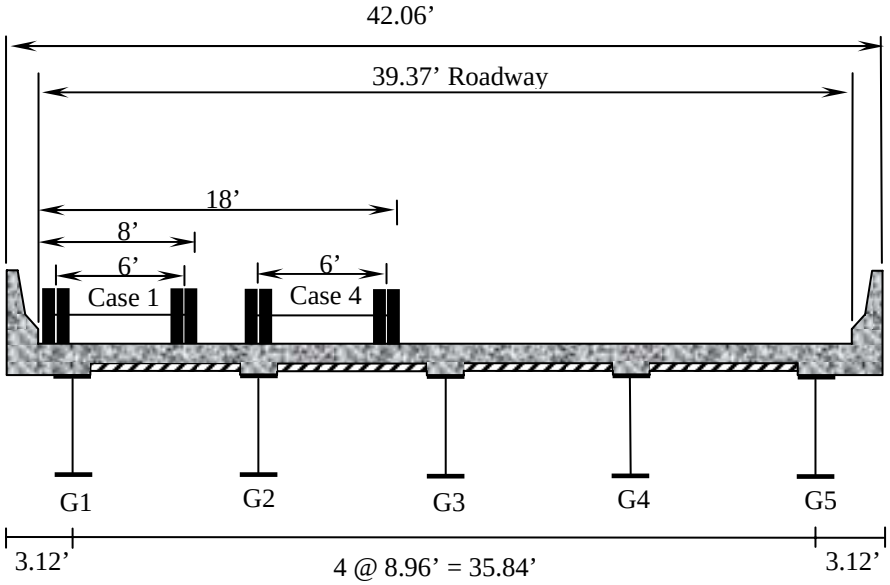

Figure 3.13(a): Maximum load positions for Girder 1 (Load Cases 1 & 4)

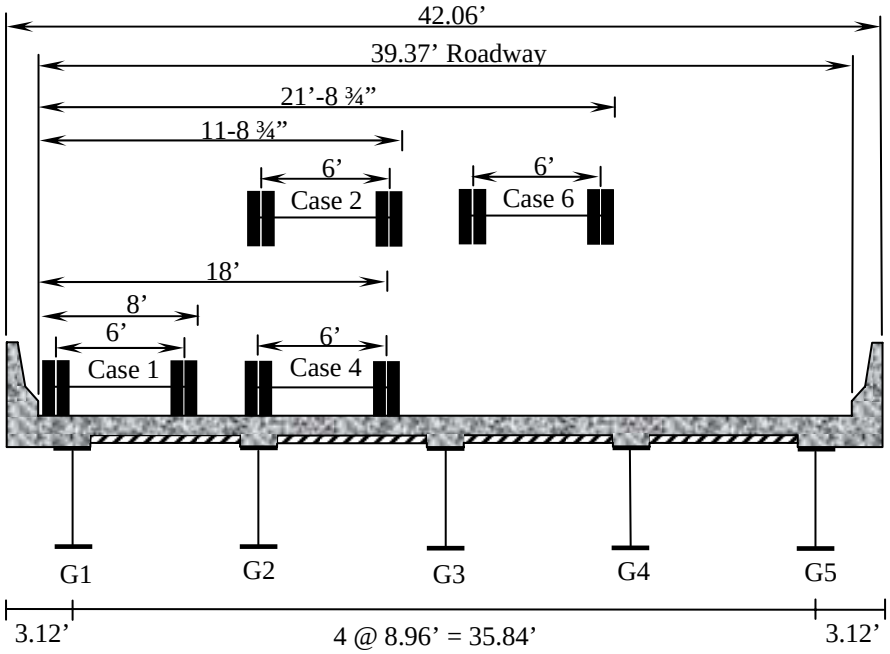

Figure 3.13(b) - Maximum load positions for Girder 2 (Load Cases 1 & 4, Load Cases 2 & 6)

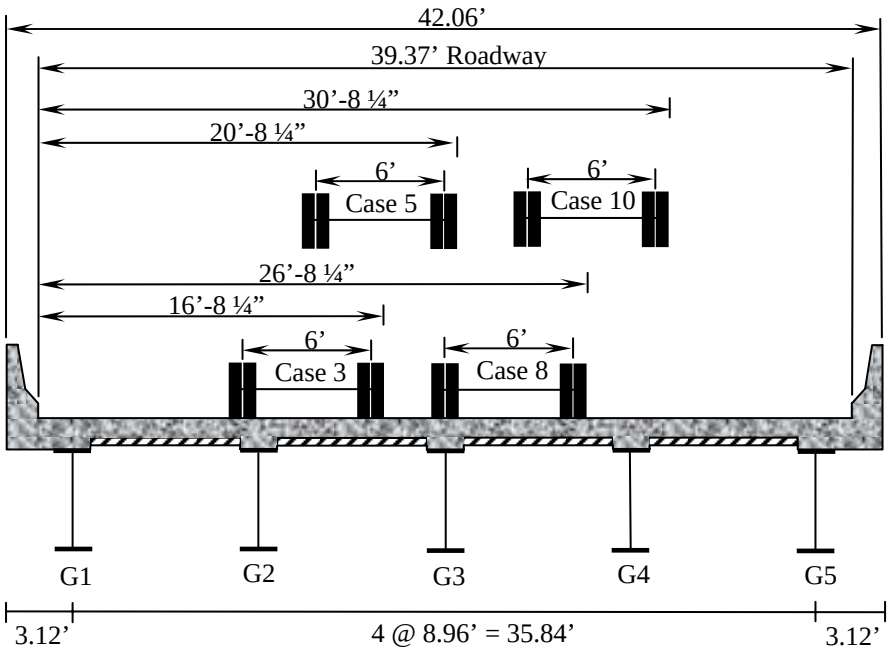

Figure 3.13(c): Maximum load positions for Girder 3 (Load Cases 3 & 8, Load Cases 5 & 10)

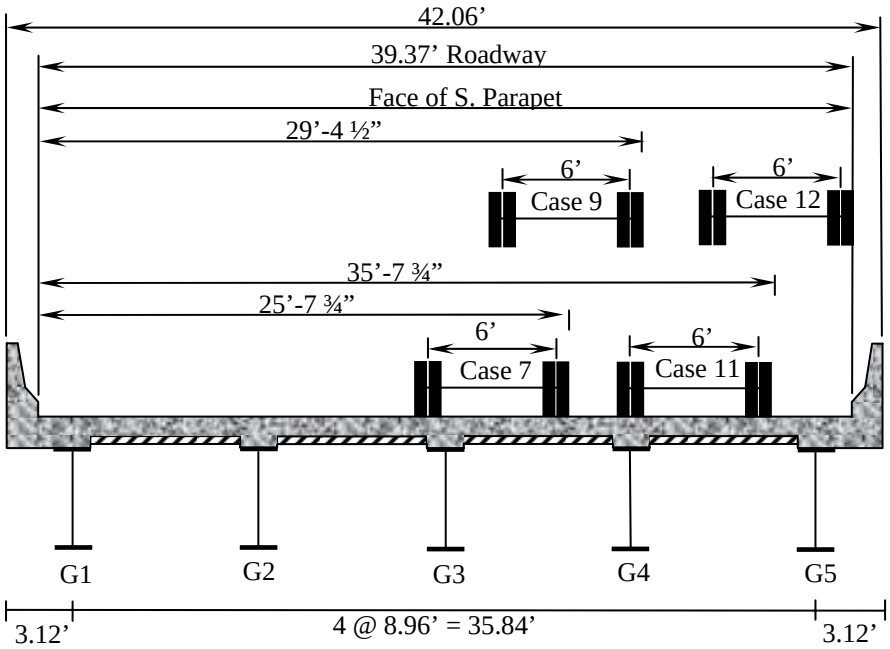

Figure 3.13(d) - Maximum load positions for Girder 4 (Load Cases 9 & 12 Load Cases 7 & 11)

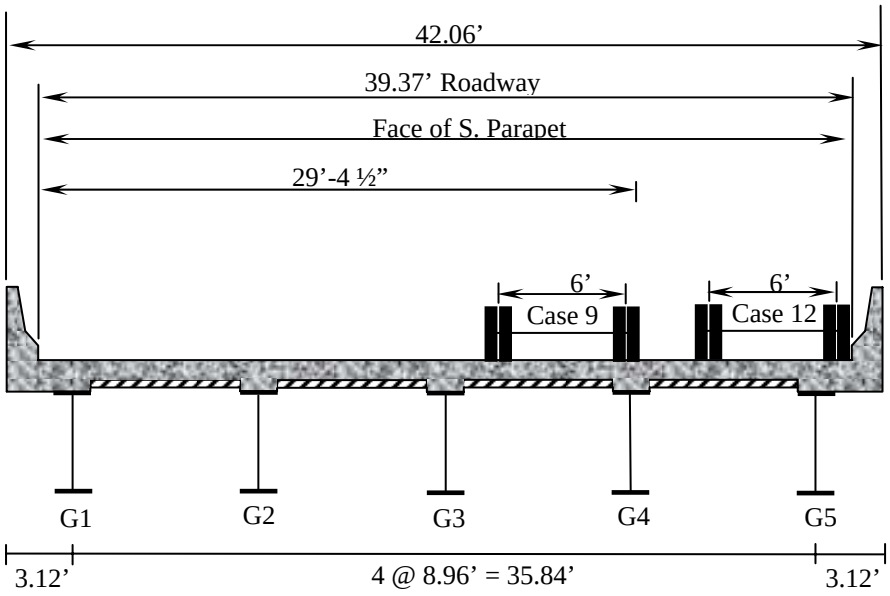

Figure 3.13(e) - Maximum load positions for Girder 5 (Load Cases 9 & 12)

From the data collected and these load combinations, the data reduction process can begin (Oesch, 2003).

3.4 FIELD TEST DATA COLLECTION PLANS

On August 18th, 2002 the University of Missouri – Columbia's Bridge Field Test Team arrived at Bridge A6101 along Route 224 over relocated Route 13. One of the first of several problems encountered by the team was that the road approaching the bridge was not complete. This posed a problem for serviceability tests (accelerations and natural periods) because the load truck would need to reach high speeds. However it was not a problem with the strength testing that was completed. It was decided that the east span would be the best choice for testing because of the cloverleaf ramp that led down to underneath the bridge had been graded and was passable by the RV. A second problem that the team encountered was the fact that the new Route 13 was not completed and

consisted of graded roadway. The weather had been nice for the week leading up to testing, but the first night before instrumentation began, a huge thunderstorm came through the area causing all of the dirt to turn into mud. The center ditch between the east and west spans filled with water as well as the ditch between the east span and the east abutment. The entire west span was unreachable as well as the east abutment. All together it rained two of the three nights during the testing dates.

3.4.1 Test Plan VI (Abandoned)

It was originally planned that Bridge A6101 would be tested using Test Plan VI as described by Frederick, "*Experimental Load Rating of a Slab-on-Steel Girder Bridge*" (1998). Test Plan VI is the most comprehensive testing plan developed by the University of Missouri's Bridge Field Test Team. When used correctly, Test Plan VI can calculate the total moment at all three cross sections that are heavily gaged, the bearing restraint moments at each pier, the elastic moments, the longitudinal moment distribution, and 8 adjustment factors that quantify the difference between the design predicted response and the actual experimental response.

Since A6101 is symmetrical, strain gages would be placed at six different cross sections on the bridge as shown in Figure 3.14.

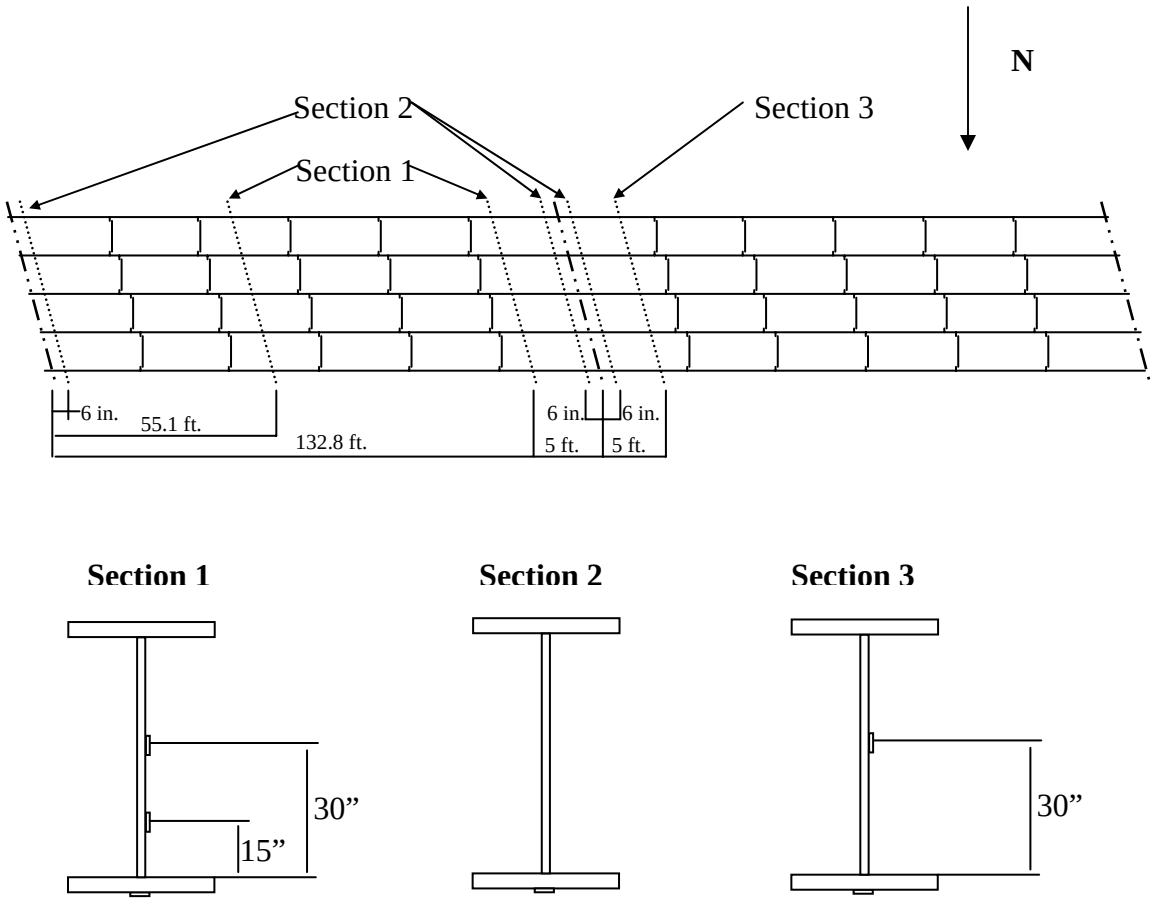

Figure 3.14 - Strain Gage Placement (Test Plan VI)

According to Test Plan VI three gages were to be placed at 55.1 ft from the east abutment in the positive moment region, which is equivalent to 0.4 times the length of the bridge. Gages were to be placed at the midpoint of the bottom flange, at a quarter of the height of the web and at the middle of the web (Figure 3.14, Section 1). Three additional gages were also to be placed at 132.8 ft from the east abutment near the maximum negative region. Gages were to be placed in these positions to produce a stress profile along the girder depth. A typical Section 1 gage placement is shown in Figure 3.15.

Figure 3.15 - Strain Gage Cross Section

The maximum negative moment occurs over the center pier, but gages are placed the height of the girder (5 ft from the interior pier) away from the pier to avoid concentrated load effects. Test Plan VI also involves the placement of gages on each side of the center bearing and east bearing on the bottom flange 6 in. from the bearing to estimate bearing restraint forces (Figure 3.14, Section 2). On the west span, 5 ft from the interior bearing, two gages were placed on each girder- one at the midpoint of the bottom flange and one at the midpoint of the girder to compare redundancy in the negative moment regions (Figure 3.14, Section 3).

3.4.2 Test Plan II (Performed)

After arriving at the site and seeing the field conditions, the team decided that it would not be possible to implement a Test Plan VI. The entire western span was unreachable as well as the eastern abutment due to the mud. It was decided that the placement of the most critical gages would result in enough data to determine bridge

performance to an acceptable level. This gage placement corresponds with a Test Plan II as described by Frederick (1998). This plan still allowed for an experimental verification of the section modulus as well as an accurate experimental total girder moment to be used in the experimental response calculations. However, with this test plan, the axial stress due to bearing restraint cannot be determined. The critical gages were determined to be the three gages on each girder 55.1 ft from the eastern abutment in the positive moment region and the gages 132.8 ft from the eastern abutment in the negative moment region. The bearing gages would not be installed, seeing as they were not considered critical. Each gage is identified by the region, girder, and position that they are located at on the girder, with Girder 1 the northernmost girder and Position 1 the bottom of the flange. For example, P1-3 was the gage in the positive region (55.1 ft from the eastern abutment), on Girder 1, and placed on the midpoint of the web (Davis, 2002). Test Plan II of Bridge A6101 is shown in Figure 3.16.

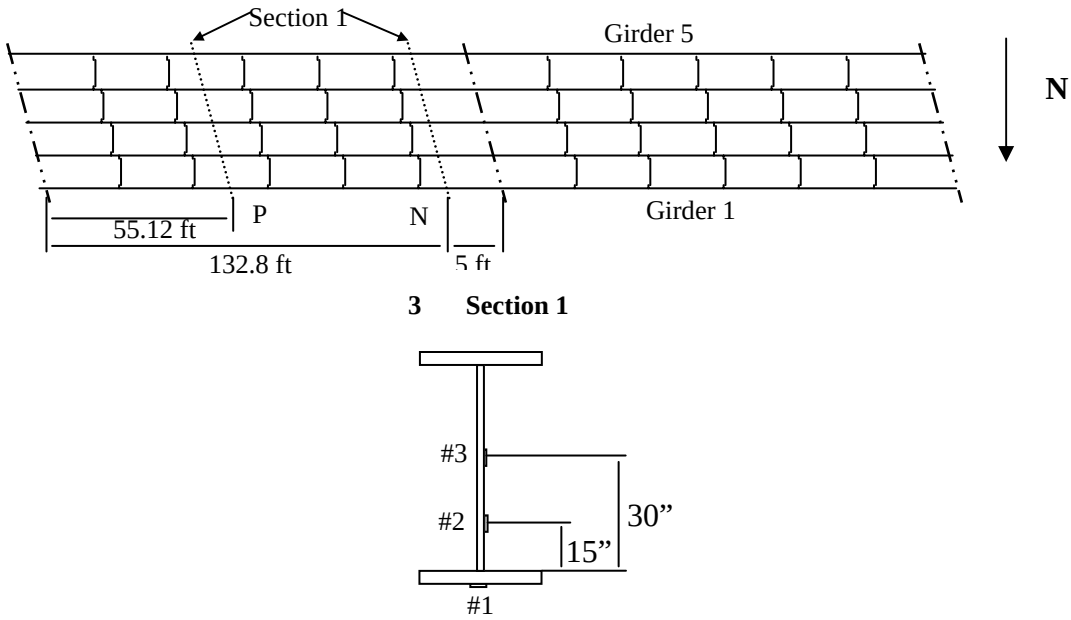

Figure 3.16 - Strain Gage Placement (Test Plan II)

3.5 FIELD TEST DATA REDUCTION

From the strain profiles taken at the critical gage sections, the experimental total moment on the girder can be calculated. The derivation of this procedure can be found in Imhoff (1998). However, using this test plan, the axial stress due to bearing restraint could not be determined and thus has not been removed from this calculation. The process is as follows:

3.5.1 Experimental Stress Profiles

After the experimental stresses have been recorded, the process starts by determining a best-fit stress profile on the girder cross sections. The gages are depicted as follows.

#1 – Bottom Flange

#2 – Quarterpoint of the Web

#3 – Midpoint of the Web

From the maximum stress values obtained during testing, a linear regression can be applied to the data points to calculate a linear strain profile of the section. The linear regression equation was derived by Imhoff (1998) using the least squares analysis as follows:

$$\begin{bmatrix} \Sigma\sigma_i^2 & \Sigma\sigma_i \\ \Sigma\sigma_i & 3 \end{bmatrix} * \begin{Bmatrix} Slope \\ Intercept \end{Bmatrix} = \begin{Bmatrix} \Sigma(\sigma * d_i \\ \Sigma d_i \end{Bmatrix} \tag{3.1}$$

Solving the matrix equation for the slope and the intercept and the writing the equation of the straight line yields:

$$Slope = \frac{3*\Sigma(\sigma_i * d_i) - \Sigma\sigma_i * \Sigma d_i}{3*\Sigma\sigma_i^2 - (\Sigma\sigma_i)^2} \tag{3.2}$$

$$Intercept = \frac{\Sigma(\sigma_i * d_i) - \Sigma\sigma_i^2 * slope}{\Sigma\sigma_i} \tag{3.3}$$

$$d = Slope * \sigma + Intercept \tag{3.4}$$

$$\sigma = \frac{1}{Slope} * d - \frac{Intercept}{Slope} \tag{3.5}$$

where,

Intercept = Neutral Axis from Bottom of Bottom Flange (in),

Slope = Slope of the Stress Profile (in/ksi),

d = Depth from Bottom of Bottom Flange (in), and

σ = Stress in Girder (ksi).

Figure 3.17 shows the maximum predicted design and equivalent experimental stress profiles along the girder for the positive moment region of Girder 4 using best fit line.

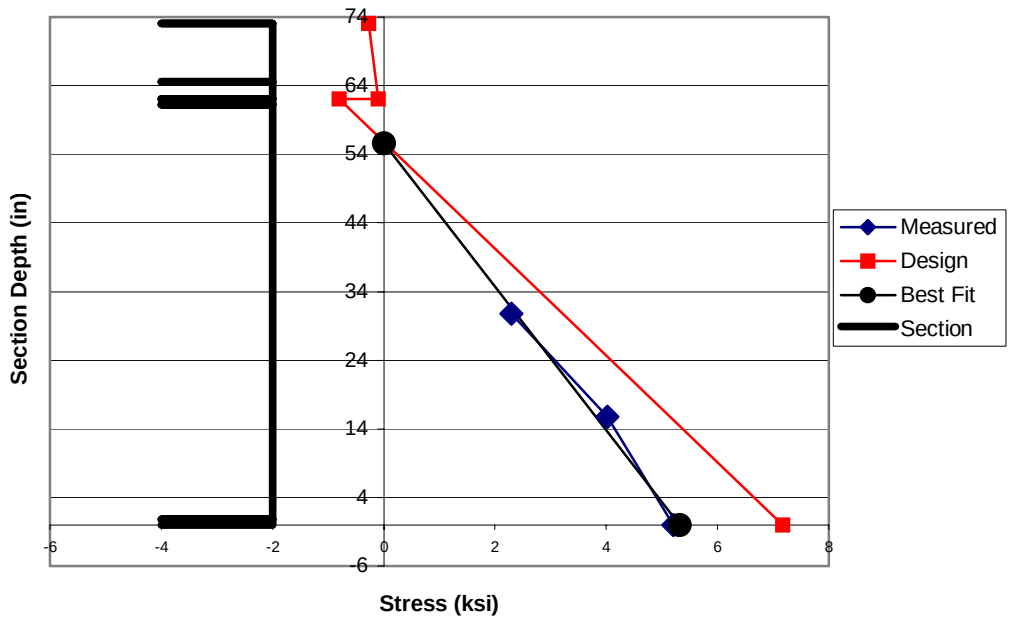

Figure 3.17 - Stress profiles along Girder 4 in the maximum positive moment region

From the equation for stress (σ), calculating the stresses at the bottom for the bottom flange and at the centroid (assumed to be at the center of gravity (CG)) of the girder yields:

$$\sigma_O = -\frac{Intercept}{Slope} \tag{3.6}$$

$$CG = \frac{\sum Area * y}{\sum Area} \tag{3.7}$$

$$\sigma_{CG} = \frac{CG - Intercept}{Slope} \tag{3.8}$$

where,

σ_o = Stress at the bottom of the bottom flange (ksi),

σ_{CG} = Stress at the centroid of the steel girder (ksi),

CG = Center of Gravity of steel girder (in),

y = Distance to centroid of steel member (in).

3.5.2 Girder Total Experimental Moment, M_T

The total moment is calculated by breaking the load carrying mechanisms into three parts (Bakht, 1988). One part is the steel girder bending about its own neutral axis, M_L. The second part is the concrete area bending about its own neutral axis, M_U. The third component is a couple that is a function of the amount of composite action between the concrete area and the steel section, Na. Figure 3.18 shows how the experimental stresses are transformed into the three components described above.

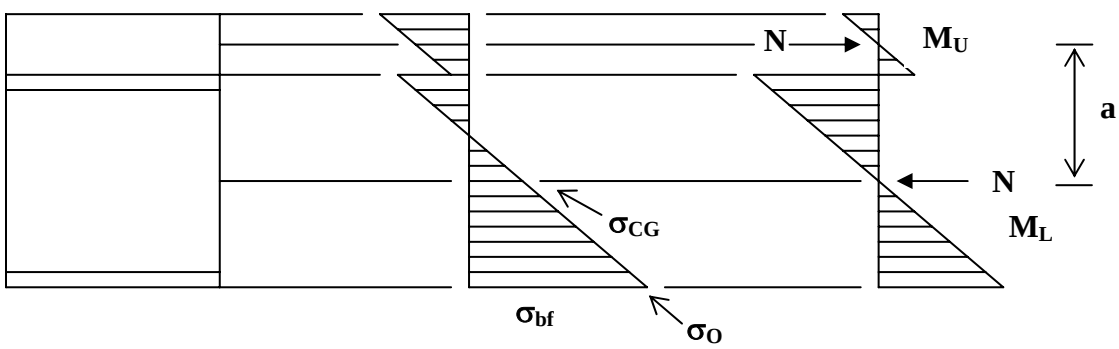

Figure 3.18 - Total Moment

The respective moment components can be calculated by:

$$S_{STL}^{ADIM} = \frac{I_{STL}^{ADIM}}{CG} \tag{3.9}$$

$$M_L = (\sigma_O - \sigma_{CG}) S_{STL}^{ADIM} \tag{3.10}$$

$$Na = \sigma_{\mathrm{CG}} A_{STL}^{ADIM} \left[\left(d_{STL}^{ADIM} - CG \right) + haunch^{ADIM} + \frac{d_{SLAB}}{2} \right] \tag{3.11}$$

$$M_U = \left[\frac{E_{SLAB} I_{SLAB}}{E_{STL} I_{STL}^{ADIM}} \right] M_L \tag{3.12}$$

$$M_{TOTAL} = M_L + Na + M_U \tag{3.13}$$

where,

S_{STL}^{ADIM} = Section Modulus of the steel using measured dimensions (in^3),

A_{STL}^{ADIM} = Area of steel girder using measured dimensions (in^2),

d_{STL}^{ADIM} = Depth of steel girder using measured dimensions (in),

$haunch^{ADIM}$ = Depth of haunch using measured dimensions (in),

d_{SLAB} = Depth of concrete slab (in),

E_{SLAB} = Modulus of Elasticity of Concrete Slab (ksi),

I_{SLAB} = Moment of Inertia of Concrete Slab (in^4),

E_{STL} = Modulus of Elasticity of Steel (ksi), and

I_{STL}^{ADIM} = Moment of Inertia of Steel using measured dimensions (in^4).

This system of calculating the total experimental moment is important because it provides a convenient method of dealing with a unintentional or partially composite section. The reduction of moment into the three components previously described can help quantify the amount of composite action for that member. Additional composite action can be attributed to the curbs and barriers, especially in the exterior girders.

3.5.3 Experimental Section Modulus, S_E

Finding the experimental moment of inertia and then dividing that by the intercept of the stress equation found earlier can determine the experimental section modulus.

$$I_E = -(M_T) * Slope \tag{3.14}$$

$$S_E = \frac{I_{EXP}}{Intercept} \tag{3.15}$$

where,

I_E = Experimental Moment of Inertia (in^4),

S_E = Experimental Section Modulus (in^3).

3.6 EXPERIMENTAL AND DESIGN LOAD CAPACITIES

Using these factors, coupled with analysis, the experimental and design load capacities can be determined. MoDOT uses an HS20 design truck for their bridge designs. The analytical and experimental bridge capacities can be represented using rating factors, which are the number of HS20 trucks that can be put on the bridge according to design limits. An HS20 truck weighs 72,000 lb. For instance, if a rating factor of 1.5 is found, the design capacity of the bridge is 1.5*72,000 lb. This would give the result that the load rating capacity for the girder would be 108,000 lb or and HS30 (1.5*20). Figure 2.19 shows the axle spacing and loadings for an HS20 design truck.

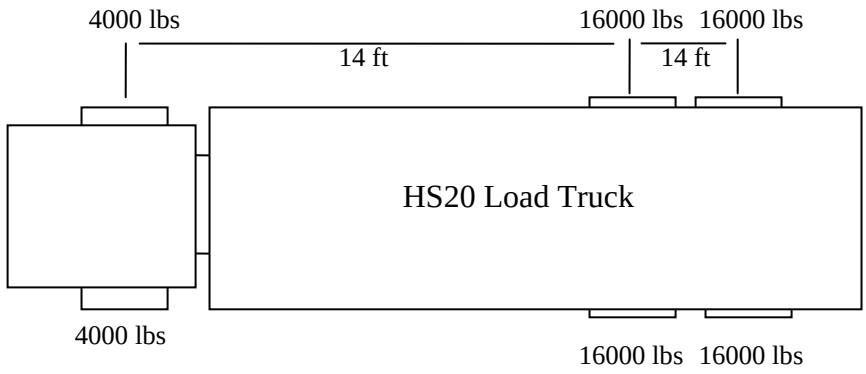

Figure 3.19 - HS20 Load Truck

Equations were developed to determine the critical experimental capacities from the experimental data based on analytical design criteria. This requires adjusting the experimental data with analytical data. For instance, the experimental data may be increased due to the fact that the maximum analytical moment is located a distance from the strain gage. Thus, the experimental data is increased by the ratio of the maximum analytical moment to the gage location analytical moment. SIMON (1996) Version 8.10b, developed by the American Institute of Steel Construction, Inc, software was used for the analytical response. To determine analytical moments, MoDOT, when designing A6101, also used the SIMON software.

First the nominal design dimensions using the design HS20 vehicle were run through SIMON to determine the analytical moments and hybrid reduction factors for an interior and exterior girder. Then the actual measured dimensions were run through SIMON using both the design HS20 truck as well as the actual test truck for an interior and exterior girder. Waypoint sections were put into SIMON at the position of the test gages so that SIMON would output moments at these positions (55.1 ft and 132.8 ft).

SIMON develops moment envelopes but cannot give a moment when a truck is at a certain position. SIMON, however, does give moment influence line diagrams, which were used to find the position of the truck that causes the maximum negative moment and the corresponding positive moment. The maximum positive moment, however, is when the center axle of the truck is directly over the gage (Davis, 2003).

The following design experimental capacity equations are based on Barker et al (1999). However, this past work only developed equations for bridges designed by AASHTO Allowable Stress Design (ASD). Therefore, since Bridge A6101 was designed using Load Factor Design (LFD), the following derives the required design and experimental capacity rating equations for LFD (Davis, 2003).

3.6.1 AASHTO LFD Design Capacity

The Design Rating Factor for an HS20 truck can be defined by the equation:

$$RF_{Design}^{HS20} = \frac{\dfrac{R_{Design}F_y}{1.3} - \left(\dfrac{M_{D_{NC}}^{HS20-MAX-ADIM}}{S^{Design}} + \dfrac{M_{D_C}^{HS20-MAX-ADIM}}{S_{3n}^{Design}} \right)}{\dfrac{5}{3}\left(\dfrac{M_{L+I}^{HS20-MAX-ADIM}}{S_n^{Design}} \right)} \qquad (3.16)$$

where,

R_{Design} = Hybrid Reduction factor using Design Dimensions,

F_y = Yield Strength of Steel (ksi),

$M_{D_{NC}}^{HS20-MAX-ADIM}$ = Dead load Non-composite moment caused by an HS20 truck using measured dimensions (k-ft),

S^{Design} = Section Modulus of girder using design dimensions (in^3),

S_n^{Design} = Short Term Section Modulus of girder plus (1/n) of the slab (in^3),

S_{3n}^{Design} = Long Term Section Modulus of girder plus (1/3n) of the slab (in^3),

$M_{D_C}^{HS20-MAX-ADIM}$ = Dead load composite moment caused by an HS20 truck using measured dimensions (k-ft),

$M_{L+I}^{HS20-MAX-ADIM}$ = Live load plus Impact moment caused by an HS20 truck using measured dimensions (k-ft).

The rating factor is the number of HS20 trucks that can be placed on the bridge and meet the design requirements.

Although design dimension are used for the section properties, actual or measured dimensions were used for the dead and composite dead load moments. This is slightly conservative, but is helpful when comparing the analytical design capacity to the experimental capacity and the effect is minimal.

To develop the experimental capacity rating, Equation 3.16 is modified for the experimental parameters. In other words, the test truck moments at the gage locations are analytically adjusted to match equivalent HS20 moments (Barker, et al, 1999):

$$RF_{Design}^{TRK} = \frac{\frac{R_{Design}F_y}{1.3} - \left(\frac{M_{D_{NC}}^{TRK-GAGE-ADIM}}{S^{Design}} \left\{ \frac{M_{D_{NC}}^{HS20-MAX-ADIM}}{M_{D_{NC}}^{TRK-GAGE-ADIM}} \right\} + \frac{M_{D_C}^{TRK-GAGE-ADIM}}{S_{3n}^{Design}} \left\{ \frac{M_{D_C}^{HS20-MAX-ADIM}}{M_{D_C}^{TRK-GAGE-ADIM}} \right\} \right)}{\frac{5}{3}\left(\frac{M_{L+I}^{TRK-GAGE-ADIM}}{S_n^{Design}} \right) \left\{ \frac{M_{L+I}^{HS20-MAX-ADIM}}{M_{L+I}^{TRK-GAGE-ADIM}} \right\}} \quad (3.17)$$

where,

$M_{D_{NC}}^{TRK-GAGE-ADIM}$ = Non-composite dead load moment caused by the test truck at the gages using measured dimensions (k-ft),

$M_{L+I}^{TRK-GAGE-ADIM}$ = Live load plus Impact moment caused by an HS20 truck using measured dimensions at the gage (k-ft),

$M_{D_C}^{TRK-GAGE-ADIM}$ = Composite dead load moment caused by the test truck at the gage using measured dimensions (k-ft),

The design-rating factor for the test truck will be the same as the design-rating factor for an HS20 because moments cancel out. The equation simplifies as follows:

$$RF_{Design}^{TRK} = \frac{\frac{R_{Design}F_y}{1.3} - \left(\frac{\cancel{M_{D_{NC}}^{TRK-GAGE-ADIM}}}{S^{Design}} \left\{ \frac{M_{D_{NC}}^{HS20-MAX-ADIM}}{\cancel{M_{D_{NC}}^{TRK-GAGE-ADIM}}} \right\} + \frac{\cancel{M_{D_C}^{TRK-GAGE-ADIM}}}{S_{3n}^{Design}} \left\{ \frac{M_{D_C}^{HS20-MAX-ADIM}}{\cancel{M_{D_C}^{TRK-GAGE-ADIM}}} \right\} \right)}{\frac{5}{3}\left(\frac{\cancel{M_{L+I}^{TRK-GAGE-ADIM}}}{S_n^{Design}} \right) \left\{ \frac{M_{L+I}^{HS20-MAX-ADIM}}{\cancel{M_{L+I}^{TRK-GAGE-ADIM}}} \right\}} \tag{3.18}$$

Resulting in:

$$RF_{Design}^{TRK} = \frac{\frac{R_{Design}F_y}{1.3} - \left(\frac{M_{D_{NC}}^{HS20-MAX-ADIM}}{S^{Design}} + \frac{M_{D_C}^{HS20-MAX-ADIM}}{S_{3n}^{Design}} \right)}{\frac{5}{3}\left(\frac{M_{L+I}^{HS20-MAX-ADIM}}{S_n^{Design}} \right)} \tag{3.19}$$

which is the same as Equation 3.16. The need to demonstrate Equation 3.16 to 3.19 is to move forward with the experimental capacity equation. The measured stresses can be used to find an equivalent HS20 experimental rating factor using the adjustments illustrated.

3.6.2 Experimental Capacity

The Experimental Rating Factor is determined by:

$$RF_{EXP}^{TRK} = \frac{\frac{R_{EXP}F_y}{1.3} - \left(\frac{M_{D_{NC}}^{TRK-GAGE-ADIM}}{S^{ADIM}} \left\{ \frac{M_{D_{NC}}^{HS20-MAX-ADIM}}{M_{D_{NC}}^{TRK-GAGE-ADIM}} \right\} + \frac{M_{D_C}^{TRK-GAGE-ADIM}}{S_{3n}^{ADIM}} \left\{ \frac{M_{D_C}^{HS20-MAX-ADIM}}{M_{D_C}^{TRK-GAGE-ADIM}} \right\} \right)}{\frac{5}{3}\sigma_O(1+I_E)\left\{ \frac{M_{L+I}^{HS20-MAX-ADIM}}{M_{L+I}^{TRK-GAGE-ADIM}} \right\}} \tag{3.20}$$

where,

R_{EXP} = Hybrid Reduction Factor for an HS20 truck using measured dimensions,

σ_O = Experimental Stress in bottom flange of girder using best fit line (ksi),

I_E = Experimental Impact Factor.

The experimental rating factor is consistent with the design procedures (Equation 3.17), but actual measured section properties are used along with the maximum measured stress at the bottom flange. This maximum stress is the superposition of the critical truck runs described in Section 3.3.

Impact needs to be put into the bottom flange stress because the tests are conducted at crawl speeds and it is assumed the experimental impact is the same as that used for the original design. Impact is calculated by AASHTO using the equation:

$$I_A = \frac{50}{125 + SpanLength} \tag{3.21}$$

3.6.3 Performance Comparison

The Design Load Rating Factor will not be the same as the Experimental Load Rating Factor. The difference between these can be defined by eight different factor adjustments: Dead Load Stress Adjustment, Lateral Distribution Factor Adjustment, Impact Factor Adjustment, Bearing Restraint Adjustment, Longitudinal Distribution Adjustment, Section Modulus Adjustment, Additional or Unintended Composite Action Adjustment, and Curb / Railing / Skew Adjustment (Barker et al 1999). From these factors, the difference between the experimental load factor capacity and the design load factor capacity is explained. These factors are found by dividing the experimental rating factor by the design rating factor. Using that σ_O is equal to the total moment divided by experimental section modulus calculated in Section 3.5.3, the following generalized equation relates the experimental and design capacities:

$$\frac{RF_{EXP}^{TRK}}{RF_{Design}^{TRK}} = \left(\frac{\frac{R_{EXP}F_y}{1.3} - \left(\frac{M_{D_{NC}}^{HS20-MAX-ADIM}}{S^{ADIM}} + \frac{M_{D_C}^{HS20-MAX-ADIM}}{S_{3n}^{ADIM}} \right)}{\frac{R_{Design}F_y}{1.3} - \left(\frac{M_{D_{NC}}^{HS20-MAX-ADIM}}{S^{Design}} + \frac{M_{D_C}^{HS20-MAX-ADIM}}{S_{3n}^{Design}} \right)} \right) * \left(\frac{DF_A}{DF_E} \right) * \left(\frac{1+I_A}{1+I_E} \right)$$

$$* \left(\frac{M_E}{M_T} \right) * \left(\frac{M_{LE}}{M_E} \right) * \left(\frac{S_n^{ADIM}}{S_n^{Design}} \right) * \left(\frac{S_E}{S_n^{ADIM}} \right) * \left(\frac{M_{WHL-Line}^{HS20-MAX-ADIM}}{\frac{M_{LE}}{DF_E} * \frac{M_{L+I}^{HS20-MAX-ADIM}}{M_{L+I}^{TRK-MAX-ADIM}}} \right) \tag{3.22}$$

The difference between the design and the experimental capacity is the product of 8 adjustment factors. Each term in Equation 3.22 represents an adjustment that qualitatively and quantitatively defines the difference between the design and experimental response. These adjustment factors are:

$$\text{(1) Dead Load Stress Adjustment} = \frac{\frac{R_{EXP}F_y}{1.3} - \left(\frac{M_{D_{NC}}^{HS20-MAX-ADIM}}{S^{ADIM}} + \frac{M_{D_C}^{HS20-MAX-ADIM}}{S_{3n}^{ADIM}} \right)}{\frac{R_{Design}F_y}{1.3} - \left(\frac{M_{D_{NC}}^{HS20-MAX-ADIM}}{S^{Design}} + \frac{M_{D_C}^{HS20-MAX-ADIM}}{S_{3n}^{Design}} \right)} \tag{3.23}$$

$$\text{(2) Distribution Factor Adjustment} = \left(\frac{DF_A}{DF_E} \right) \tag{3.24}$$

$$\text{(3) Impact Factor Adjustment} = \left(\frac{1+I_A}{1+I_E} \right) \tag{3.25}$$

$$\text{(4) Bearing Restraint Adjustment} = \left(\frac{M_E}{M_T} \right) \tag{3.26}$$

$$\text{(5) Longitudinal Distribution Adjustment} = \left(\frac{M_{LE}}{M_E} \right) \tag{3.27}$$

$$\text{(6) Section Modulus Adjustment} = \left(\frac{S_n^{ADIM}}{S_n^{Design}} \right) \tag{3.28}$$

$$(7)\ \text{Additional or Unintended Composite Action Adjustment} = \left(\frac{S_E}{S_n^{ADIM}} \right) \tag{3.29}$$

$$(8)\ \text{Curb / Railing / Skew Adjustment} = \left(\frac{M_{WHL-Line}^{HS20\text{-}MAX-ADIM}}{\frac{M_{LE}}{DF_E} * \frac{M_{L+I}^{HS20-MAX-ADIM}}{M_{L+I}^{TRK-MAX-ADIM}}} \right) \tag{3.30}$$

where,

F_y = Yield Stress of Structural Steel (ksi),

R_{EXP} = Experimental Hybrid Reduction Factor,

R_{Design} = Design Hybrid Reduction Factor,

I_E = Experimental Impact Factor,

DF_A = Analytical Distribution Factor,

DF_E = Experimental Distribution Factor,

M_E = Experimental Elastic Moment with Bearing Restraint Effects Removed (k-ft),

M_T = Experimental Total Moment (k-ft),

$M_{WHL-Line}^{HS20\text{-}MAX-ADIM}$ = Analytical Wheel Line Moment for RVW Truck (k-ft),

M_{LE} = Experimental Elastic Moment Adjusted for Longitudinal Distribution (k-ft),

S_n^{ADIM} = Analytical Section Modulus with Actual Measured Dimensions (in^3),

S_E = Experimental Section Modulus (in^3).

These adjustment factors describe the difference between the design capacity and the experimental capacity and show the source of additional capacity or reduced capacity of the structure. For a full description of these factors the reader is directed to “Experimental

Load Rating of a Slab-on-Steel Girder Bridge" (Frederick, 1998). A brief description is also presented in the example calculations.

3.7 DATA, STRESSES AND MAXIMUM BRIDGE RESPONSE

The raw data collected by the strain gages consisted of hundreds of lines of an Excel spreadsheet. For each gage the data was collected relative to time since, as the truck drove across the bridge and back, the purpose was to locate maximum response. The first process in the reduction was a smoothing of the data. This was done by taking a running average of the data, which is 0.6 times the data at the specific time point plus 0.2 times the data at time point above it plus 0.2 times the data at the time point below it. This procedure has a smoothing effect on the data and takes out some of the noise that might be caused by vibrations and electrical noise. A comparison of the original raw data and data smoothed once is shown in Figures 3.20 (a-b). The data comes from the gage at the bottom flange of Girder 1 using Test Run 1 (Gage P1-1).

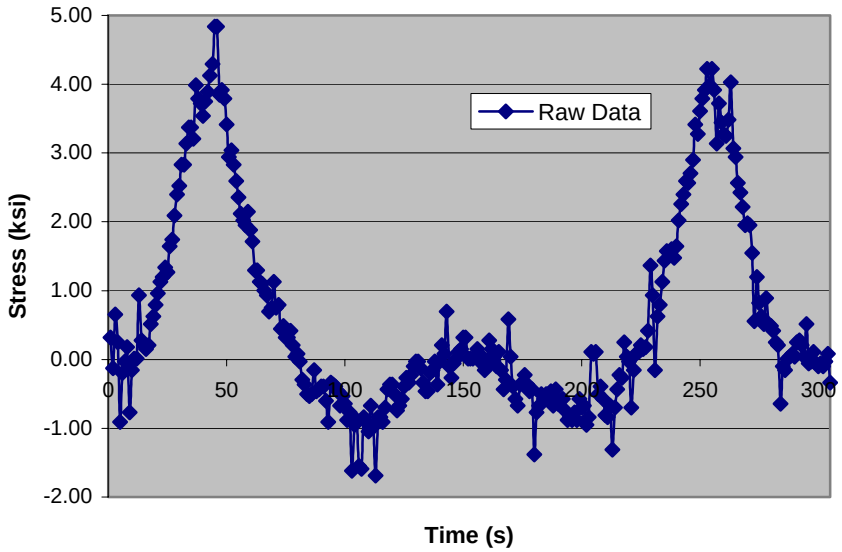

Figure 3.20 (a) - Raw Data (Not Smoothed) (Gage P1-1)

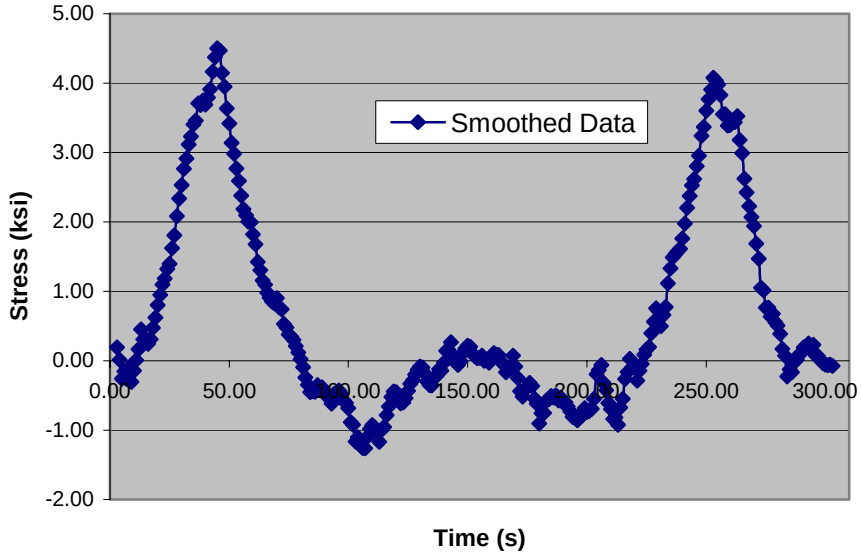

Figure 3.20 (b): Raw Data (Smoothed) (Gage P1-1)

On the plot, distinct peaks show where moments are maximized. From this smoothed data, the maximum stresses in the girders can be found for each run. In the data, the maximum stress is found for the girder that is being examined and all of the stresses for the other four girders are collected at the same time point. For a given truck run, this represents the stresses for the maximum moment in this particular girder and corresponding stresses and, thus, moments for all the other gaged sections. In other words, the set of stresses represents the equilibrium response of the system when the one particular girder is maximized. Superposition of truck run sets of maximums are used to model two side-by-side trucks on the bridge. The load combinations that maximize each girder in the positive and negative are shown in Table 3.1.

Table 3.1: Maximum Run Combinations

Girder	Run Combinations to cause Maximum Positive Moments	Run Combinations to cause Maximum Negative Moments
1	1+4	1+4
2	1+4	1+4
3	3+8	3+8
4	9+12	9+12
5	9+12	9+12

Table 3.2 shows the maximum stresses for individual load runs and superposition of the critical runs that maximize an individual girder and the corresponding stresses for all other girders. For instance, Girder 4 is maximized by superposition of Runs 9 and 12. The other stresses shown in Girders 1, 2, 3 and 5 for positive and negative moment regions are the corresponding stresses when Girder 4 is maximized. Thus, the Girder 4 stress set represents the bridge response from two side-by-side trucks in a single position. Equilibrium is applicable. Table 3.3 shows an analogous set of stresses for maximum negative moments in each girder and corresponding stresses at all other sections. Gage positions are the locations of the gages on the girders corresponding to Test Plan II described in Figure 3.16.

Table 3.2 – Girder Stresses When Truck at Maximum Positive Position

Girder 1		Maximum Positive Stress (ksi) Girder #					Correlating Negative Stress (ksi) Girder #				
Run #	Gage Pos.	1	2	3	4	5	1	2	3	4	5
1	1	4.50	2.56	1.12	0.40	-0.24	-1.31	-0.81	-0.40	-0.02	0.22
	2	3.71	2.23	0.76	0.22	-0.21	-1.39	-0.29	-0.40	0.01	0.14
	3	2.25	1.54	0.08	-0.12	-0.21	-0.89	-0.15	-0.55	-0.62	0.00
4	1	1.96	2.37	1.81	1.20	0.49	-0.61	-0.63	-0.65	-0.54	-0.23
	2	2.15	2.38	1.16	0.88	0.41	-0.75	-0.52	-0.54	0.03	0.011851
	3	1.22	1.43	0.23	0.38	0.35	-0.39	-0.21	0.27	1.00	-0.05205
Run 1+4	1	6.46	4.93	2.93	1.60	0.24	-1.93	-1.43	-1.05	-0.56	0.00
	2	5.86	4.61	1.91	1.10	0.21	-2.14	-0.81	-0.93	0.04	0.16
	3	3.48	2.97	0.31	0.26	0.14	-1.28	-0.36	-0.29	0.39	-0.05
Girder 2											
1	1	4.17	2.67	1.09	0.47	-0.22	-1.28	-0.77	-0.45	0.00	0.21
	2	3.61	2.30	0.71	0.25	-0.20	-1.36	-0.34	-0.41	-0.01	0.11
	3	2.32	1.63	0.02	0.00	-0.18	-0.89	-0.17	-0.51	-0.31	0.04
4	1	1.88	2.48	2.03	1.19	0.61	-0.62	-0.60	-0.64	-0.52	-0.22
	2	1.99	2.40	1.23	0.82	0.42	-0.72	-0.49	-0.53	0.02	-0.05
	3	1.21	1.49	0.17	0.36	0.16	-0.40	-0.21	0.21	1.18	-0.05
Run 1+4	1	6.05	5.15	3.12	1.65	0.39	-1.90	-1.37	-1.09	-0.52	-0.01
	2	5.60	4.70	1.94	1.06	0.21	-2.08	-0.83	-0.93	0.01	0.06
	3	3.52	3.12	0.19	0.36	-0.02	-1.29	-0.38	-0.30	0.87	-0.01
Girder 3											
3	1	2.23	2.48	2.02	0.96	0.36	-0.70	-0.64	-0.54	-0.43	-0.04
	2	2.07	2.26	1.10	0.80	0.25	-0.72	-0.31	-0.47	0.06	-0.09
	3	1.24	1.41	0.11	0.28	0.11	-0.50	-0.16	-0.30	0.57	0.02
8	1	1.11	1.43	2.24	2.10	1.64	-0.24	-0.53	-0.67	-0.72	-0.56
	2	0.91	1.20	1.28	1.69	1.15	-0.31	-0.12	-0.51	0.08	-0.32
	3	0.53	0.93	0.26	0.92	0.53	-0.17	-0.13	-0.59	-0.37	-0.15
Run 3+8	1	3.34	3.91	4.26	3.06	2.00	-0.94	-1.17	-1.21	-1.15	-0.60
	2	2.98	3.46	2.38	2.49	1.40	-1.03	-0.43	-0.99	0.14	-0.40
	3	1.77	2.34	0.37	1.20	0.65	-0.67	-0.29	-0.89	0.19	-0.13
Girder 4											
9	1	0.85	1.08	1.99	2.54	1.99	-0.14	-0.35	-0.61	-0.85	-0.74
	2	0.54	1.07	1.05	1.91	1.37	-0.16	-0.15	-0.50	0.08	-0.37
	3	0.43	0.69	0.09	1.15	0.62	-0.11	-0.09	-0.15	0.03	-0.18
12	1	-0.10	0.47	1.34	2.70	4.01	0.08	-0.09	-0.38	-0.85	-1.44
	2	-0.21	0.35	0.62	2.20	2.86	0.10	0.03	-0.27	0.15	-0.94
	3	-0.23	0.22	0.08	1.18	1.36	0.06	-0.02	-0.04	0.20	-0.35
Run 9+12	1	0.75	1.55	3.33	5.24	6.00	-0.06	-0.44	-0.99	-1.69	-2.18
	2	0.33	1.42	1.67	4.11	4.24	-0.06	-0.12	-0.77	0.23	-1.31
	3	0.19	0.91	0.18	2.32	1.98	-0.05	-0.12	-0.19	0.23	-0.52
Girder 5											
9	1	0.56	1.11	1.62	2.05	2.08	-0.17	-0.35	-0.46	-0.75	-0.60
	2	0.50	0.99	0.80	1.57	1.45	-0.14	-0.14	-0.42	0.09	-0.48
	3	0.47	0.54	0.01	0.91	0.70	-0.10	-0.11	-0.25	-0.10	-0.15
12	1	-0.24	0.44	1.39	2.66	4.12	0.05	-0.04	-0.36	-0.78	-1.44
	2	-0.24	0.33	0.65	2.11	2.95	0.11	-0.01	-0.28	-0.02	-0.98
	3	-0.16	0.22	0.07	1.14	1.41	0.05	-0.04	0.02	0.41	-0.30
Run 9+12	1	0.31	1.55	3.01	4.71	6.20	-0.12	-0.39	-0.82	-1.53	-2.04
	2	0.26	1.31	1.46	3.68	4.40	-0.03	-0.15	-0.70	0.07	-1.46
	3	0.31	0.76	0.08	2.05	2.11	-0.06	-0.15	-0.23	0.30	-0.44

Table 3.3 – Girder Stresses When Truck at Maximum Negative Position

Girder 1		Correlating Positive Stress (ksi) Girder #					Minimum Negative Stress (ksi) Girder #				
Run #	Gage Pos.	1	2	3	4	5	1	2	3	4	5
1	1	3.42	2.00	1.05	0.31	-0.17	-1.35	-0.83	-0.46	-0.05	0.16
	2	2.95	1.88	0.70	0.21	-0.24	-1.44	-0.43	-0.33	-0.01	0.14
	3	1.92	1.22	-0.09	0.30	-0.18	-0.85	-0.18	-0.21	-0.04	0.01
4	1	1.65	1.68	1.32	0.99	0.71	-0.67	-0.66	-0.69	-0.53	-0.14
	2	1.78	1.87	0.83	0.60	0.46	-0.69	-0.52	-0.53	0.01	-0.07
	3	1.16	1.20	0.11	0.38	0.24	-0.46	-0.21	0.14	1.20	-0.01
Run 1+4	1	5.07	3.68	2.37	1.30	0.53	-2.03	-1.49	-1.15	-0.57	0.02
	2	4.74	3.75	1.53	0.81	0.21	-2.13	-0.95	-0.86	0.00	0.07
	3	3.08	2.42	0.02	0.67	0.06	-1.31	-0.39	-0.07	1.15	0.01
Girder 2											
1	1	3.95	2.32	1.09	0.33	-0.18	-1.35	-0.89	-0.47	-0.11	0.17
	2	3.38	2.11	0.76	0.21	-0.23	-1.44	-0.34	-0.37	0.01	0.18
	3	2.07	1.34	-0.01	0.22	-0.18	-0.88	-0.17	-0.28	-0.46	-0.01
4	1	1.73	1.36	1.05	0.99	0.65	-0.61	-0.75	-0.71	-0.52	-0.12
	2	1.65	1.49	0.66	0.77	0.31	-0.64	-0.47	-0.55	0.02	-0.04
	3	1.08	1.06	0.15	0.38	0.22	-0.45	-0.20	-0.01	0.60	-0.05
Run 1+4	1	5.68	3.68	2.14	1.32	0.47	-1.96	-1.63	-1.18	-0.63	0.06
	2	5.03	3.60	1.42	0.98	0.08	-2.08	-0.81	-0.92	0.03	0.13
	3	3.15	2.40	0.13	0.60	0.04	-1.32	-0.37	-0.29	0.13	-0.06
Girder 3											
3	1	2.30	1.71	1.31	0.89	0.33	-0.74	-0.83	-0.68	-0.55	-0.05
	2	1.97	1.68	0.79	0.69	0.25	-0.80	-0.39	-0.56	0.02	0.09
	3	1.24	0.81	0.18	0.31	0.14	-0.53	-0.17	0.09	0.12	-0.03
8	1	1.18	0.97	0.99	1.04	1.30	-0.15	-0.52	-0.75	-0.86	-0.41
	2	0.71	1.05	0.63	0.72	1.02	-0.24	-0.18	-0.50	0.08	-0.15
	3	0.26	0.86	0.10	0.43	0.43	-0.14	-0.08	-0.25	-0.45	-0.18
Run 3+8	1	3.48	2.68	2.31	1.92	1.63	-0.89	-1.35	-1.43	-1.41	-0.46
	2	2.68	2.72	1.43	1.41	1.26	-1.04	-0.57	-1.06	0.10	-0.05
	3	1.49	1.67	0.28	0.74	0.56	-0.67	-0.25	-0.16	-0.34	-0.21
Girder 4											
9	1	0.79	0.82	0.98	1.05	1.42	-0.12	-0.40	-0.67	-0.98	-0.57
	2	0.51	0.87	0.56	0.82	0.94	-0.11	-0.18	-0.52	0.12	-0.31
	3	0.21	0.53	0.13	0.49	0.41	-0.08	-0.11	-0.16	0.26	-0.06
12	1	-0.19	0.40	1.19	2.10	2.94	0.08	-0.05	-0.40	-0.98	-1.49
	2	-0.29	0.34	0.57	1.61	1.99	0.10	-0.06	-0.33	0.17	-0.83
	3	-0.13	0.16	0.25	0.92	0.86	0.10	-0.01	0.30	0.66	-0.29
Run 9+12	1	0.60	1.22	2.17	3.16	4.36	-0.05	-0.45	-1.07	-1.97	-2.06
	2	0.21	1.21	1.13	2.43	2.93	-0.01	-0.24	-0.84	0.29	-1.14
	3	0.08	0.70	0.38	1.41	1.28	0.03	-0.12	0.15	0.92	-0.35
Girder 5											
9	1	0.84	1.08	1.96	2.51	1.94	-0.17	-0.37	-0.59	-0.88	-0.75
	2	0.51	1.09	1.12	1.90	1.30	-0.16	-0.14	-0.53	0.05	-0.41
	3	0.39	0.56	0.14	1.14	0.61	-0.13	-0.13	-0.16	0.04	-0.19
12	1	-0.29	0.34	1.17	2.04	2.81	0.11	-0.01	-0.38	-0.94	-1.52
	2	-0.28	0.30	0.59	1.52	1.89	0.11	-0.08	-0.34	0.12	-0.82
	3	-0.15	0.19	0.10	0.87	0.79	0.09	0.00	0.32	0.88	-0.26
Run 9+12	1	0.55	1.42	3.14	4.55	4.75	-0.07	-0.38	-0.97	-1.82	-2.27
	2	0.23	1.39	1.72	3.42	3.19	-0.05	-0.22	-0.86	0.17	-1.23
	3	0.25	0.75	0.24	2.00	1.40	-0.04	-0.13	0.15	0.92	-0.44

3.8 FEM STRESS COMPARISONS

The University of West Virginia worked with the University of Missouri – Columbia's Field Test Team on this project. They developed a finite element model using ABAQUS finite element software for Bridge A6101 and were able to develop bottom flange stresses in the girders for Runs 9 and 12 (Wu 2003). The model considered the skew of the bridge, the railings and curbs, and composite and non-composite actions at the various locations. These stresses were compared to the experimental stresses found by the University of Missouri – Columbia's team. Table 3.4 shows West Virginia's finite element stresses compared to University of Missouri – Columbia's measured stresses and σ_o's found from stress profiles when Girder 4 is maximized for positive moment from Runs 9 and 12.

Table 3.4 - Stress Comparison between West Virginia FEM and Missouri Measured Stresses

Maximum Positive Stresses (Run 9+12)

Girder	1	2	3	4	5
MO Measured	0.315	1.550	3.007	4.715	6.196
MO σ_O	0.617	1.629	2.992	4.853	6.307
WVU FEM	0.124	1.553	3.664	5.650	6.262

Corresponding Negative Stresses (Run 9+12)

Girder	1	2	3	4	5
MO Measured	-0.125	-0.388	-0.825	-1.529	-2.036
MO σ_O	-0.141	-0.387	-0.920	-1.529	-2.140
WVU FEM	0.042	-0.427	-1.059	-1.717	-2.346

Maximum Negative Stresses (Run 9+12)

Girder	1	2	3	4	5
MO Measured	-0.065	-0.379	-0.970	-1.822	-2.272
MO σ_O	-0.064	-0.372	-1.254	-1.822	-2.241
WVU FEM	0.035	-0.461	-1.141	-1.829	-2.485

Corresponding Positive Stresses (Run 9+12)

Girder	1	2	3	4	5
MO Measured	0.548	1.421	3.136	4.550	4.748
MO σ_O	0.556	1.619	3.159	4.616	4.804
WVU FEM	0.116	1.465	2.684	3.851	4.844

Table 3.5 shows the maximum positive stresses for the individual girders subject to their respective maximum loading. Unfortunately, a difference between Table 3.5 and Table 3.4 is that the FEM analysis assumes composite action in the negative moment region. Therefore, shown are only comparisons of the positive stresses. It is assumed that the difference in the positive region is minimal. The positive moment region comparison

is shown to support the experimental results where the critical experimental capacity (lowest rating factor) for the bridge is from the exterior Girder 1 (discussed in Section 3.10).

Table 3.5 - Maximum Positive Stresses for Individual Girders from Particular Maximum Loading

Maximum Positive Stresses in Girders

Girder	1	2	3	4	5
Truck Runs	1+4	1+4	3+8	9+12	9+12
MO Measuered	6.46	5.15	4.26	5.24	6.2
MO σ_O	6.959	5.46	4.297	5.391	6.307
WVU FEM	6.361	5.784	4.601	5.538	6.23

The FEM stresses compare well, demonstrating that the finite element model can predict how the bridge actually performed during field-testing. The corresponding serviceability study of Bridge A6101 in Chapter 4 uses the finite element model results to extend the experimental results to draw conclusions on serviceability in steel bridges.

3.9 MOMENTS

From the stress combinations in Tables 3.2 and 3.3, the moments for each girder can be calculated using the method shown in Section 3.5.2. An example spreadsheet for the maximum positive moment in Girder 4 is shown in Table 3.6. In the table, the maximum moment in Girder 4, from superposition of truck Runs 9 and 12 is 706.3 k-ft. The moments shown for Girders 1, 2, 3, and 5 represent corresponding moments when the two side-by-side trucks are positioned to maximize Girder 4.

Section 3.9.1 shows a sample calculation for the maximum positive interior moment for Girder 4.

Table 3.6 – Maximum Stresses Caused from Load Case 9+12(Positive Section)

Girder 4

Gir 1	Run 9+12									
0.75	0		m	b	s_0	s_{CG}	M_L (k-ft)	M_U (k-ft)	Na (k-ft)	M_T (k-ft)
0.33	15.79		-51.2359	37.25473	0.727121	0.157452	50.91749	1.05396	27.49193	79.46338566
0.19	30.79									
			0.727121	0						
			0	37.25473						
Gir 2	Run 9+12		y=mx+b							
1.55	0		m	b	s_0	s_{CG}	M_L	M_U (k-ft)	Na (k-ft)	M_T (k-ft)
1.42	15.79		-42.7732	70.88183	1.657156	0.974776	60.99164	1.262489	170.2013	232.4554574
0.91	30.79									
			1.657156	0						
			0	70.88183						
Gir 3	Run 9+12		y=mx+b							
3.33	0		m	b	s_0	s_{CG}	M_L	M_U (k-ft)	Na (k-ft)	M_T (k-ft)
1.67	15.79		-9.76132	32.37451	3.316612	0.326489	267.2596	5.532105	57.00683	329.7984937
0.18	30.79									
			3.316612	0						
			0	32.37451						
Gir 4	Run 9+12		y=mx+b							
5.24	0		m	b	s_0	s_{CG}	M_L	M_U (k-ft)	Na (k-ft)	M_T (k-ft)
4.11	15.79		-10.3556	55.82482	5.390809	2.572269	251.9233	5.214655	449.1324	706.2703996
2.32	30.79									
			5.390809	0						
			0	55.82482						
Gir 5	Run 9+12		y=mx+b							
6.00	0		m	b	s_0	s_{CG}	M_L	M_U (k-ft)	Na (k-ft)	M_T (k-ft)
4.24	15.79		-7.62339	46.56796	6.108566	2.279881	342.2109	7.083551	398.0798	747.3742676
1.98	30.79									
			6.108566	0						
			0	46.56796						
										Total Moment
										2095.362004 k-ft

Sample Calculation: Maximum Positive Interior Moment (Girder 4)

Stresses From Table 3.2 (Locations are measured up from the bottom flange, See Figure 3.16):

Location (in) Run 9	Stress (ksi) Run 9
0	2.54
15.79	1.91
30.79	1.15

Location (in) Run 12	Stress (ksi) Run 12
0	2.70
15.79	2.20
30.79	1.18

Location (in) Run 9+12	Stress (ksi) Run 9+12
0	5.24
15.79	4.11
30.79	2.32

$$\sum \sigma_i^2 = 5.24^2 + 4.11^2 + 2.32^2 = 49.73$$

$$\sum \sigma_i = 5.24 + 4.11 + 2.32 = 11.67$$

n = 3

$$\sum d_i * \sigma_i = 0 * 5.24 + 15.79 * 4.11 + 30.79 * 2.32 = 136.34$$

$$\sum d_i = 0 + 15.79 + 30.79 = 46.58$$

$$\begin{bmatrix} 49.73 & 11.67 \\ 11.67 & 4 \end{bmatrix} * \begin{Bmatrix} a \\ b \end{Bmatrix} = \begin{Bmatrix} 136.34 \\ 46.58 \end{Bmatrix} \rightarrow a = -10.356 \rightarrow b = 55.825$$

$$d = -10.356 * \sigma + 55.825$$

$$y_1 = 55.825 \text{ in}$$

$$\sigma_O = -\frac{55.825}{-10.356} = 5.39 \text{ ksi}$$

$$CG = \frac{[(16.625*0.8125)*0.406] + [(0.5*60.4375)*31.031] + [(12.625*0.8125)*61.656]}{(16.625*0.8125) + (0.5*60.4375) + (12.625*0.8125)} = 29.1876 \text{ in}$$

$$\sigma_{CG} = \frac{29.1876 - 55.825}{-10.356} = 2.572 \text{ ksi}$$

$$S_{STL}^{ADIM} = \frac{31305.67}{29.1876} = 1072.57 \text{ in}^3$$

$$M_L = (5.39 - 2.572) * \frac{1072.57}{12} = 251.923 \text{ k - ft}$$

$$Na = \left(\frac{2.572 * 53.984}{12}\right)\left[(62.0625 - 29.1876) + 1.6875 + \left(\frac{8.5}{2}\right)\right] = 449.132 \text{ k - ft}$$

$$M_U = \left[\frac{3.6 * 10^6 (5220.06)}{2.9 * 10^7 (31305.67)}\right] 251.923 = 5.215 \text{ k - ft}$$

$$M_{TOTAL} = 251.923 + 449.132 + 5.215 = 706.27 \text{ k - ft}$$

3.9.1 Experimental Moment Results

Table 3.7 shows the results for maximum positive moments with corresponding moments for each girder and minimum negative moments with corresponding moments for each girder. The positive moments are the moments from the gages at 55.1 ft from the eastern abutment and the negative moments are from the gages at 132.8 ft from the eastern abutment. Each sub-table represents the experimental moments in equilibrium from two side-by-side trucks placed on the bridge to maximize the moment at a particular section.

Table 3.7 - Moment Summary

Maximum Positive and Corresponding Negative Moments when Girder 1 is Maximum Positive

Run 1+4

Girder	Maximum Positive Moment (k-ft)	Corresponding Negative Moment (k-ft)
1	949.9	-503.6
2	748.1	-256.8
3	323.8	-222.7
4	184.3	-47.1
5	35.3	36.3

Maximum Negative and Corresponding Positive Moments when Girder 1 is Maximum Negative

Run 1+4

Girder	Maximum Negative Moment (k-ft)	Corresponding Positive Moment (k-ft)
1	-509.5	770.8
2	-278	589.8
3	-213.8	250
4	33.3	168.4
5	22.9	51.4

Maximum Positive and Corresponding Negative Moments when Girder 2 is Maximum Positive

Run 1+4

Girder	Maximum Positive Moment (k-ft)	Corresponding Negative Moment (k-ft)
1	909.3	-493.2
2	775.6	-253.1
3	331.9	-226.7
4	190.8	12.25
5	37.46	-24.3

Maximum Negative and Corresponding Positive Moments when Girder 2 is Maximum Negative

Run 1+4

Girder	Maximum Negative Moment (k-ft)	Corresponding Positive Moment (k-ft)
1	-499.2	831.5
2	-281.3	578.2
3	-234.4	233.6
4	-84.2	175.1
5	20	38.9

Maximum Positive and Corresponding Negative Moments when Girder 3 is Maximum Positive

Run 3+8

Girder	Maximum Positive Moment (k-ft)	Corresponding Negative Moment (k-ft)
1	486.6	-246.4
2	579.9	-192.2
3	442.8	-280.1
4	410.7	-159.9
5	247.7	-112.1

Maximum Negative and Corresponding Positive Moments when Girder 3 is Maximum Negative

Run 3+8

Girder	Maximum Negative Moment (k-ft)	Corresponding Positive Moment (k-ft)
1	-244.7	463.6
2	-221	424.5
3	-268.3	252
4	-256.6	248.1
5	-80.5	211

Maximum Positive and Corresponding Negative Moments when Girder 4 is Maximum Positive

Run 9+12

Girder	Maximum Positive Moment (k-ft)	Corresponding Negative Moment (k-ft)
1	79.5	-15.2
2	232.5	-70.1
3	329.8	-193.4
4	706.3	-241.1
5	747.4	-395.6

Maximum Negative and Corresponding Positive Moments when Girder 4 is Maximum Negative

Run 9+12

Girder	Maximum Negative Moment (k-ft)	Corresponding Positive Moment (k-ft)
1	-4.2	56.9
2	-79.8	188.3
3	-191.2	230.1
4	-210.1	422.9
5	-356.5	526.7

Maximum Positive and Corresponding Negative Moments when Girder 5 is Maximum Positive

Run 9+12

Girder	Maximum Positive Moment (k-ft)	Corresponding Negative Moment (k-ft)
1	57.1	-22.4
2	218.5	-68.5
3	290.8	-171.3
4	632.7	-207.1
5	776.8	-388.8

Maximum Negative and Corresponding Positive Moments when Girder 5 is Maximum Negative

Run 9+12

Girder	Maximum Negative Moment (k-ft)	Corresponding Positive Moment (k-ft)
1	-14.5	63.2
2	-71.2	214.8
3	-183.7	322.3
4	-186.8	603.6
5	-394.5	573.9

3.10 RATING FACTORS

From these moments, rating factors for positive and negative interior and positive and negative exterior girders can be calculated using the method described in Section 3.6.1 and 3.6.2. The eight adjustment factors can also be calculated using the method described in Section 3.6.3. Sample calculations for these rating factors and adjustment factors are shown below. The dead, composite dead, analytical live load moments, the nominal design and actual dimension section properties are from the various SIMON runs described in Section 3.6.

3.10.1 Sample Calculation: Maximum Positive Interior Rating Factor (Girder 4)

Design Rating Factor (HS20) eqn 3.16

$$RF_{Design}^{HS\,20} = \frac{\frac{(0.9581)(70)}{1.3} - \left(\frac{1388}{83.27} + \frac{592}{108.6}\right)}{\frac{5}{3}\left(\frac{1769.4}{118.8}\right)} = 1.19$$

Adjusted HS20 Truck Design Rating Factor eqn 3.17

$$RF_{Design}^{TRK} = \frac{\frac{(0.9581)(70)}{1.3} - \left(\frac{1374}{83.27}\left\{\frac{1388}{1374}\right\} + \frac{590}{108.6}\left\{\frac{592}{590}\right\}\right)}{\frac{5}{3}\left(\frac{1152}{118.8}\left\{\frac{1769.4}{1152}\right\}\right)} = 1.19$$

Experimental Truck Rating Factor eqn 3.20

$$I = \frac{50}{125 + 137.8} = 0.19$$

$$RF_{EXP}^{TRK} = \frac{\frac{(0.9563)(70)}{1.3} - \left(\frac{1374}{89.38}\left\{\frac{1388}{1374}\right\} + \frac{590}{119.5}\left\{\frac{592}{590}\right\}\right)}{\frac{5}{3}(5.39)(1 + 0.19)\left\{\frac{1769.4}{1152}\right\}} = 1.89$$

The difference between the Experimental Rating Factor and the Design Rating Factors is described by the eight factors from Section 3.6.3. This example, examining the experimental capacity compared to design, will fully describe the procedures to calculate the various factors.

(1) Dead Load Stress Adjustment

$$\frac{\frac{R_{EXP}F_y}{1.3}-\left(\frac{M_{D_{NC}}^{HS20-MAX-ADIM}}{S^{ADIM}}+\frac{M_{D_C}^{HS20-MAX-ADIM}}{S_{3n}^{ADIM}}\right)}{\frac{R_{Design}F_y}{1.3}-\left(\frac{M_{D_{NC}}^{HS20-MAX-ADIM}}{S^{Design}}+\frac{M_{D_C}^{HS20-MAX-ADIM}}{S_{3n}^{Design}}\right)}=\frac{\frac{0.9563(70)}{1.3}-\left(\frac{1374}{89.38}\left\{\frac{1388}{1374}\right\}+\frac{590}{119.5}\left\{\frac{592}{590}\right\}\right)}{\frac{0.9563(70)}{1.3}-\left(\frac{1374}{83.27}\left\{\frac{1388}{1374}\right\}+\frac{590}{108.6}\left\{\frac{592}{590}\right\}\right)}=1.056$$

(2) Distribution Factor Adjustment

AASHTO Design Manual calculates the distribution factor for an interior girder to be:

$$DF_{Interior}=\frac{S}{5.5}$$

where,

S = Girder spacing (ft).

For an exterior girder, AASHTO uses the design equation:

$$DF_{Exterior}=\frac{S}{4+\frac{S}{4}}$$

These equations are used to determine the analytical distribution factors to compare to the experimental distribution factors.

$$DF_A=\frac{8.96}{5.5}=1.629$$

The experimental distribution factor is found by the ratio of the girder moment to the total bridge section moment. The maximum positive moment for the Girder 4 was found to be 706 k-ft. The total moments of all girders across the positive section is 2095 k-ft. When 706 k-ft is divided by 2095 k-ft, the distribution factor for one wheel line is found

for Girder 4. This number must be multiplied by 4 because when load superposition is used there are 4 wheel lines causing the maximum moment. This result is the experimental distribution factor.

$$DF_E = \frac{706}{2095} * 4 = 1.348$$

The distribution factor adjustment is then found by dividing the analytical distribution factor by the experimental distribution factor.

$$\frac{DF_A}{DF_E} = \frac{1.629}{1.348} = 1.209$$

(3) Impact Factor Adjustment

$$\frac{I_A}{I_E} = \text{Assumed to be } 1.0$$

Impact Factor Adjustment is assumed to be 1.0 because no impact testing was conducted.

(4) Bearing Restraint Adjustment

$$\frac{M_E}{M_T} = \text{Assumed to be } 1.0$$

The Bearing Restraint Adjustment is assumed to be 1.0 because no bearing restraint gages were used during testing. Thus, $M_E = M_T$.

(5) Longitudinal Distribution Adjustment

$$M_{GIR4}^{MAXPOS} = 706 \text{ k - ft}$$

$$M_{GIR4}^{CORSNEG} = -241 \text{ k - ft}$$

Using Influence Line Diagrams, the Analytical Statical Moments can be calculated as follows (Barker et al 1999):

$$M_A^{MAXPOS-GAGE} = 21.6(2.55) + 29.1(14.85) + 23(3.61) + 17.3(1.59) = 597.75 \text{ k - ft}$$

The position of the truck that maximizes the positive moment is when the middle axle is directly over the gage position. SIMON gives Influence Line Points at 1/10 points along the span (example 13.78 ft, 27.56 ft, 41.34 ft). The gage in the negative moment region is in between the 9th and 10th points along the span so the moments must be found at these points and then interpolated between to find the corresponding negative moment at the gage position of 132.8 ft from the eastern abutment. The process is as follows:

$$M_{Pt9} = -3.1(2.55) - 3.5(14.85) - 3.3(3.61) - 2.4(1.59) = -75.61\,\text{k - ft}$$

$$M_{Pt10} = -8(2.55) - 10(14.85) - 11.3(3.61) - 11.8(1.59) = -228.46\,\text{k - ft}$$

Interpolating between these points gives:

$$M_A^{CORSNEG-GAGE} = -75.61 + \frac{8.78}{13.78}(-228.46 + 75.61) = -173\,\text{k - ft}$$

Figure 3.21 shows the tenth points from SIMON along one span of the bridge and shows the positioning of the axles to maximize the moment at the positive gage. The point loads from the axles are also shown and the distributed loads to the 10th points.

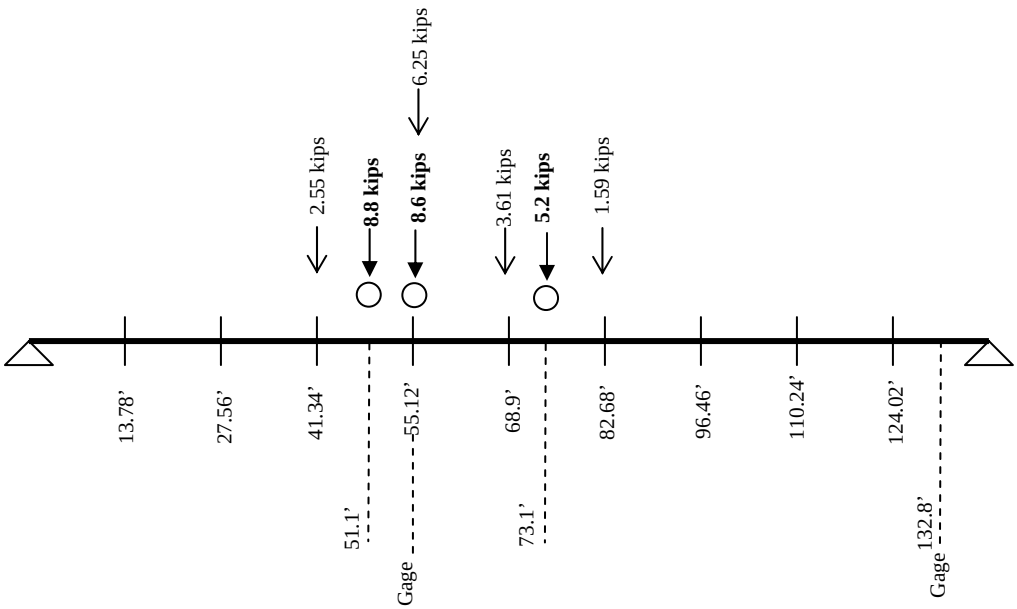

Figure 3.21 - Load position for Influence Line Diagram

The analytical statical moment is calculated by dividing the ratio of the distances that the gages are placed along the span and then multiplying it by the $M_A^{CORSNEG-GAGE}$. The $M_A^{MAXPOS-GAGE}$ is then added to this to find the $STAT_A$.

$$STAT_A = \frac{55.1}{132.8}(173) + 597.75 = 669.5 \text{ k - ft}$$

The experimental statical moment is calculated by using same ratio of the distance the gages are placed along the bridge and multiplying it by $M_{GIR4}^{CORSNEG}$ and adding M_{GIR4}^{MAXPOS} to it.

$$STAT_E = \frac{55.1}{132.8}(241) + 706 = 806 \text{ k - ft}$$

The statical moments are defined as being the total moment that is applied to the bridge. If the analysis and experimental response have the same longitudinal distribution, the

ratio of the positive moment to the statical moment for each would be identical. Figure 3.22 shows what the statical moments look like when plotted along the span.

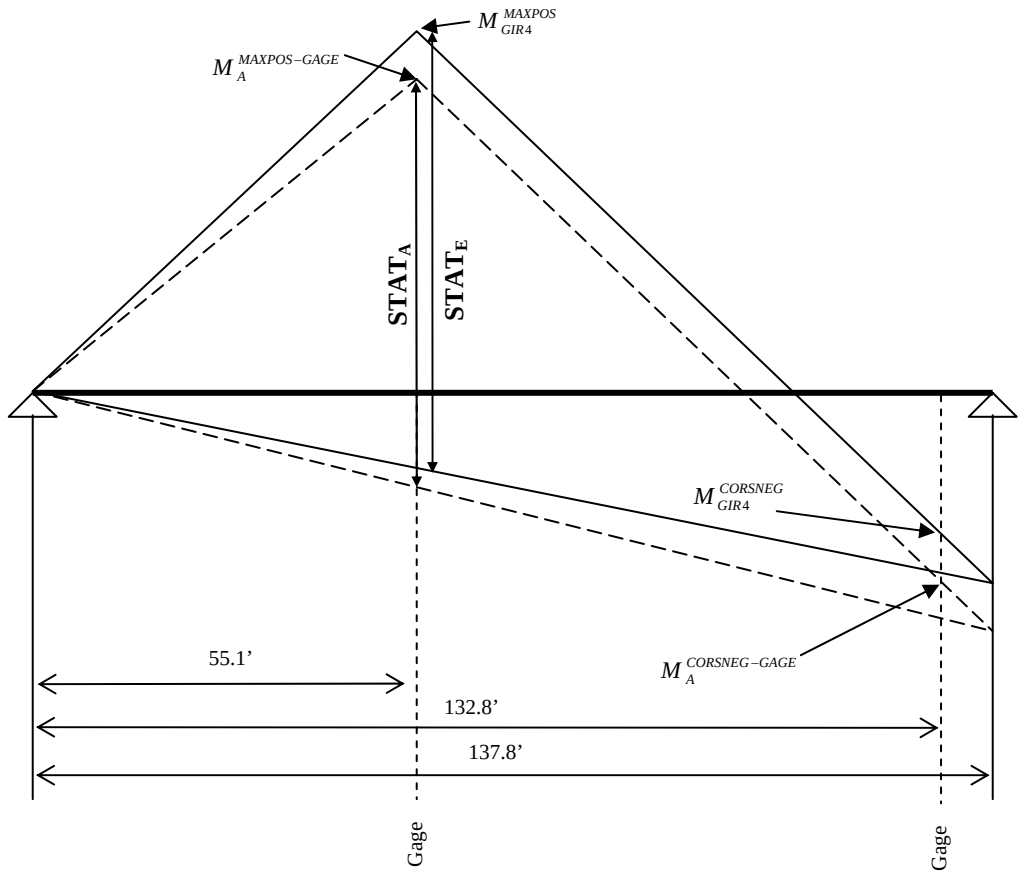

Figure 3.22 - Statical Moment Diagram along Span

Thus, the adjusted moment, M_{LE}, represents the experimental moment that would be on the bridge if the experimental longitudinal distribution factor followed the behavior of the analytical analysis (Frederick, 1998). This moment is found by dividing the $STAT_E$ by the $STAT_A$ and then multiplying it by $M_{A}^{MAXPOS-GAGE}$.

$$M_{LE}^{P} = \frac{806}{669.5}(597.75) = 719.6 \text{ k - ft}$$

The Longitudinal Distribution Adjustment is then found by dividing M_{LE} by the M_{GIR4}^{MAXPOS} which, here, is equal to M_E.

$$\frac{M_{LE}}{M_E} = \frac{719.6}{706} = 1.019$$

(6) Section Modulus Adjustment

The difference between the actual dimensions of the girder and the girder's nominal dimensions (fabrication and construction tolerances) is accounted for with the section modulus adjustment factor (Frederick, 1998). It is found by dividing the short term section modulus of girder plus (1/n) of the slab using measured dimensions by the short term section modulus of girder (1/n) of the slab using design dimensions.

$$\frac{S_n^{ADIM}}{S_n^{Design}} = \frac{130.4}{118.8} = 1.098$$

(7) Additional or Unintended Composite Action Adjustment

A second adjustment factor for the section modulus is the additional or unintended composite action adjustment. This factor is the ratio of the experimentally determined section modulus to the section modulus that is determined using the true bridge dimensions. The increase in section modulus is due to unintended or additional action from the concrete slab and barrier curbs (Frederick, 1998). Calculation of the experimental moment of inertia, I_E, is found using the Equation 3.14 in Section 3.5.3.

$$I_E = -706(-10.36)(12) = 87770 \text{ in}^4$$

The experimental section modulus, S_E, is calculated using Equation 3.15.

$$S_E = \frac{87770}{55.82} = 1572.4 \text{ in}^3$$

The additional or unintended composite action adjustment factor is then found by dividing the experimental section modulus by the short term section modulus of girder plus (1/n) of the slab using measured dimensions.

$$\frac{S_E}{S_n^{ADIM}} = \frac{1572.4}{130.4(12)} = 1.005$$

(8) Curb / Railing/ Skew Adjustment

The curb / railing / skew adjustment is used to account for extra strength in the load carrying system. The extra strength reduces the observed moment in the girders because other parts of the bridge are also resisting the applied load. This adjustment is found by using eqn 3.30. $M_{WHL-Line}^{HS20-MAX-ADIM}$ is found by dividing the $M_{L+I}^{HS20-MAX-ADIM}$ by the distribution factor DF_E for either an interior or exterior girder and then by $(1+I_A)$ to get an equivalent experimental wheel line moment.

$$\frac{M_{WHL-Line}^{HS20-MAX-ADIM}}{\frac{M_{LE}}{DF_E} * \frac{M_{L+I}^{HS20-MAX-ADIM}}{M_{L+I}^{TRK-MAX-ADIM}}} = \frac{\frac{1769.4}{1.629(1.19)}}{\frac{719.6}{1.348}\left(\frac{1769.4}{1152}\right)} = 1.113$$

Experimental Capacity

$$\frac{ExpCap}{DesCap} = \frac{1.89}{1.19} = 1.59$$

This Experimental Capacity / Design Capacity Ratio means that the bridge demonstrates an experimental capacity that is 59 % stronger than design for Girder 4. The addition to the design capacity is broken up into the 8 adjustment factors in the following:

Adjustment Factor	Percent Addition to Experimental Capacity
Dead Load Stress Adjustment	5.6 %
Impact Factor Adjustment	0 %
Distribution Factor Adjustment	20.9 %
Bearing Restraint Adjustment	0 %
Curb / Railing / Skew Adjustment	11.3 %
Section Modulus Adjustment	9.8 %
Longitudinal Adjustment	1.9 %
Additional Composite Adjustment	0.5 %

$$\frac{RF_E}{RF_A} = (1.056)(1.00)(1.209)(1.00)(1.113)(1.098)(1.019)(1.005) = 1.59$$

$$RF_E = 1.19(1.59) = 1.89$$

3.10.2 Design and Experimental Rating Factor Results

Rating Factors were calculated for Maximum Positive and Maximum Negative Moments for all girders. Table 3.8 gives the values for the Design Rating Factors and the Experimental Rating Factors for both Max Positive and Max Negative moments. Tables 3.9 and 3.10 show the Rating Factors and the Adjustment Factors for all 5 girders, both positive and negative.

Table 3.8 - Maximum Positive and Maximum Negative Rating Factors

Maximum Positive Rating Factors

Girder	HS20 Design Rating Factor	Experimental Rating Factor
1	1.440	1.310
2	1.190	1.860
3	1.190	2.370
4	1.190	1.890
5	1.440	1.440

Maximum Negative Rating Factors

Girder	HS20 Design Rating Factor	Experimental Rating Factor
1	1.523	1.333
2	1.217	2.148
3	1.217	2.176
4	1.217	1.734
5	1.523	1.423

Table 3.9 - Maximum Positive Rating Factors and Adjustment Factors

Maximum Positive Rating Factors and Adjustment Factors

Girder	1	2	3	4	5
HS20 Design Rating Factor	1.440	1.190	1.190	1.190	1.440
Experimental Rating Factor	1.310	1.860	2.370	1.890	1.440
Dead Load Stress Adjustment	1.045	1.056	1.056	1.056	1.045
Impact Factor Adjustment	1.000	1.000	1.000	1.000	1.000
Distribution Factor Adjustment	0.847	1.179	1.993	1.208	0.913
Bearing Restraint Adjustment	1.000	1.000	1.000	1.000	1.000
Longitudinal Adjustment	1.089	1.014	1.127	1.019	1.078
Curb / Railing / Skew Adjustment	0.816	1.044	0.973	1.113	0.935
Section Modulus Adjustment	1.090	1.098	1.098	1.098	1.090
Additional Composite Adjustment	1.061	1.064	0.790	1.005	0.957

Table 3.10 - Maximum Negative Rating Factors and Adjustment Factors

Maximum Negative Rating Factors and Adjustment Factors

Girder	1	2	3	4	5
HS20 Design Rating Factor	1.523	1.217	1.217	1.217	1.523
Experimental Rating Factor	1.333	2.148	2.176	1.734	1.423
Dead Load Stress Adjustment	1.032	1.039	1.039	1.039	1.032
Impact Factor Adjustment	1.000	1.000	1.000	1.000	1.000
Distribution Factor Adjustment	0.668	1.563	1.626	1.632	0.774
Bearing Restraint Adjustment	1.000	1.000	1.000	1.000	1.000
Longitudinal Adjustment	0.690	0.884	0.485	0.869	0.669
Curb / Railing / Skew Adjustment	1.324	1.063	1.954	1.386	1.516
Section Modulus Adjustment	1.031	1.031	1.031	1.031	1.031
Additional Composite Adjustment	1.355	1.121	1.090	0.678	1.118

3.11 SUMMARY

Bridge A6101 was tested to evaluate the performance compared to design predictions. This chapter demonstrates the testing equipment, testing, data reduction, and results for the analytical and experimental design capacities. The experimental capacity procedures illustrated can also estimate what contributors are responsible for the difference between the experimental and analytical capacities. Table 3.9 for positive

moment regions and 3.10 for negative moment regions summarize the experimental performance comparison to design.

For design, the minimum design rating factor is 1.19 located at the positive moment region of an interior girder. This represents a capacity of an HS23.8 truck loading using design procedures. The critical experimental rating factor is 1.31 located at the positive moment region of an exterior girder. This represents an experimental capacity of an HS26.2 truck loading using testing procedures. Thus, this bridge does exhibit additional capacity over the design prediction specifications as is expected.

However, there are a few important behaviors to note. At the critical design location, an interior girder, the design rating factor is 1.19, but the experimental rating factor is 1.86. This represents an experimental capacity 56% larger than design predictions. Most of this additional capacity is due to lateral distribution characteristics.

For the critical experimental location, an exterior girder, the design rating factor is 1.44 while the experimental rating factor is only 1.31. This represents that the experimental capacity is only 91% of the design prediction. This insinuates that the design equations are unconservative for the exterior girder. The difference is mostly attributed to the lateral distribution factor; design equations underpredict the exterior girder distribution. However, two notes about this exterior girder behavior. First, the overall experimental rating is still above 1.0 meaning the bridge meets design requirements. Second, the experimental testing placed the loads only 1 ft from the curb whereas the specifications assume 2 ft from the curb. This resulted in a loading on the exterior girder more severe than design procedures dictate.

Chapter 5 summarizes the findings and conclusions of this research.

CHAPTER 4 – SERVICEABILITY FIELD TESTING OF BRIDGE A6101

4.1 SERVICEABILITY BACKGROUND INFORMATION

Serviceability design for bridge design can be broken down into two primary categories: live load deflection and acceleration or vibration. These two categories may be related in that a bridge with unacceptable vibration may also, but not necessarily, have excessive deflections. According to a 1930 Bureau of Public Roads Study, it was concluded that bridges that exhibited intolerable acceleration had calculated deflections of greater than the span length (L) divided by 800 (Barth and Christopher, 2000). This corresponds with the present AASHTO (1996) LFD specifications that a bridge meets a live load deflection of less than L/800 for non-pedestrian bridges and L/1000 for bridges with sidewalks used by pedestrians.

The AASHTO limits, although controlling deflection, are actually intended to limit the bridge's acceleration (Barth and Christopher, 2000). However, in the past, acceleration of a bridge was much harder to predict and measure than deflection, so it has been more practical to limit the deflection.

In addition to causing user discomfort, it has also been thought that deflections cause deterioration of the concrete deck. However, recent studies are finding that factors such as surface roughness, damping, and vehicle characteristics and volume are more to blame (Barth and Christopher, 2000).

Serviceability is important to bridge design even if it does not affect the life span of the structure. People will not use a structure that they do not trust. If a bridge deflects or vibrates excessively, the public will not be comfortable in its safety. Another aspect of

serviceability is the resonant frequency of a bridge. The resonant frequency is the frequency that the bridge exhibits during free vibration. If traffic or other forces acting on the bridge match the resonant frequency, the deflections and accelerations can be magnified significantly. It is with this in mind that the Ontario Highway Bridge Design Code (1983) limits deflection as a function of the resonant frequency of the structure.

Serviceability criteria take form in most United States bridge design codes as some type of live load deflection limit. States are allowed to make their own limitations, although most state codes relate to the criteria used by AASHTO (Barth and Christopher, 2000). Several states, Missouri included, have more conservative deflection criteria than AASHTO. So, it is of interest to know how the MoDOT and AASHTO codes differ in both the deflection allowed and the way that deflection is distributed to the girders, along with the economic impact of conservative deflection limits.

4.1.1 AASHTO Deflection Criteria

AASHTO (1996) LFD design, according to article 10.6.2, states that the allowable deflection of a bridge depends on the pedestrian traffic on the bridge. For a rural or non-pedestrian bridge, the allowed deflection of a span is the length of that span divided by 800. For a bridge with sidewalks or an urban bridge, the allowed deflection is the span length divided by 1000. The allowable deflection in a pedestrian bridge is less because of the higher sensitivity to deflection and acceleration of a pedestrian than that of a person riding in a vehicle.

It should also be noted that in the AASHTO Load and Resistance Factor Design code (1998), deflection criteria is optional. It is up to the design engineer's discretion, or

the owner, whether allowable deflection limits are enforced and, if so, what are those limits.

The analysis of deflection in the AASHTO LFD code, article 10.6.4, explains that the live load deflection of the bridge is distributed equally to all of the girders. The deflection of a girder caused by one wheel line is calculated and then multiplied by the deflection distribution factor. This distribution factor depends on the width of the bridge (number of traffic lanes), an intensity reduction factor, and the number of girders. In AASHTO, the traffic lanes are 12 feet wide, and the number of lanes is the truncated integral value of the width of the bridge divided by 12. The number of lanes on the bridge then determines the value of the intensity reduction factor, as AASHTO (Section 3.12.1) assumes that it is less likely for every lane to have a design truck side by side as the number of lanes grow. So the intensity reduction factor equals

1.0 for one or two traffic lanes

0.9 for three traffic lanes

0.75 for four or more traffic lanes

Therefore the AASHTO live load deflection distribution factor is represented by

$$D.F. = \frac{n * 2(wheels / axle) * i}{G} \tag{4.1}$$

Where,

n = Number of 12 ft Traffic Lanes (integer)

i = Intensity Reduction Factor

G = Number of Girders

4.1.2 MoDOT Deflection Criteria

A notable difference between the AASHTO and MoDOT deflection criteria is the allowable deflection. As opposed to different limits for pedestrian and non-pedestrian bridges, MoDOT (2002) separates bridges as either composite or non-composite (MoDOT B.M 3.40.3.4). Non-composite bridges are allowed to deflect the span length divided by 800, while composite bridges are limited to the span length divided by 1000. This is because of the perception that deflection causes cracking in the deck in composite bridges. This is more conservative than AASHTO for composite bridges with no sidewalks since they still must meet the stricter Span/1000 limit.

The distribution factor used for the MoDOT deflection analysis is also more conservative than AASHTO. The MoDOT distribution factor is explained in article 1.3.2-2 of the MoDOT Bridge Manual. First, the traffic lanes are only ten feet wide, allowing for the possibility of more lanes. Also, the intensity reduction factor is not taken into account. Finally, for each girder's deflection distribution factor, the moment distribution factor is averaged with the value of the traffic lanes distributed equally between the girders. So the MoDOT live load deflection distribution factor is

$$D.F. = \frac{(MDF) + \left(\frac{n * 2(wheels/axle)}{G}\right)}{2} \tag{4.2}$$

Where,

MDF = Moment Distribution Factor for that Girder

n = Number of 10 ft Traffic Lanes (integral)

G = Number of Girders

4.1.3 Comparison to Other State's Deflection Criteria

In an effort to compare the conservative deflection criteria used in Missouri to that of other states, MoDOT conducted a survey in 1999 (Criswell, 1999). A short questionnaire was sent to all 50 state DOT's asking the deflection that was allowed, the method used in calculating the deflection distribution factor, and how the state's code differed from AASHTO, if at all. While only 11 states responded to the survey, it is clear that Missouri is in the minority with its conservative deflection criteria. Of the 11 responses, 8 states use the AASHTO code as their deflection policy. Two states, Illinois and Arkansas, are actually slightly less conservative than AASHTO. Illinois uses the deflection limits only on pedestrian bridges, and Arkansas uses a moment distribution factor of S/7.0 for non-pedestrian bridges. Of the respondents, only Iowa has a slightly more conservative approach than AASHTO, and its only difference is that it may use a limit of L/1000 on some "special bridges" that are non-pedestrian. MoDOT was alone in using a different (and more conservative) live load deflection distribution factor than AASHTO.

4.1.4 Ontario Bridge Code

While not widely used in bridge design in the United States, the Ontario Highway Bridge Design Code (1983) is an important resource in determining the serviceability of a bridge. The Ontario Bridge Code does not limit the deflection based directly on span length. Instead, Section 2-6.2 explains that the deflection is limited as a function of the bridge's natural frequency, which depends not only on span length, but also the bridge's stiffness and weight. Allowable deflections are smaller for higher resonant frequencies. The Ontario Code also breaks bridges into three categories: bridges with sidewalks and

high pedestrian use, those with sidewalks and little pedestrian use, and those without sidewalks. Bridges with heavy pedestrian use are allowed less deflection than those with little pedestrian use, which in turn are allowed less deflection than a bridge with no sidewalk. The limits are shown in the Ontario Bridge Code in a graph shown as Figure 4.1.

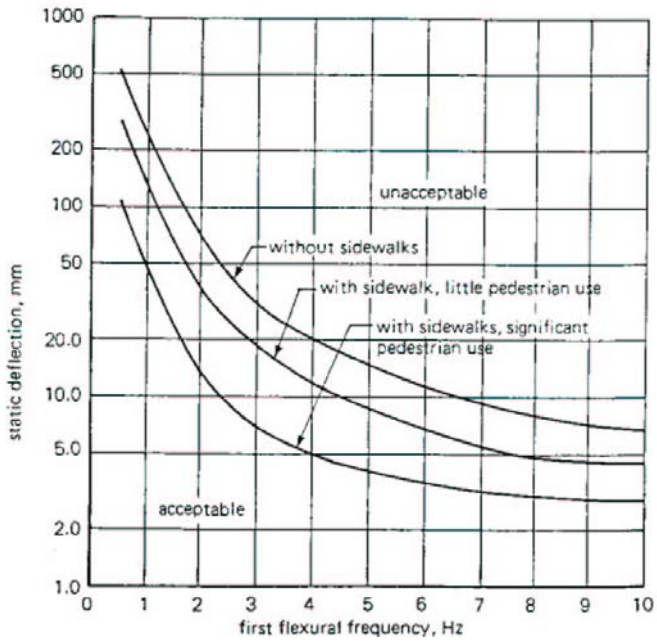

Figure 4.1 – Ontario Bridge Code Allowable Deflection Chart (Ontario, 1983)

To use the graph, the designer must be able to estimate the first natural frequency of the bridge, which is the frequency that dominates the vibration of the bridge. This is accomplished by finding the base frequency of the bridge. The base frequency can be found using the equation (Billing, 1979)

$$f_b = \frac{\pi}{2L^2}\sqrt{\frac{EI}{m}} \tag{4.3}$$

Where,

L = Longest Span Length

E = Young's Modulus of Elasticity

I = Moment of Inertia

m = mass per unit length

The resonant frequency is a ratio, depending on the ratio of span lengths, of this base frequency. For example, if a two-span bridge has one span half as long as the other, the first resonant frequency is 1.282 times the base frequency. If the two spans are equal in length, the first resonant frequency equals the base frequency. The frequency of other modes of resonance is also a factor of the base frequency. The modal frequency factors for a two-span beam, such as Bridge A6101, are shown in Table 4.1.

A structure exhibits multiple modes of resonant frequency because of the characteristics of a bridge system. A two span bridge, such as Bridge A6101, exhibits two major resonant frequencies, but also has other resonant frequencies that exist and do not play as large of role in the bridge deflection. The first two modes of resonant frequency cause deflection shapes as illustrated in Figure 4.2.

Table 4.1 – Modal Frequency Factors for Two-Span Beam (Billing, 1979)

Span Ratio L_2/L_1	Mode 1	2	3	4
0.40	1.318	4.339	7.584	10.364
0.45	1.300	4.210	6.426	10.015
0.50	1.282	4.000	5.593	9.828
0.55	1.264	3.677	5.100	9.672
0.60	1.245	3.290	4.844	9.482
0.65	1.226	2.918	4.703	9.162
0.70	1.206	2.594	4.610	8.574
0.75	1.183	2.322	4.536	7.792
0.80	1.156	2.098	4.467	7.026
0.85	1.126	1.915	4.393	6.359
0.90	1.090	1.768	4.300	5.806
0.95	1.048	1.652	4.174	5.373
1.00	1.000	1.562	4.000	5.062

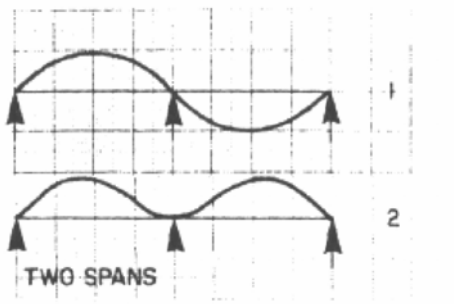

Figure 4.2 – 1st and 2nd Resonant Frequency Mode Shapes for Two-Span Beam (Billing, 1979)

If the bridge is already built, it is possible to find an accurate natural frequency using experimental methods. To find the natural frequency, the different modes must be excited by some kind of introduced vibration. If acceleration measurements are taken during free vibration, a Fast Fourier Transform can translate the acceleration and time to frequency and power. The power of each frequency can then be plotted, and the resonant frequency occurs where there is a spike in the power vs. frequency graph. Different spikes refer to the different modes of resonant frequency.

4.1.5 Effect of Serviceability Criteria on HPS Bridges

In most typical structures using the AASHTO deflection criteria, the deflection limitations do not control the design. In a conventional steel girder bridge, the cross section of the girders is designed for the required strength, and the resulting bridge is usually stiff enough that the deflection limits are satisfied. However, recent advances in steel production may increase the role that serviceability has in bridge design.

High Performance Steel (HPS) is a recent development in steel production. The most common HPS steel used in bridges at this time is HPS70W. HPS70W refers to steel with a yield strength of 70 ksi, compared to the steel used in conventional bridges that

has a yield strength of 50 ksi. Because of the added strength of the steel, a smaller HPS girder cross section can be used to carry the same load as a conventional steel girder. HPS is more expensive, however, so it is not practical to make an entire girder out of HPS, even with the savings in material weight. Past research (Barker, 2000) has found that in order to gain the most benefit, HPS should be used only in the high stress areas, namely the bottom flange in the positive moment composite section, and both flanges in the negative moment non-composite area. The web and other low stress areas are made using conventional 50 ksi steel. Using HPS in a hybrid design takes advantage of both the smaller HPS cross section and the less expensive conventional steel.

In using less material, however, the stiffness of the girder, and therefore the bridge, is less than the stiffness of a bridge with the larger conventional steel cross section. This reduction in stiffness results in an increase in live load deflection. If a bridge is designed using the AASHTO code, this increase in deflection is usually still allowable. But it is a concern that if the designer imposes more conservative serviceability criteria, as MoDOT does, the HPS girders would not meet allowable deflections. The HPS girder would then need to use a larger cross section to increase the stiffness. Therefore, if deflection controls the design of the bridge as opposed to strength, the advantage of using a hybrid HPS girder is not realized.

4.2 SERVICEABILITY FIELD TESTING PROCEDURES

On August 18, 2002, the University of Missouri Bridge Field Test Team arrived at Bridge A6101 near Lexington, Missouri, for the purpose of field testing the strength and serviceability performance (Davis, 2003). Instrumentation and preparation for the field

testing took two days to complete, and actual testing began on August 20th. Chapter 3 describes the field test system. The following sections detail the serviceability field testing preparation and procedures.

4.2.1 Loading System

The serviceability testing of Bridge A6101 was completed for the most part using the same equipment as for the strength testing described in Chapter 3. The lone difference is that, for the acceleration portion of field testing, it was a concern that the load truck would not excite the bridge adequately. The road approaching the bridge had not been completed at the time of testing, so the truck did not have adequate space to gain speed or brake. In order to ensure adequate vibration, the field test team obtained the services of the construction supervisor to drive a backhoe across the bridge, as the backhoe accelerates and brakes much quicker than the load truck. The backhoe used is pictured in Figure 4.3.

Figure 4.3 – Side View of Backhoe

4.2.2 Data Acquisition System

The data acquisition system used for collecting the serviceability data is also largely identical to the equipment discussed in Chapter 3, including the data acquisition RV and the data acquisition boxes. However, additional instrumentation was installed for deflection and acceleration measurements. String pots and a laser deflection device measured the vertical deflection of the girders, and accelerometers measured the acceleration of the bridge. Details on the placement of the instruments are included in the following sections.

4.2.2.1 String Pots

In order to measure the vertical displacement of each girder, variable resistors in the form of string pots were placed under the bridge. To avoid confusion, girders were labeled, with the north exterior girder being Girder 1 and increasing in number up to the south exterior Girder 5. A string pot was placed directly below the 4/10 point of each girder, or 55.1 ft from the East bearing support, as illustrated in Figure 4.4. To avoid any accidental movement, the string pots were anchored to the ground by sections of steel cut from an I-beam. Fishing line ran from the string pot to the bottom flange of the girder, where the line was clamped to avoid slippage. A close-up of an individual string pot is shown in Figure 4.5.

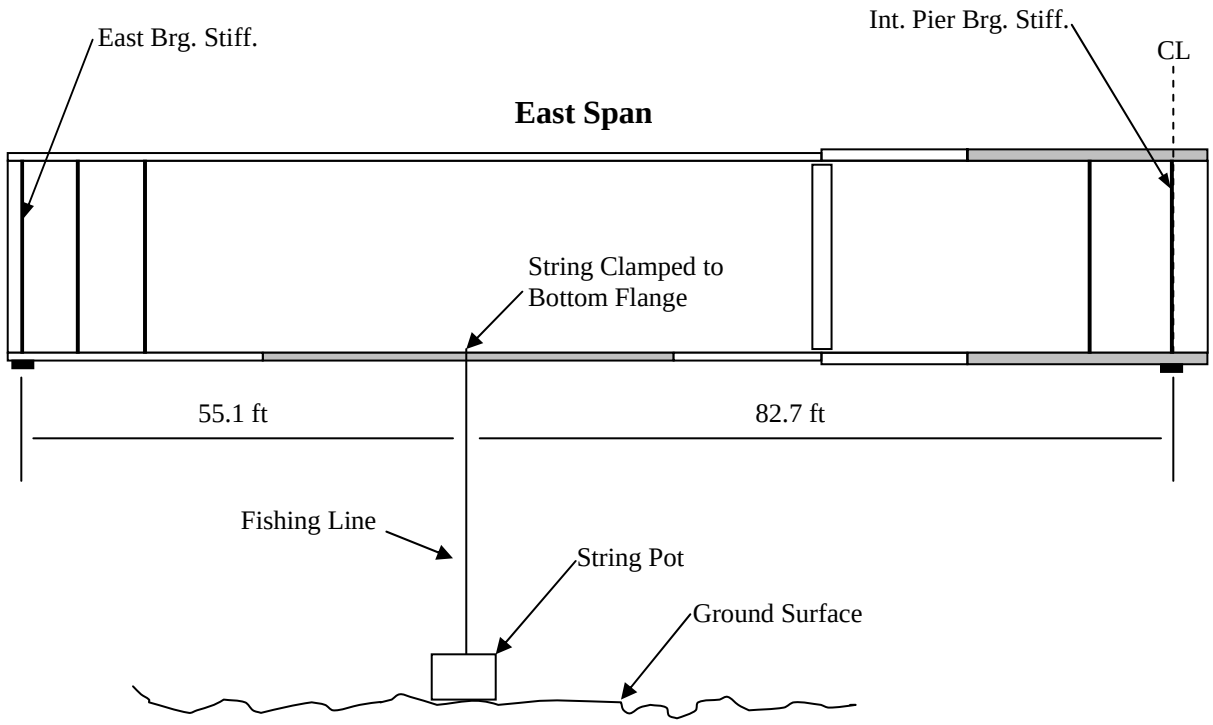

Figure 4.4 – String Pot Placement (Girders 1 – 5)

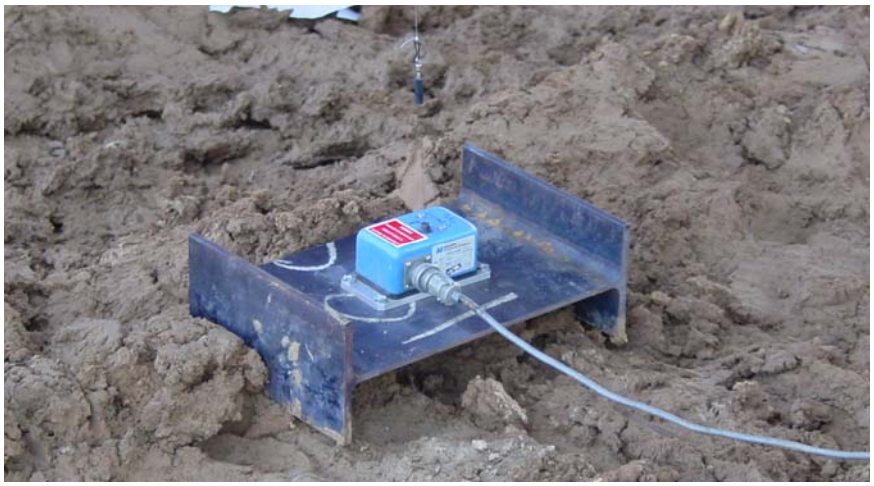

Figure 4.5 – Close-up of String Pot on Ground

4.2.2.2 Laser Deflection Device

In addition to the string pots, a laser deflection system developed by the University of Missouri-Columbia's Department of Civil Engineering was used to measure deflections of Bridge A6101. The laser deflection device was placed on the bottom flange of Girder 2 at a position 55.1 ft from the East bearing support. The system works by placing a Helium-Neon gas laser on a tripod at a reasonable distance from the bridge. The laser is aimed at the deflection device, which has two phototransistors mounted on a high helix screw. The laser acts as a reference point as the bridge deflects. In its initial position, the two transistors receive an equal amount of light from the laser. As the bridge deflects and moves the entire deflection device, one transistor catches more light than the other, causing a voltage difference. This voltage difference causes a servomotor to turn the helix screw, which turns the shaft and raises or lowers the transistors to keep the voltage difference at zero. The amount the phototransistors move equals the deflection. A more detailed discussion on the laser deflection system can be found in Imhoff (1997) and Schrage (1998). The setup of the laser deflection system is illustrated in Figure 4.6. Figure 4.7 shows the laser and tripod and Figure 4.8 shows the laser deflection device in position on Girder 2.

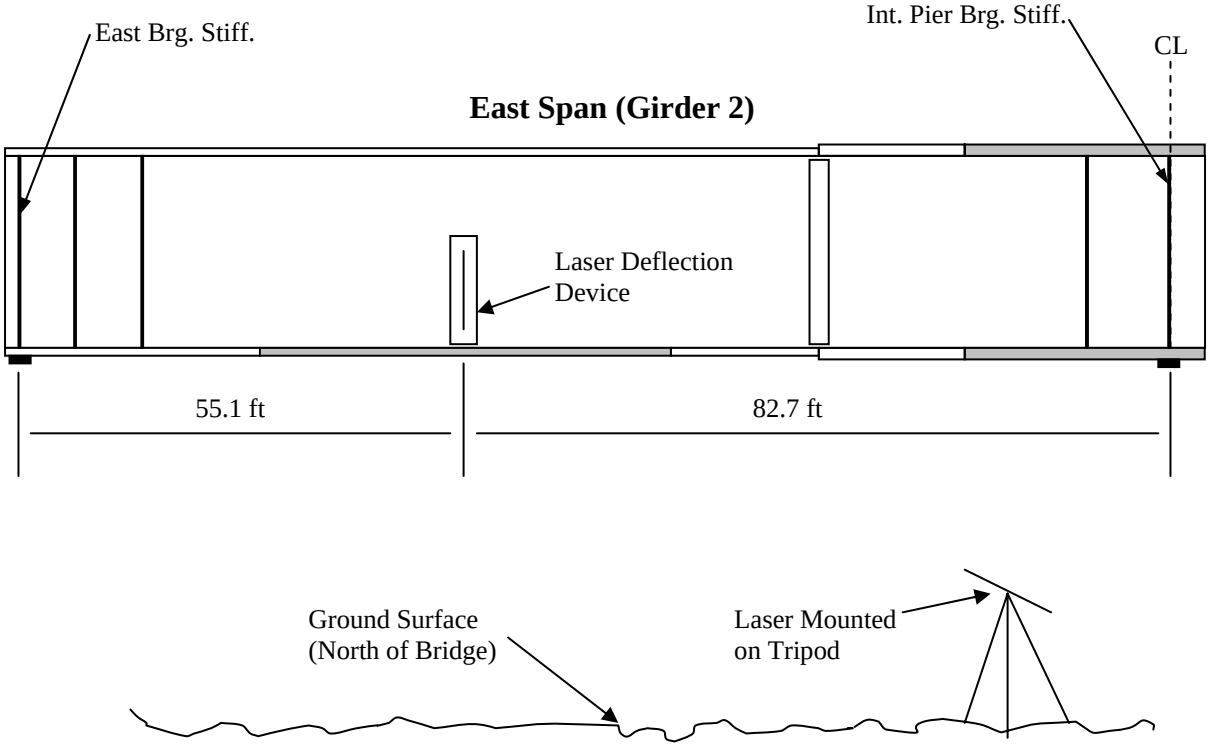

Figure 4.6 – Laser Deflection Device Setup (Girder 2 only)

Figure 4.7 – Laser Mounted on Tripod

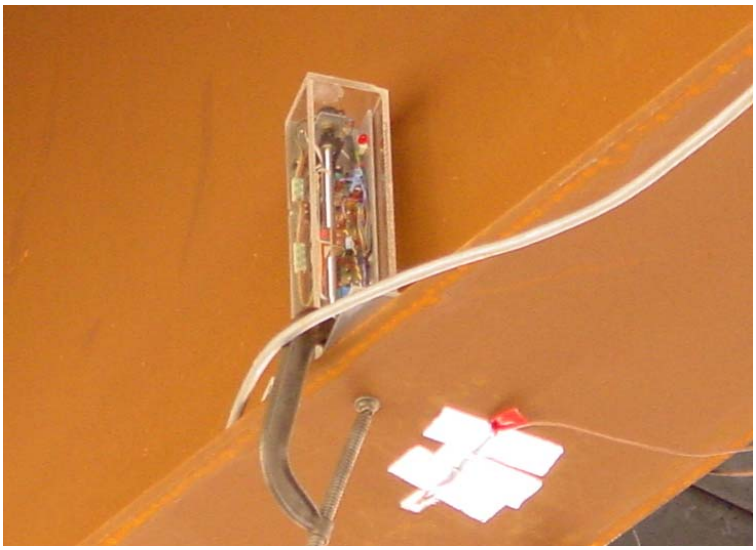

Figure 4.8 – Laser Deflection Device in Position on Girder 2

4.2.2.3 Accelerometers

Vibrations of Bridge A6101 were measured with accelerometers that were placed 55.1 ft from the East bearing support on Girder 2 and Girder 3, as shown in Figure 4.9. The accelerometers were clamped to the bottom flange. The bridge was excited and the accelerometers measured the girder vibrations in terms of accelerations. The natural frequencies of the structure can be found through examination of the accelerations in the bridge after the load excitation and the bridge is in free vibration.

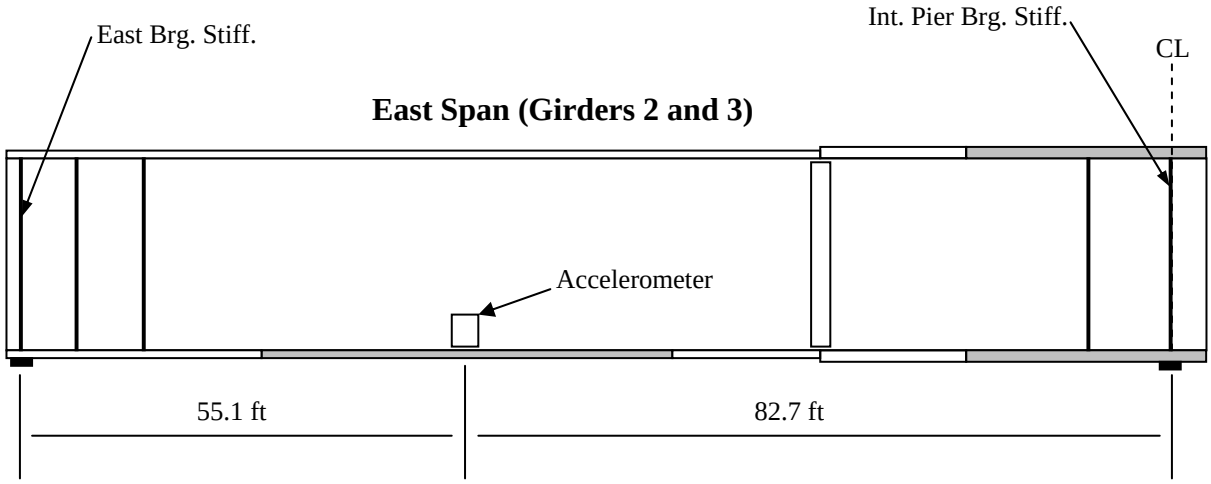

Figure 4.9 – Accelerometer Placement (Girders 2 and 3)

4.3 SERVICEABILITY FIELD CONDITIONS

Bridge A6101 itself had just been completed, so it was in new condition. Route 224, which the bridge carries, however, was unpaved. The area of the road just past the approach slab on both sides of the bridge was gravel. The west approach had reinforcement in place so that vehicles had to drive to the side of the road and make a sharp turn onto the bridge. The east approach did not have reinforcement in place, but had a ramp on only the north lane to get on the bridge. This did not affect the deflection procedure, but it did affect the acceleration testing as explained in Section 4.5. Dimensions of the girders were measured in order to compare to the design. The measured dimensions were slightly larger than the design dimensions due to construction tolerances. The measured dimensions of the girder cross section are shown in Figure 4.10.

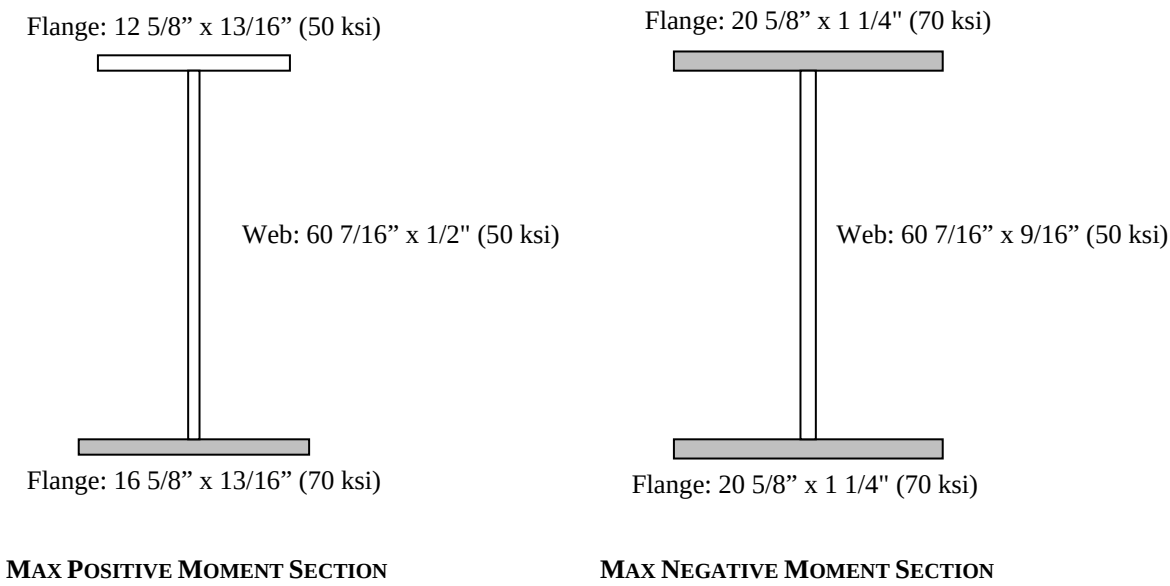

Figure 4.10 – Measured Dimensions of Girder Cross Sections

4.4 DEFLECTION TESTING PROCEDURE

Live load static deflection testing of Bridge A6101 was accomplished by running the load truck on the bridge at “crawl” speed, as described in Chapter 3. Deflection data was collected from the string pots and laser device during the same 12 test runs performed for the strength performance testing discussed in Chapter 3.

Immediately after static deflection testing, the field test team measured the load truck’s wheel weights using the weighing pads, as explained in Chapter 3. An accurate measurement of how the truck’s weight is dispersed is important for calculating an estimated deflection, and for comparing the load truck to an HS20 loading. The wheel weights measured are illustrated in Figure 3.9.

4.5 ACCELERATION TESTING PROCEDURE

In past field tests conducted by the University of Missouri Bridge Field Test Team, the dynamic loading was accomplished by driving the load truck at various speeds across the bridge (Imhoff, 1998). Past testing has also shown that the truck needs to be traveling at least 25 mph to correctly place a dynamic load on the bridge. As explained earlier, this was not possible on Bridge A6101 because of the placed reinforcement just past the west approach slab. While the east approach had a clear path for the truck to gain speed, the approach slab on the west side did not provide enough braking area. In order for the truck to stop without going off the west approach slab, the truck either had to be going slower than 25 mph, or had to begin braking before the approach slab which places unwanted horizontal loading on the bridge. Since additional horizontal forces interfere with the vertical free vibration trying to be obtained, the truck was driven slower than 25 mph. A few attempts were made with the truck, but there was concern that the bridge was not being excited enough to determine natural frequencies.

The solution to the problem for exciting the bridge was for a backhoe that was onsite for construction purposes to supply the excitation for the acceleration testing. The backhoe was able to brake much quicker than the load truck, so it was able to go across the bridge at a higher speed and still be able to stop on the west approach slab. Although it was not equipped with a speedometer, the test team estimates the backhoe reached at least 25 mph. Also, the conditions at the east end of the bridge and the behavior of the backhoe were perfect for inducing vibrations in the bridge. The ramp to go on the East approach slab somewhat launched the front tires of the backhoe in the air. Since the backhoe's bucket is behind the back wheels, the backhoe sort of balances on the back

wheels. This caused the front wheels to bounce repeatedly while going across the bridge, inducing even more vibration. Figure 4.11 illustrates how much the front wheels left the surface.

Figure 4.11 – Front Tires of Backhoe Bouncing on Surface of Bridge

While not entirely possible, because the ramp was to the side of the bridge, the backhoe passed over the bridge in a transverse position close to that of Run 4 from the deflection runs. Run 4 is a prime position to vibrate both Girders 2 and 3, which were instrumented with the accelerometers. The backhoe would go over the bridge, careful not to brake until completely off the bridge so that horizontal forces were not introduced. Data was collected while the backhoe made its pass, and measurements continued until the vibrations were insignificant, which took between 20 and 30 seconds after the backhoe had passed. Several passes were made to ensure a clean vibration would be

recorded. The backhoe's dimensions and weight distribution were then measured and are illustrated in Figure 4.12.

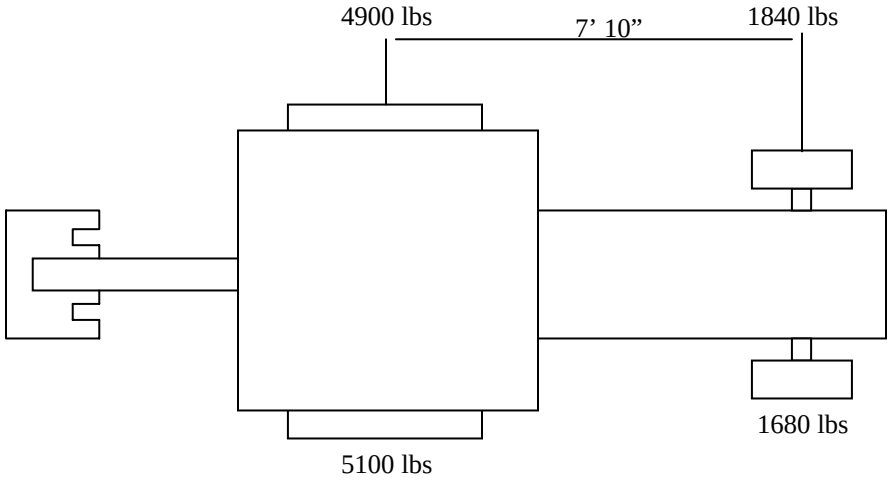

Figure 4.12 – Backhoe Testing Wheel Weights

4.6 SERVICEABILITY MEASUREMENT EQUIPMENT PERFORMANCE

A large amount of data was collected during the field test of Bridge A6101, including data from string pots, the laser deflection device, and the accelerometers. This data must all be confirmed before being used in conclusions. Several methods of verifying the data exist. Patterns in the data can be examined, for example deflection should be maximized in the girder that the truck wheels are nearest. Different measurements can also be compared, for example between the laser device and the string pots. The measured values can also be established by comparing them to predicted values from computer software analysis. Finally, repetition and consistency of measured values can validate accuracy. The data from all measuring devices used in the field test is proven accurate or inaccurate in the following section.

4.6.1 String Pot Performance

The string pots measure deflection as a change in voltage as the string is pulled out of the device. The voltage difference is then multiplied by a calibration factor to find the deflection in inches. When plotted versus time, the string pot data should show a maximum downward deflection as the truck passes over span one, a smaller upward deflection as the truck passes over span two, and should level out at near zero while the truck pauses on the West approach slab. As the truck makes its pass in reverse, the girder should behave the same, that is a slight upward deflection while the truck is on span two, a larger downward deflection for span one, and level out back at zero at the end of the test run. An example of the data taken by the string pots is shown in Figure 4.13, which is data taken during Run 3.

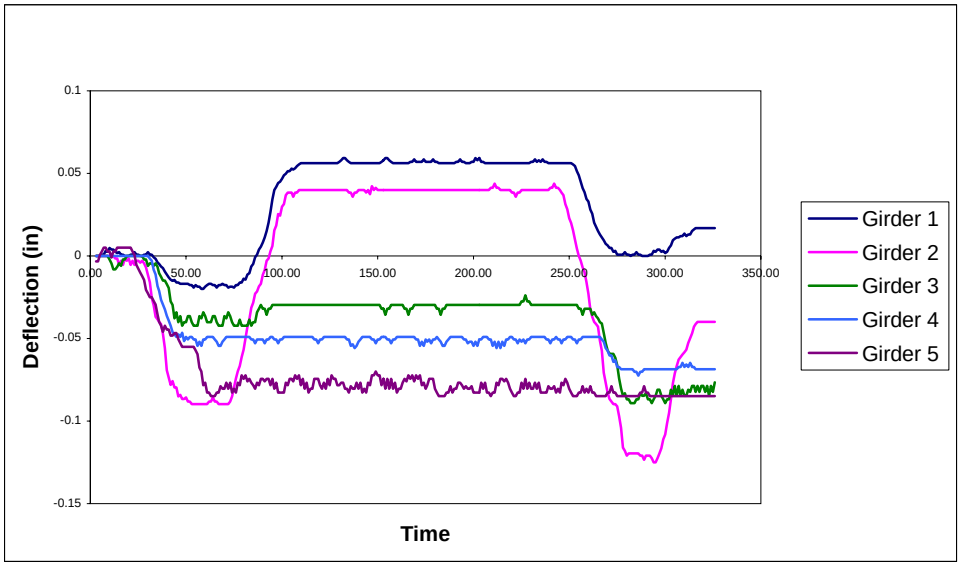

Figure 4.13 – String Pot Measurements for Load Test Run 3

It is easy to see that the string pots did not work properly. Most of the string pots run flat and just show noise for most of the test. Run 3 is still relatively close to the north edge of the bridge, so Girder 2 should display the greatest deflection, with Girders 1 and 3 close behind. Girder 4 should have the next highest deflection, and Girder 5 should see very little deflection at all. However, the graph shows that Girders 2 and 5 have the highest deflection, followed by Girder 4, then Girder 3, and finally Girder 1 with the least deflection. Another verification that the data is corrupt is that none of the string pots measure a deflection near zero while the truck is off the bridge either at the middle of the test, or at the end of the test. Finally, the deflections of Girder 2, which should be approximately equal to the values measured by the laser deflection device, which are discussed in the next section, are not even close. The other truck runs show similarly erroneous results.

Unfortunately, the string pots cannot be used for any comparisons or conclusions in this research. The reason for the string pot failure is not known. While every effort was made to keep the string pots out of the elements, it is possible that the electronics could have been exposed to moisture during the inclement weather during the tests.

4.6.2 Laser Deflection Device Performance

Using the same procedure as the string pots, the laser deflection device data is plotted vs. time in order to verify results. Figure 4.14 is an example of one of these plots; it is the data taken during Test Run 3, the same run as shown in the string pot example plot. Note that in this plot, the deflection of Girder 2 behaves appropriately. It deflects downward when the load truck is on Span 1, slightly upward when the truck is on Span 2, and has periods at the middle and end where the deflection is very close to zero because

the truck is not on the bridge. The other test run data had similarly successful results, so it is evident that the laser deflection device performed its duties very well.

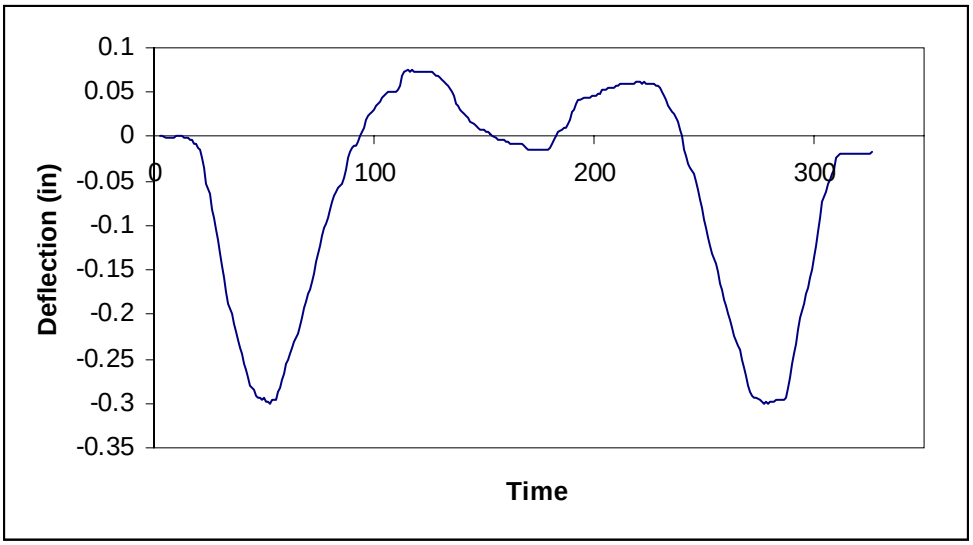

Figure 4.14 – Laser Deflection Device Measurements for Load Run 3

However, just before run 9, the laser deflection device stopped taking measurements. This can most likely be attributed to the laser moving off of the sensors. For Runs 1 – 8, the largest deflection measured was picked out of the data, making sure to use the values while the load truck was on Span 1. This value should represent the maximum deflection of Girder 2 for the load truck while at the transverse positions of the test runs. The maximum deflections of Girder 2 for Test Runs 1 – 8 are listed in Table 4.2, with a negative value representing downward deflection. The values are largest for Runs 1, 2, and 3, where the load truck is near over Girder 2, and decrease steadily the further the truck is from Girder 2.

Table 4.2 – Maximum Deflection of Girder 2 Measured by Laser Deflection Device

Load Truck Position	Maximum Deflection (in)
1	-0.310
2	-0.308
3	-0.300
4	-0.271
5	-0.243
6	-0.230
7	-0.209
8	-0.190
9	-
10	-
11	-
12	-

4.6.3 Accelerometer Performance

While testing Bridge A6101, the field test team was unable to get the accelerometer placed on Girder 3 to produce a signal. The other accelerometer that was on Girder 2 was working well, so data was collected only from it. As was mentioned earlier, several testing runs were done with both the truck and the backhoe. The run that produced the largest, cleanest vibrations in the bridge, which was made with the backhoe during Backhoe Run 6, is the data used in this report (Davis, 2003).

Acceleration data was recorded every hundredth of a second. A process of smoothing was used to make the information easier to read. The smoothing process was simply to take a weighted average of a data point and the points directly above and below it. The smoothing process was completed twice to produce Figure 4.15.

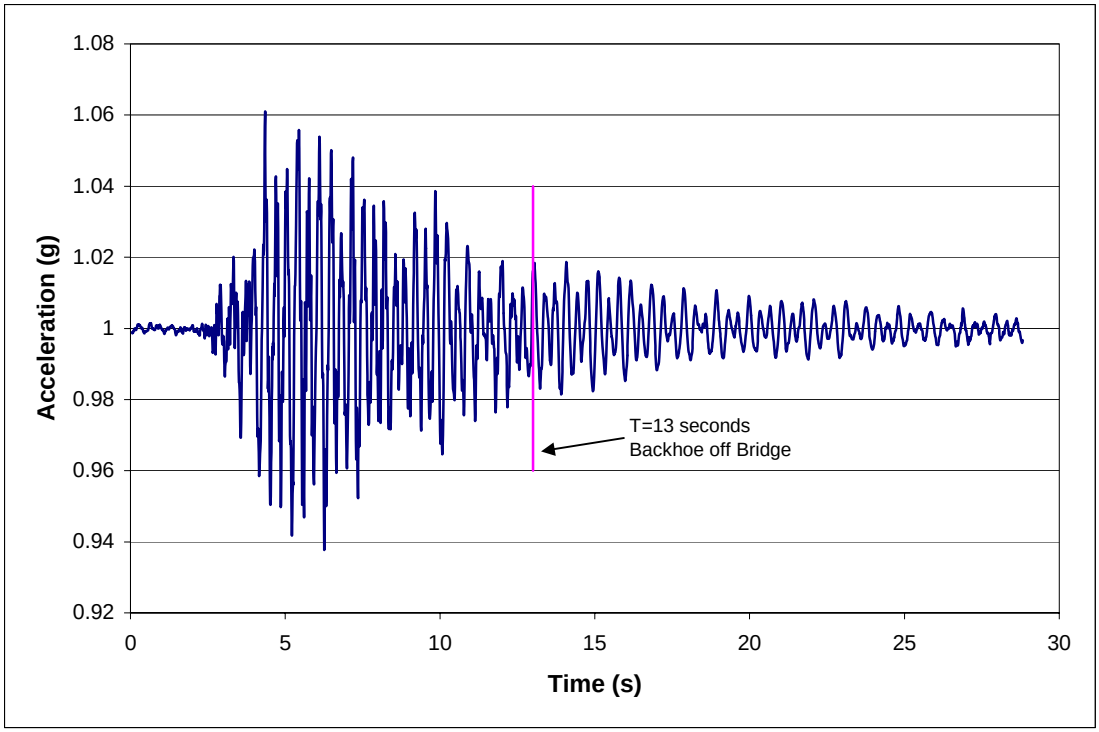

Figure 4.15 – Girder 2 Accelerometer Data for Backhoe Run 6 (smoothed twice)

Very little vibration was detected before the backhoe reached the bridge, and then relatively large vibrations were measured while the backhoe was on the bridge. It is also possible to see when the backhoe had completed its pass and was off the bridge. While the backhoe is on the bridge, vibrations are large and jagged, and are not very uniform. At about 13 seconds into the test, the vibrations become much more regular and show a steady decline caused by damping. It can also be observed that the bridge is vibrating in at least two modes because the measurements after 13 seconds are not completely regular and vary in amplitude. It is this data that is taken after the backhoe is off the bridge that is used in later sections to find the 1st and 2nd natural resonant frequencies of Bridge A6101.

4.7 ABAQUS FINITE ELEMENT MODEL

In addition to comparing deflection measurements to the design deflection of the girder, a Finite Element Model of the bridge was conducted by Wu at West Virginia University (2003). The model was designed using Abaqus modeling software, and is a solid model that incorporates the conditions in the field, including the skew and parapet. Just as in the actual testing, a model of the load truck with the same wheel weights made 12 analytical test runs at varying transverse distances. The transverse positions of the truck in the model also matched the actual test runs. Data was collected on the deflection of all five girders during each run. In theory, the maximum deflection of the girders in the Abaqus model should match the measurements taken by the string pots and the laser device. However since the string pots malfunctioned, only the laser deflection device can be compared. The maximum deflection of each girder in the solid model for each run is listed in Table 4.3. As before, the deflections predicted by the Abaqus FEM are shown where a negative value represents a downward deflection.

Table 4.3 – Abaqus FEM Maximum Predicted Deflections for All Girders

Testing Truck Locations	Girder Deflection (in)				
	1	2	3	4	5
1	-0.5033	-0.3443	-0.1892	-0.06516	-0.03891
2	-0.4106	-0.3347	-0.2174	-0.1071	-0.01088
3	-0.2944	-0.3029	-0.2536	-0.1659	-0.08267
4	-0.2707	-0.2921	-0.2602	-0.1796	-0.1
5	-0.2141	-0.2617	-0.2713	-0.2145	-0.1458
6	-0.1966	-0.2509	-0.2732	-0.2262	-0.1617
7	-0.1292	-0.2048	-0.2706	-0.2732	-0.2323
8	-0.111	-0.1913	-0.2668	-0.2861	-0.2546
9	-0.07046	-0.16	-0.2537	-0.3122	-0.3111
10	-0.05205	-0.1453	-0.2445	-0.3218	-0.34
11	0.013584	-0.09142	-0.2106	-0.3461	-0.455
12	0.037981	-0.07073	-0.1966	-0.3493	-0.5016

The deflections estimated by the Abaqus solid model appear to be valid, as the deflections for each girder is maximized by a run that places a wheel line close if not directly on top of it. Figure 4.16 illustrates this by showing that Girders 1 and 2 show decreasing deflection with increasing truck position, while Girders 4 and 5 exhibit increasing deflections for higher truck position. The deflection of Girder 3 changes very little for all truck positions. Also, it appears that the total deflection of the bridge for each run is relatively equal to that of other runs.

More evidence that the FEM is an accurate portrayal of Bridge A6101 is found when comparing the predicted deflection of Girder 2 to the deflections measured by the laser deflection device. Table 4.4 compares the predicted and measured deflections, and Figure 4.17 shows the similarities graphically.

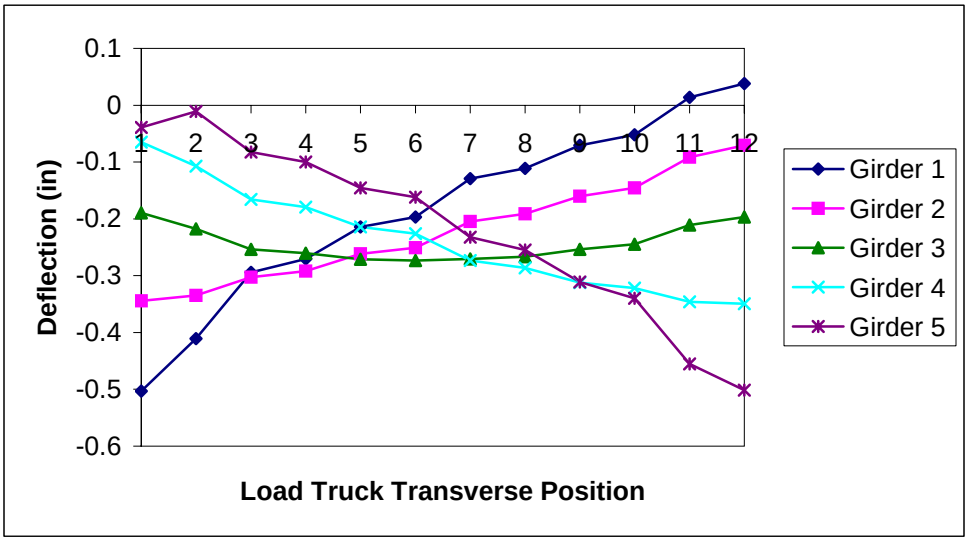

Figure 4.16 – Abaqus FEM Predicted Deflections

Table 4.4 – Girder 2 Deflection Comparison

Load Truck Position	Measured Laser Deflection (in)	Abaqus Predicted Deflection (in)	% Off Laser Measurement
1	-0.310	-0.344	11.06%
2	-0.308	-0.335	8.67%
3	-0.300	-0.303	0.97%
4	-0.271	-0.292	7.79%
5	-0.243	-0.262	7.70%
6	-0.230	-0.251	9.09%
7	-0.209	-0.205	-2.01%
8	-0.190	-0.191	0.68%
9	-	-0.160	
10	-	-0.145	
11	-	-0.091	
12	-	-0.071	

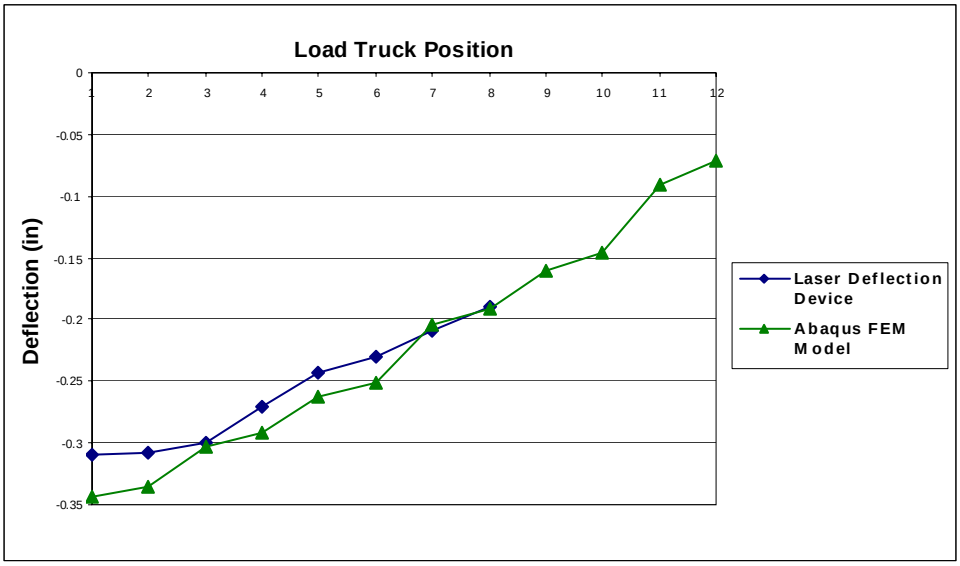

Figure 4.17 – Measured and FEM Predicted Deflection Comparison

Because the Abaqus predicted deflections closely match the deflections measured by the laser device, with all but one within 10%, it can be assumed that the laser device would match the model for the rest of the test runs as well. Also, since the string pots did

not work, another method of obtaining an "equivalent" measured deflection is needed. The accuracy of the Abaqus FEM in predicting Girder 2 deflections shows that the rest of the girder predictions should also be accurate. Furthermore, as almost all the deflections predicted by Abaqus are slightly larger than the laser device measurements, this assumption should be slightly conservative. Therefore, the "measured" deflection of Bridge A6101 will refer to the Abaqus FEM deflections for the rest of this report. While the laser deflection device measurements could be used for Girder 2, the Abaqus model will still be used for uniformity.

4.8 MEASURED DEFLECTION RESULTS

The deflections found by the Abaqus model can now be used to compare the measured deflections to the deflections used for AASHTO and MoDOT design procedures. The deflections from each run must be superimposed and analytically factored to produce a total girder deflection for an HS20 truck loading. The following sections contain information about the calculation of the girder deflections, and how the resulting deflections compare to MoDOT and AASHTO live load deflection criteria.

4.8.1 Conversion of Field Test Load Truck Deflection to HS20 Deflection

While the live load deflection criteria for both MoDOT and AASHTO use an HS20 vehicle, the measured deflections are caused by the field test load truck, which is much lighter than the HS20 and has slightly different axle spacing. Consequently, the measured deflections need to be factored to an equivalent HS20 deflection. This is accomplished by multiplying the measured deflection by a constant that equals the ratio

of the HS20 analytical estimated deflection divided by the load truck estimated analytical deflection, or

$$HS20em = (HS20p / LTp) * LTm \tag{4.4}$$

Where,

HS20em = HS20 Truck Equivalent Measured Deflection

HS20p = Predicted HS20 Deflection

LTp = Predicted Load Truck Deflection

LTm = Measured Load Truck Deflection

To calculate the predicted deflections of an HS20 truck and the load truck on Bridge A6101, SIMON (AISC, 1996) was again utilized, this time using the measured dimensions of the bridge. Also, for these SIMON runs, the full depth of the slab was used for the effective slab depth, and the effective slab width was calculated from that value. Other assumptions such as loads and distribution factors remained the same as discussed earlier in Chapter 2. These SIMON runs should represent the conditions of Bridge A6101 at the time of testing. It does not matter which deflection distribution factor is used, either MoDOT or AASHTO, because the ratio of HS20 / LT would remain the same. As SIMON automatically uses the AASHTO deflection distribution factor, the predicted deflections will also use AASHTO.

SIMON already contains a loading condition for HS20 trucks so nothing needs to be added as load. The load truck, however, must be input manually into SIMON. The wheel weights of the load truck, measured during the field test, are added together in

pairs to make axle weights. The axle weights and the distance between the axles is then input into SIMON. Figure 4.18 illustrates the axle weights of the user defined load truck.

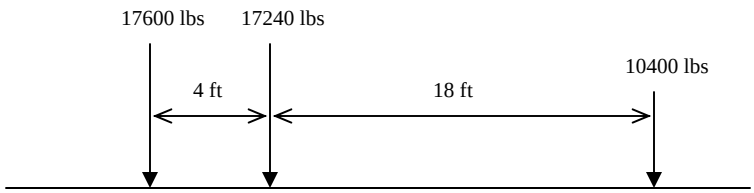

Figure 4.18 – User Defined Load Truck Axle Weights

The resulting live load deflection found by SIMON for an HS20 loading for the measured dimensions of Bridge A6101 is 1.363 in. For the user defined load truck, SIMON finds a live load deflection of 0.70 in. The ratio to be used to find an equivalent HS20 measured deflection from the load truck measured deflection is then

1.363 in / 0.70 in = 1.947

4.8.2 Load Combinations

The measured deflections must be combined in a way that represents AASHTO or MoDOT design methods. For each girder, several combinations must be checked. In general, the critical load combination for each girder is to use the deflection found with one of the truck's wheel lines close to if not on top of it. Then the deflection found from the closest truck positions possible in the other traffic lanes is added to find the maximum total deflection of the girder. As MoDOT uses 10 ft lanes instead of the 12 ft lanes used by AASHTO, there are some differences in the loading combinations that must be

checked. This is most evident by examining the exterior girders. The critical combination for each exterior girder is when a truck is in each traffic lane and is as far to the outside of the bridge as possible. However, because the lanes are wider in AASHTO than in MoDOT, there must be more space between trucks since the trucks must fully fit inside the traffic lane. Also, as discussed earlier, Bridge A6101 actually has four MoDOT traffic lanes as it was designed as a metric bridge with 3 m (9.9 ft) wide lanes. The difference in critical loading positions for exterior Girder 1 is shown in Figure 4.19.

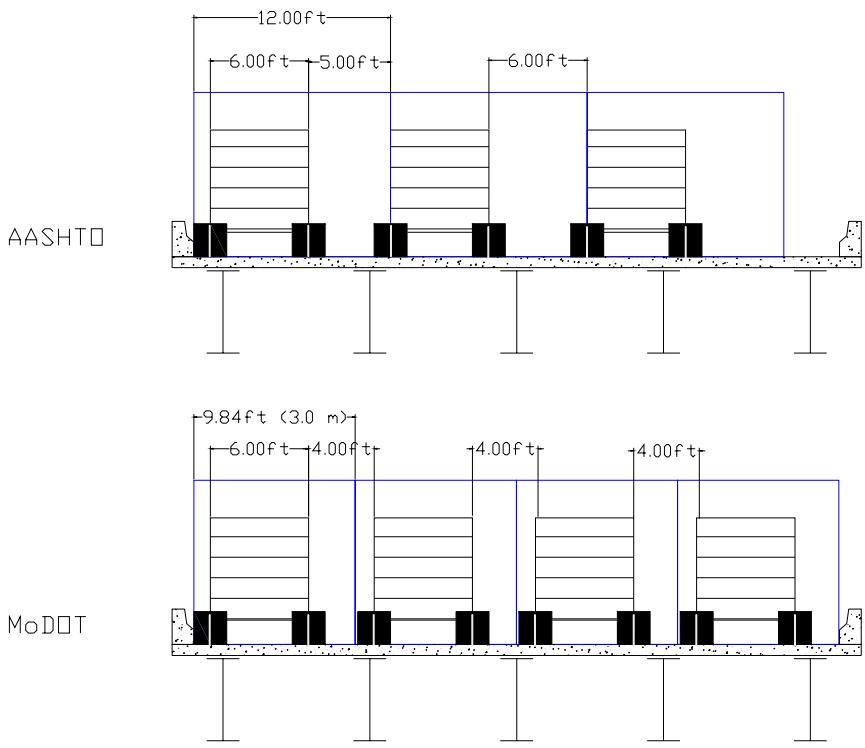

Figure 4.19 – Comparison of AASHTO, MoDOT Girder 1 Critical Loading

Similarly, the critical truck positions can be found for the other girders. The positions can then be matched to the corresponding field test transverse truck position. The critical loading combinations that need to be checked for each girder are listed in

Table 4.5. All the load combinations in the table must be checked in a manner reflecting either the MoDOT or AASHTO standards.

Table 4.5 – Possible Load Combinations for Bridge A6101

Girder	Load Truck Field Test Transverse Position	
	AASHTO Load Combinations	MoDOT Load Combinations
1	1,4,10	1,4,9,12
2	1,4,10	1,4,9,12
	2,6,10	2,6,10
3	3,8,12	3,8,12
	1,5,10	1,5,10
		1,4,9,12
4	3,7,11	4,9,12
	3,9,12	3,7,11
		1,4,9,12
5	3,9,12	1,4,9,12

4.8.3 AASHTO Measured Girder Deflections

Using the load combinations discussed in the previous section, the total maximum measured girder deflections can be found. However, the load combinations must be broken down even further to find the maximum deflection. One, two, or three load truck positions could maximize each girder, as an upward deflection is possible if the load truck is on the opposite edge of the bridge than the girder. Also, as in the AASHTO design procedures, a deflection found with three load truck positions is multiplied by an intensity reduction factor of 0.90. Therefore, each AASHTO critical load combination actually has three loading scenarios to be checked. For instance, Girder 1 could be maximized by Load Truck Position 1 only, Load Truck Position 1 and 4 together, or by 0.90 times the sum of Load Truck Position 1, 4, and 10. The resulting maximum measured deflection of each girder is then multiplied by the HS20/Load Truck Ratio,

1.947, to find the equivalent measured maximum girder deflection caused by an HS20 truck. Table 4.6 lists the AASHTO maximum girder live load deflections as well as the loading scenario that causes the maximum deflection, and also the equivalent HS20 maximum measured deflection.

Table 4.6 – AASHTO Measured Total Live Load Deflections

Girder	Controlling Truck Position Load Scenario	Load Truck Total Girder Deflection (in)	HS20/Load Truck Ratio	Equivalent HS20 Total Girder Deflection (in)
1	1+4	-0.774	1.947	**-1.507**
2	.9(1,4,10)	-0.704	1.947	**-1.370**
3	.9(3,8,12)	-0.645	1.947	**-1.256**
4	.9(3,9,12)	-0.745	1.947	**-1.450**
5	9+12	-0.813	1.947	**-1.582**

The equivalent measured HS20 deflection can be compared to the live load deflection predicted by the AASHTO design discussed in Chapter 2. In theory, the measured deflections should be approximately equal to the design deflections. Table 4.7 compares the measured and design deflections, and shows the percentage of the design value that is measured.

Table 4.7 – AASHTO Measured, Design Live Load Deflection Comparison

Girder	Equivalent HS20 Total Girder Deflection (in)	AASHTO Design Live Load Deflection (in)	Percentage of Design Value
1	-1.507	-1.565	**96.3%**
2	-1.370	-1.540	**89.0%**
3	-1.256	-1.540	**81.6%**
4	-1.450	-1.540	**94.2%**
5	-1.582	-1.565	**101.1%**

All of the girders of Bridge A6101 have measured deflection within 20% of the AASHTO design live load deflection, and most are within 10%. Also, all but one measured girder deflection is less than the design deflection, and even it is only 1% higher than the design deflection. This shows that the AASHTO design procedure is a rather accurate method in maximum deflection estimation.

It should also be noted that the measured deflections are slightly conservative. While the AASHTO code states that the truck should be placed two feet away from the barrier curb, Truck Positions 1 and 12 place the wheel line one foot from the barrier. Placing the wheel line two feet away from the barrier curb would slightly decrease the measured deflection of Girders 1 and 5, and would probably make the Girder 5 measured deflection even slightly less than the design deflection.

4.8.4 MoDOT Measured Girder Deflections

Similar to AASHTO, the load combinations for the MoDOT critical deflection must be checked for various loading scenarios, except MoDOT can be controlled by 1, 2, 3, or 4 load trucks. There is also no intensity reduction factor so the total deflection is just the sum of the deflections for the controlling loading positions. Just as before, the load truck deflections are multiplied by the HS20/Load Truck Ratio to find the HS20 equivalent deflection. The MoDOT measured total deflections and equivalent HS20 deflection, as well as the loading scenario that causes the maximum deflection, are listed in Table 4.8.

Table 4.8 – MoDOT Measured Total Live Load Deflection

Girder	Controlling Truck Position Load Scenario	Load Truck Total Girder Deflection (in)	HS20/Load Truck Ratio	Equivalent HS20 Total Girder Deflection (in)
1	1,4,9	-0.844	1.947	**-1.644**
2	1,4,9,12	-0.867	1.947	**-1.688**
3	1,4,9,12	-0.900	1.947	**-1.752**
4	1,4,9,12	-0.906	1.947	**-1.765**
5	1,4,9,12	-0.952	1.947	**-1.853**

As before, the equivalent HS20 deflection can be compared to the design deflection, except this time with the MoDOT design procedures, as discussed in Chapter 2. Table 4.9 is a comparison of MoDOT measured and design deflections.

Table 4.9 – MoDOT Measured, Design Live Load Deflection Comparison

Girder	Equivalent HS20 Total Girder Deflection (in)	MoDOT Design Live Load Deflection (in)	Percentage of Design Value
1	-1.644	-2.200	**74.7%**
2	-1.688	-2.302	**73.3%**
3	-1.752	-2.302	**76.1%**
4	-1.765	-2.302	**76.7%**
5	-1.853	-2.200	**84.2%**

With MoDOT design procedures, almost all of the measured deflections are roughly 25% less than the design deflection. The closest measured deflection is still 16% less than the design value, even though the measured deflections are slightly conservative as discussed earlier. Also note that while the largest measured deflection occurs on an exterior girder, MoDOT design deflection procedures predict less deflection in exterior

girders than for interior girders. This data shows that the MoDOT design deflection may be overconservative in approximating deflections.

4.9 NATURAL FREQUENCY RESULTS

As discussed earlier in the chapter, the Ontario Bridge Code defines the allowable live load deflection as a function of the first flexural frequency of the bridge. This harmonic frequency is a result of many factors, including weight, inertia, and span length. Several methods of finding the first resonant frequency and the resulting allowable deflections are compared in this section.

4.9.1 Ontario Equation Harmonic Frequency

From Equation 4.3, the base frequency of Bridge A6101 can be found. To recall, the equation for base frequency is

$$f_b = \frac{\pi}{2L^2}\sqrt{\frac{EI}{m}}$$

As the bridge is made of more than one material, and has different cross sections for positive and negative moment regions, finding the value of the variables in the base frequency equation can be confusing. A report by J.R. Billing (1979) of the Ontario Ministry of Transportation gives some information about the determination of the more confusing variables, in particular the moment of inertia. According to Billing, the vibration caused by a vehicle is very small and there is not much slippage between the concrete deck and steel girder, so composite action should always be assumed. He goes on to say

> "For steel and concrete bridges, it has been found in some cases that the composite bending moment of inertia at the point where the deck is

ignored for design, in the negative moment region adjacent to piers, provides a good value" (Billing, 1979).

Therefore, a moment of inertia was calculated at the pier, including the concrete deck, as shown in Table 4.10. The calculated base frequency of Bridge A6101 is presented in Table 4.11. Because Bridge A6101 is symmetric, the base frequency equals the first resonant frequency.

Table 4.10 – Calculation of Negative Composite Moment of Inertia

Section	Dimensions		Centroid			Inertia	
	Base (b)	Height (h)	Area (A)	Centroid (y)	A*y	(b*h^3)/12	A*(y-Y)^2
Bottom Flange	20.625	1.250	25.78	0.63	16.11	**3**	**70845**
Web	0.563	60.438	34.00	31.47	1069.81	**10348**	**15827**
Top Flange	20.625	1.250	25.78	62.31	1606.49	**3**	**2214**
Deck	13.492	8.500	114.68	67.19	7705.23	**690**	**22935**
Reinforcement			9.01	77.94	702.22	**0**	**5583**

Girder Centroid (Y) = Sum (A*y) / Sum (A)	53.05	M. Of Inertia = Sum	**128450**

Table 4.11 – Base Frequency Calculation using Ontario Bridge Code Equation

Acceleration due to Gravity	g (ft/s^2)	32.2
PI		**3.142**
Span Length	L (ft)	**137.8**
Young's Modulus of Steel	E (ksi)	**29000**
Moment of Inertia (Composite Negative)	I (in^4)	**128450**
Composite Dead Load	w (k/ft)	0.436
Non-Composite Dead Load	w (k/ft)	1.022
Girder Weight	w (k/ft)	0.216
Total Weight	w (k/ft)	1.674
Total Mass (w/g)	m (k*s^2 / in^2)	**7.486**

Bridge A6101 Base Frequency (Hz)	$f_b = \frac{\pi}{2L^2}\sqrt{\frac{EI}{m}}$	**1.845**

Because the two spans are the same length, the first harmonic frequency of Bridge A6101 is equal to its base frequency of 1.845 Hz. This equation is very useful because it allows a designer to estimate the harmonic frequency of a bridge without performing some type of vibration analysis.

West Virginia University, using the same Abaqus FEM solid model that predicted the deflections well, also estimated the first and second resonant frequencies of Bridge A6101. The resulting first harmonic frequency was 1.83 Hz, and the second harmonic frequency was 2.88 Hz.

4.9.2 Natural Frequency by Fast Fourier Transform

The acceleration data from the field test of Bridge A6101 can also be used to find the resonant frequencies of the structure by performing a Fast Fourier Transform (FFT) on the data taken during free vibration. The FFT works by determining the power associated with each frequency found in the data. The FFT can be performed by a variety of software packages. Performing an FFT on the data using different software multiple times will ensure an accurate resonant frequency is found, as there are different forms of FFT methods. Three different FFT's will be compared in this section. The first was performed by Origin (2002) Version 7 software, which has FFT capabilities included. Another FFT was performed using Microsoft Excel, using a spreadsheet produced for examining data from earthquake accelerations (Davis, 2003). Finally, students at West Virginia University (Wu, 2003) performed another FFT analysis using the Origin (2002) software.

As shown earlier, the bridge is in free vibration after the backhoe is completely off the bridge, which happens at approximately t = 13 s. in the accelerometer data. A

FFT must use a number of data points that is a power of 2, so 1024 points of data from the accelerometer were used, which is equivalent to just over 10 seconds of free vibration data. For the two FFT's performed by the University of Missouri, one using Origin and the other Excel, the same data points were used. Figure 4.20 shows the data used in the FFT's performed at the University of Missouri.

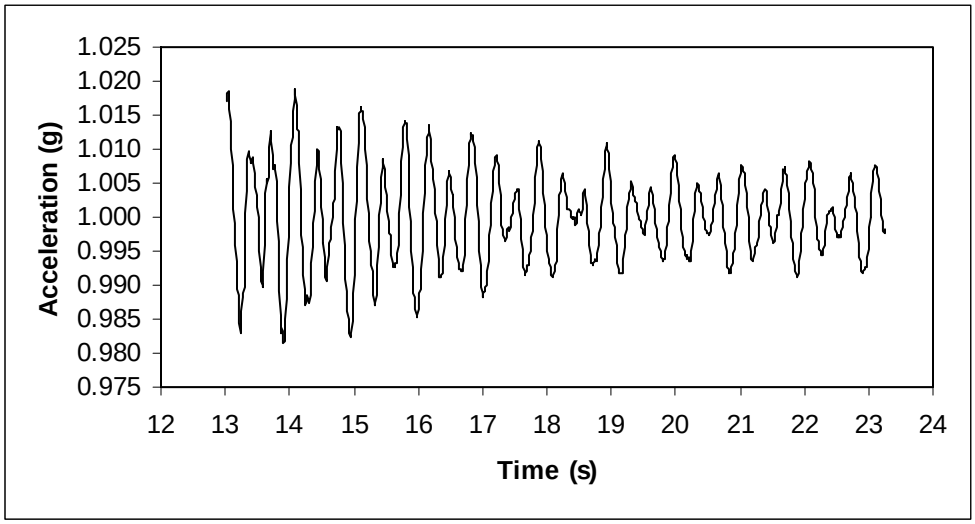

Figure 4.20 – Acceleration Data Used for University of Missouri Origin and Excel FFT's

After the FFT is completed, the power, or Fourier Coefficient, can be plotted vs. frequency. The natural frequency is seen as the frequency with the most power and should exhibit a large spike in the graph. Each spike represents a mode of vibration, with the first spike being the first harmonic frequency, the second spike the second harmonic frequency, and so on. The power vs. frequency graph and the resulting harmonic frequencies found by the Origin FFT is shown in Figure 4.21, and the Excel FFT is shown in Figure 4.22.

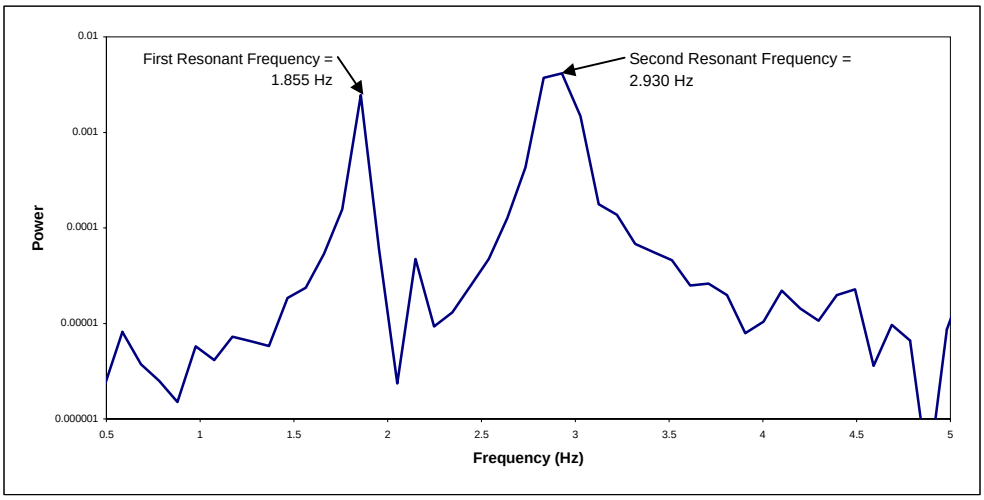

Figure 4.21 – Origin FFT Resonant Frequencies

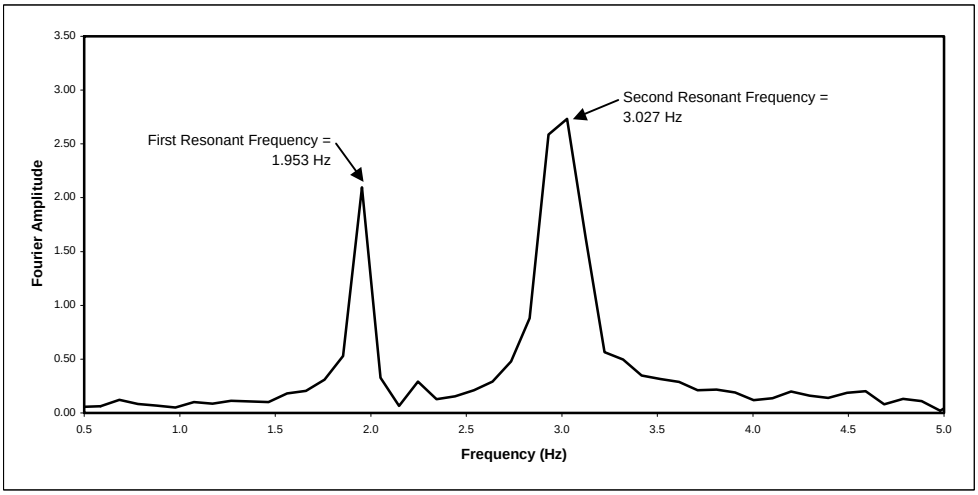

Figure 4.22 – Excel FFT Resonant Frequencies

The slight difference in the resonant frequencies from the Origin FFT and the Excel FFT are most likely due to different methods of manipulating the frequencies and data for the FFT. The Origin software used a rectangular method, while it is unknown

what method Excel uses. It should also be noted that the Origin FFT performed at West Virginia University produced a first harmonic frequency of 1.86 Hz, and a second harmonic frequency of 2.87 Hz. The slight difference between the two Origin FFT's is most likely because different data points may have been used, for instance WVU may have started using data at 15 seconds instead of 13.

4.9.3 Resonant Frequency Comparison

The results from the five estimations of the first resonant frequency can now be compared to each other to determine if a conclusive result is found. The resonant frequencies found by the various methods are listed in Table 4.12.

Table 4.12 – Bridge A6101 First Resonant Frequency Comparison

Method	1st Resonant Frequency (Hz)
Ontario B.C. Equation	**1.845**
UM Origin FFT	**1.855**
UM Excel FFT	**1.953**
WVU Abaqus FEM	**1.830**
WVU Origin FFT	**1.860**

Average	**1.869**
Standard Deviation	**0.049**

The resonant frequency found with each method is very similar. Even the frequency farthest from the average is less than a tenth of an Hz different than the average, and the standard deviation of the results is also minimal. The frequency found using the Ontario Bridge Code equation is also accurate even though it is generally thought of as a rough estimate. Therefore the value used for the first resonant frequency

in the Ontario Bridge Code graph to determine an allowable deflection will be the average of the five values, 1.869 Hz.

4.9.4 Second Harmonic Frequency

Examination of the second harmonic frequency of the five procedures yields further evidence that the estimations are accurate. As explained in Section 4.1.4, the second harmonic frequency is a multiple of the base frequency. From Table 4.1 for a symmetric two span bridge, the modal frequency factor for the 2nd resonant frequency is 1.562 times the base, or 1st resonant frequency. If used on the first resonant frequency found by the Ontario Bridge Code, the factor results in a second resonant frequency of

1.845 Hz * 1.562 = 2.882 Hz

Table 4.13 lists the second harmonic frequency of the Ontario equation as well as the other estimations and also calculates the ratio of the second frequency divided by the first.

Table 4.13 – Bridge A6101 Second Harmonic Frequency Comparison

Method	2nd Resonant Frequency (Hz)	1st Resonant Frequency (Hz)	2nd / 1st
Ontario B.C. Equation	**2.882**	1.845	**1.562**
UM Origin FFT	**2.930**	1.855	**1.580**
UM Excel FFT	**3.027**	1.953	**1.550**
WVU Abaqus FEM	**2.880**	1.830	**1.574**
WVU Origin FFT	**2.870**	1.860	**1.543**

The second harmonic frequency of all the procedures are very close to each other. The Excel FFT is the furthest from the Ontario equation, and it is still within 5%. The others are all within 3% of the equation. Even more impressive is that the ratio of the second harmonic frequency over the first is within 1.5% of 1.562 for every different

procedure used. These results establish not only the validity of the Ontario equation for estimating natural frequency, but also further evidence of the accuracy of the Abaqus FEM and the field test data.

4.9.5 Ontario Bridge Code Allowable Deflection

The graph shown in Section 4.1.4 from the Ontario Bridge Code is very difficult to accurately use. To solve this problem, a new graph was made by using easily identifiable points from the graph in the code. The points were plotted in Excel and were matched by a best-fit power function. This allows specific values of allowable deflection to be found using the equation of the best-fit line. Figure 4.23 shows the determination of allowable deflections for a bridge with a first resonant frequency of 1.869 Hz, such as Bridge A6101. The allowable deflections are then converted to English units and listed in Table 4.14. Although Bridge A6101 is non-pedestrian, all values for allowable deflection are examined.

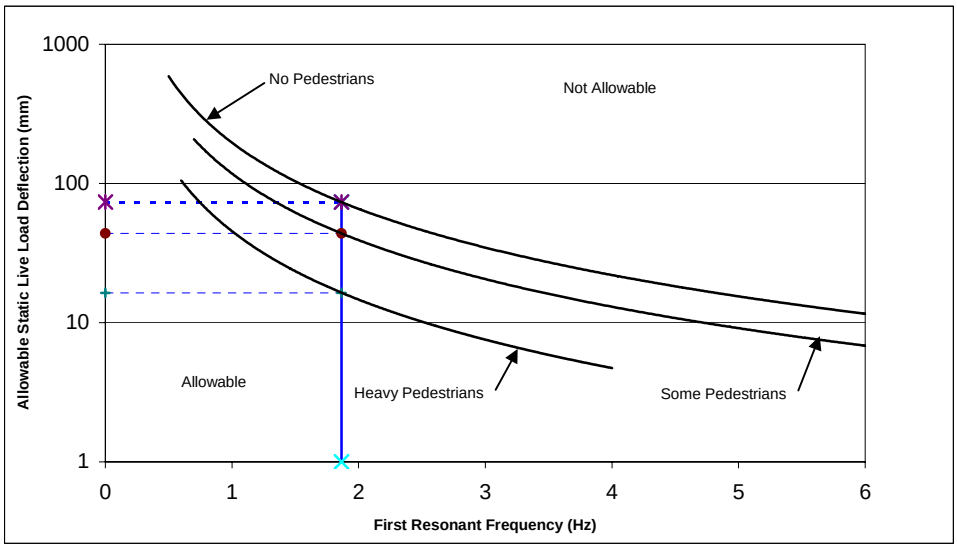

Figure 4.23 – Ontario Bridge Code Allowable Deflections for f = 1.869 Hz

Table 4.14 – Ontario Bridge Code Allowable Deflection of Bridge A6101 (f = 1.869 Hz)

	Allowable Deflection (in)
Heavy Pedestrian	**0.64**
Light Pedestrian	**1.72**
Non-Pedestrian	**2.88**

The results from the Ontario Bridge code are interesting upon examination. The allowed deflection of a bridge with heavy pedestrian traffic is only 0.64 in and deflection would surely control the design. The reasoning for the conservative value is that, apparently, a pedestrian has much more sensitivity to deflections and accelerations. On the other extreme, the allowed deflection for a bridge with no sidewalks or pedestrian traffic is allowed a rather large deflection. Strength parameters would surely control this design. Because Bridge A6101 does not have sidewalks, the Ontario Bridge Code would require an allowed deflection of less than 2.88 in. Both the measured and design live load deflections of Bridge A6101 meet this value considerably, whether using MoDOT or AASHTO deflection procedures. However, because the Ontario non-pedestrian allowed deflection is so large, it is difficult to draw conclusions about the AASHTO and MoDOT deflection criteria. Consequently, the deflection of Bridge A6101 is compared with that of a bridge with some pedestrians, which is 1.72 in. Comparison of the MoDOT and AASHTO allowed deflections, design deflections, and maximum measured deflection to the Ontario allowed deflection can be seen in Table 4.15.

Table 4.15 – Comparison of MoDOT, AASHTO, Ontario Deflection Criteria

	MoDOT Deflection Criteria	AASHTO Deflection Criteria
Ontario Bridge Code Allowed Deflection (some pedestrians)	**1.720**	**1.720**
Bridge A6101 Allowed Deflection	**1.654**	**2.067**
Bridge A6101 Design Deflection	**2.302**	**1.565**
Bridge A6101 Maximum Measured Deflection	**1.853**	**1.582**

The first point to notice is the different results of the design and measured deflections. Using AASHTO deflection criteria, the deflection predicted in design, as well as the maximum measured deflection from field testing, meet the Ontario allowed deflection. However, both the MoDOT values are greater than the deflection allowed by the Ontario Bridge Code. In fact, the MoDOT predicted deflection is over 30% higher than the Ontario allowed deflection. The MoDOT measured deflection is only 8% higher, again showing that the MoDOT design deflection may not accurately depict the actual behavior of the bridge.

Also, note that the MoDOT allowed deflection is actually slightly less than the Ontario value, even though Bridge A6101 is non-pedestrian. The AASHTO allowed deflection, on the other hand, is larger than that of the value for some pedestrians in the Ontario Bridge Code. However, AASHTO still allows 28% less deflection than the Ontario non-pedestrian deflection. While AASHTO and Ontario restrict deflections based on pedestrian traffic, MoDOT restrictions are based on Bridge A6101 being a composite design.

4.10 SERVICEABILITY RESULTS SUMMARY

Several observations can be made from the field testing results. First, it has been shown that the laser deflection device is a very useful and accurate method of measuring live load deflection. Comparing the measurements of the laser device to an Abaqus FEM showed the solid model is also accurate and can be used as the measured deflection of all five girders of Bridge A6101. By converting the load truck deflection to an equivalent experimental HS20 deflection, a comparison of the design values by MoDOT and AASHTO procedures with field test results was accomplished. This comparison shows that while AASHTO design deflections are within 1% of the maximum measured deflection, the MoDOT design deflection is about 24% greater than the maximum measured deflection.

Next, the data from acceleration testing was examined to find the resonant frequency of the bridge. Several Fast Fourier Transforms produced a first resonant frequency that is within 5% of the estimated frequency from both the Ontario base frequency equation and the Abaqus solid model. The second resonant frequency found by the FFT's are also very accurate when compared to the two estimations, further validating the vibration analysis. When examined in the Ontario Bridge Code graph, the allowed deflection for a non-pedestrian bridge is 2.88 in. This value is 40% higher than the AASHTO allowed deflection, and a full 75% larger than the MoDOT allowed deflection. Indeed, the MoDOT allowed deflection for the non-pedestrian Bridge A6101 is even less than that of the Ontario allowed deflection for a bridge with some pedestrian traffic.

While it would have been preferred to have the string pots function correctly so that direct measured deflections for all five girders could be obtained, it is believed that the Abaqus FEM solid model is confirmed as accurate. The model has proven vital in deflection analysis. Between the FEM, the laser deflection device, and the accelerometer, a very accurate picture of the serviceability characteristics of Bridge A6101 has been obtained.

CHAPTER 5 – SUMMARY AND CONCLUSIONS

5.1 MISSOURI HPS BRIDGE A6101

Bridge A6101 in Lafayette County, Missouri, was MoDOT's first use of High Performance Steel (HPS) in a bridge structure. The introduction of HPS (70 ksi) into the highly stressed regions of the hybrid bridge allowed for an efficient design that was cost effective and provided a lighter superstructure than if designed using conventional strength steel (50 ksi). MoDOT built A6101 as part of the FHWA Innovative Bridge Research and Construction Program (IBRC). One of the conditions of funding from the FHWA was to complete a strength and serviceability performance field-testing of the bridge once it was built. The University of Missouri – Columbia's Bridge Field Test Team was chosen for this task using methods described in "Field Testing and Load Rating Procedures for Steel Girder Bridges" (Barker, et al., 1999).

5.2 STRENGTH PERFORMANCE CONCLUSIONS

From the strength field-testing, stresses were measured in the girders, which allowed for load capacity rating factors to be calculated to compare Bridge A6101's performance to its design calculations.

The critical maximum positive experimental rating factors are Girder 1 (north exterior) and Girder 2 (first north interior) from Figure 3.13 with rating factors of 1.31 and 1.86, respectively, as can be seen in Table 3.8. The rating factor represents how many HS20 equivalent trucks can be applied to the structure within the design limits. For instance, for the positive moment region, the design capacity is an HS37.2 (1.86*HS20) for an interior girder and an HS26.2 (1.31*HS20) for an exterior girder. The critical

maximum negative experimental rating factors are in Girders 1 and 4 with experimental rating factors of 1.33 (HS26.7) and 1.73 (HS34.7), respectively, as can be seen in Table 3.8.

5.2.1 Critical Experimental Bridge Capacity

Girder 1 in the positive region is the critical experimental capacity for the entire bridge. It has an experimental rating factor of 1.31 (HS26.2), which is only 91% of the design rating factor for an exterior girder, but it is still above an HS20 loading. Much of this reduction is due to the Distribution Factor Adjustment as shown in Table 3.9.

The design distribution factor for an exterior girder is 1.436. The experimental distribution factor for Girder 1 in the positive region was 1.695 and in the negative region it was 2.157. These numbers show that Girder 1 experiences 18% (1.695/1.436) more of the truckload in the positive region and 50% (2.157/1.436) more of the truck load in the negative region. In other words, the exterior girders are being stressed more than the design process predicts. The finite element verifies that the exterior girders have higher stresses than predicted. Thus, Bridge A6101 showed a capacity 9% lower than the design load. However, it needs to be noted that the experimental testing loaded the exterior girder beyond the design procedures. MoDOT and AASHTO design exterior girders with a wheel line 2 ft. from the barrier curb. In the field tests, wheel lines were run only 1 ft. from the barrier curb. This added more than the design load to the exterior girder and certainly increased the stress over that required from design. The result is that the experimental bridge capacity is less than the design load with the “extreme” test loading and would probably be about equal to the design load if the test loads followed the 2 ft. from the barrier curb procedure.

5.2.2 Bridge Strength Performance

Table 5.1 shows the design rating factors compared to the experimental rating factors for all girders in both the positive and negative regions.

Table 5.1 Design and Experimental Rating Factors

Positive Rating Factors

Girder	1	2	3	4	5
Experimental	1.310	1.860	2.370	1.890	1.440
Design	1.440	1.190	1.190	1.190	1.440
Exp / Design	0.910	1.563	1.992	1.588	1.000

Negative Rating Factors

Girder	1	2	3	4	5
Experimental	1.333	2.148	2.176	1.734	1.423
Design	1.523	1.217	1.217	1.217	1.523
Exp / Design	0.875	1.765	1.788	1.425	0.934

Overall the interior girders performed well compared to design. Girder 2 was the critical girder in maximum positive and Girder 4 was the critical girder for the maximum negative regions with experimental rating factors of 1.86 (HS37.2) and 1.73 (HS43). The respective design rating factors are 1.190 and 1.217. All of the interior girders showed an experimental rating capacity significantly greater than design predicts. This increase of capacity is most attributed to the distribution factors compared to the AASHTO S/5.5 formula as shown in Tables 3.9 and 3.10. However, the exterior girders did not fair near so well.

The respective design rating factors for the exterior girders are 1.440 (HS28.8) and 1.523 (HS30.5) for positive and negative moment regions. Both of the exterior girders showed an experimental capacity either equal to or less than design predicts. The

worst performing girder was Girder 1 in the negative region with a reduction in capacity of 12.5% but was not the overall critical girder. This decrease of capacity in both exterior girders is mostly attributed to the experimental distribution factors compared to the AASHTO S/(4+(S/4)) formula as shown in Tables 3.9 and 3.10.

5.2.3 Strength Summary

Hybrid girder bridges using HPS have become economical alternatives to conventional steel bridges. Hybrid HPS bridges have been used in several other states, but Bridge A6101 is MoDOT's first bridge using HPS. The University of Missouri – Columbia's Bridge Field Test team was able to place measurement devices at critical locations on Bridge A6101, coupled with the SIMON bridge software and finite element analysis, to develop experimental rating factors and determine how Bridge A6101 performed. The results show that, unlike in the design, the exterior girders were the critical component in the experimental tests. More of the truckload was distributed to the exterior girders than design predicts. This was also confirmed by finite element analysis. The experimental capacity of the exterior girder was only 91% of the design capacity, but still above the HS20 legal loading. Therefore, the exterior girders performed poorly compared to design theory. The interior girders, however, consistently performed better than design theory. The major factor for both the interior and exterior performance was the lateral distribution factor of the loads.

5.3 SERVICEABILITY PERFORMANCE CONCLUSIONS

Bridge A6101 in Lexington, Missouri, is the first bridge to utilize High Performance Steel in Missouri. By using HPS, the bridge is lighter and less costly than a

conventional design. With the cost benefits of using HPS girders, the popularity of such designs is growing considerably nationwide. However, because of conservative MoDOT deflection criteria, Bridge A6101 actually does not meet Missouri deflection standards. MoDOT applied a design exception so that the bridge needed only to meet standard AASHTO deflection criteria. It is a concern that future MoDOT designs will be similarly controlled by deflection, not strength, and will not be given the benefit of a design exception. Doing so severely limits the benefit of utilizing HPS, as more material must be used to increase the stiffness of the bridge. The serviceability field testing of Bridge A6101 has resulted in a large amount of information about the serviceability characteristics of the bridge.

5.3.1 Comparison of MoDOT, AASHTO, and Ontario Serviceability Criteria

When compared to AASHTO deflection criteria, it is easily seen that MoDOT uses conservative standards. Put side by side with AASHTO, MoDOT uses narrower lanes, which allows for the possibility of an extra lane on some bridges. MoDOT also does not include an intensity reduction factor in the deflection distribution as AASHTO does, and MoDOT also includes moment distribution in its deflection criteria, raising its predicted deflection. MoDOT also bases its allowed deflection on whether the bridge is composite or non-composite as opposed to its pedestrian traffic. The result of MoDOT's conservative criteria is that for a bridge similar in design to Bridge A6101, the predicted deflection is 49% higher than AASHTO, while allowing 20% less deflection as shown in Chapter 4. The total outcome is that MoDOT would require 87% more stiffness than AASHTO in Bridge A6101.

In the design of Bridge A6101, the AASHTO deflection criteria are met. The predicted deflection is nearly 25% less than the allowed deflection. After calculation of the Ontario Bridge Code allowed deflection using the first harmonic frequency of the bridge, it is found that the AASHTO deflection prediction also meets this code. The AASHTO predicted deflection is 46% less than the Ontario allowable deflection for non-pedestrian bridges, and 9% lower than the allowable deflection for a bridge with some pedestrians.

MoDOT deflection criteria are not satisfied in Bridge A6101. The predicted deflection of the bridge is 40% higher than the allowable deflection. The MoDOT predicted deflection also meets the Ontario Bridge Code allowed deflection for non-pedestrian bridges, although only by 20%. However, the design does not meet Ontario's deflection for some pedestrians, as the predicted deflection is 34% larger.

It should also be noted that even a homogeneous 50 ksi design for Bridge A6101 does not meet MoDOT deflection standards. The hybrid HPS and the conventional 50 ksi designs would both have to be larger to increase stiffness, meaning both would essentially need to be the same size to meet deflection requirements. This means that there is not a need for the HPS since deflection controls and the 17% material savings and 11% cost savings demonstrated in Chapter 2 would not be realized

5.3.2 Comparison of Measured and Predicted Deflection Values

By combining the measured deflections of the different test runs in a method similar to the design procedures, the total deflection of each girder can be measured as shown in Chapter 4. Comparison to predicted values can confirm the accuracy of the design. While string pots used in the deflection testing did not function properly, the

laser deflection device validated the precision of the Abaqus FEM deflection estimations. Thus, the results from the solid model are considered as the measured values.

When the measured deflections are combined with the AASHTO method and factored to an equivalent HS20 deflection, the resulting maximum girder deflection is 1.582 in as shown in Table 4.7. This occurs in Girder 5 with trucks in two lanes corresponding with Runs 9 and 12. The maximum deflection is very close to the predicted AASHTO deflection of 1.565 in (within 1%). It is also 23% less than the allowed AASHTO deflection of 2.07 in (L/800).

When combined using MoDOT procedures, the maximum equivalent HS20 girder deflection is 1.853 in in Girder 5 (Table 4.8). This corresponds to four trucks at Positions 1, 4, 9, and 12. This measured deflection is almost 20% lower than MoDOT's estimated deflection, and is 12% higher than its allowed deflection of 1.65 in (L/1000). It should be noted that the MoDOT measured deflection does meet AASHTO's allowable deflection.

Table 5.2 summarizes the design and experimental deflection results. The table shows the controlling truck run superposition, the test truck measured deflection, and the equivalent HS20 deflections for each girder. Immediately below the table are the maximum equivalent HS20 measured deflection, the deflection predicted by design procedures, and the respective deflection limit.

Table 5.2 Deflection Results for AASHTO and MoDOT

	AASHTO			MoDOT		
Girder	Controlling Load	Test Truck	Equivalent HS20	Controlling Load	Test Truck	Equivalent HS20
1	1+4	-0.77	-1.51	1,4,9	-0.84	-1.64
2	.9(1,4,10)	-0.70	-1.37	1,4,9,12	-0.87	-1.69
3	.9(3,8,12)	-0.65	-1.26	1,4,9,12	-0.90	-1.75
4	.9(3,9,12)	-0.74	-1.45	1,4,9,12	-0.91	-1.76
5	9+12	-0.81	-1.58	1,4,9,12	-0.95	-1.85

Max Defl = 1.58”
Predicted = 1.54”
L/800 = 2.07”

Max Defl = 1.85”
Predicted = 2.30”
L/1000 = 1.65”

5.3.3 Serviceability Field Testing Summary

The field test of Bridge A6101 contains a wealth of information for serviceability characteristics. The test has further confirmed the procedures used by the University of Missouri-Columbia Bridge Field Test System. While the string pots and one of the accelerometers were faulty, all other systems worked well. This allowed for confirmation of system response compared to design theory.

First, the accuracy of the Abaqus FEM has been confirmed in multiple ways. The deflections of the solid model match the measured laser deflection device deflections of Girder 2. Also, the 1st and 2nd resonant frequency of Bridge A6101 predicted by Abaqus are almost exactly the values obtained by performing an FFT of the acceleration data, and the Ontario base frequency equation.

By using the Abaqus predicted deflections as the measured deflections, it was confirmed that AASHTO design deflections are an accurate representation of the behavior of Bridge A6101. It is also seen that MoDOT design deflections are more

conservative than what the bridge actually exhibits, and that the MoDOT allowable deflection is based on different conditions than AASHTO and Ontario. While this is conservative for Bridge A6101, it could actually be less conservative in some cases. For instance, if a bridge with sidewalks is designed as non-composite, the MoDOT allowable deflection would be more than AASHTO's, allowing for larger deflections.

Finally, the Ontario Bridge Code was examined. The equation for base frequency produced a 1st and 2nd mode of resonance that almost exactly matches the Abaqus model and FFT results. By using the allowable deflection vs. resonant frequency graph, it is found that the allowable deflection for a bridge with some pedestrians is 1.72 in, which is only 4% higher than AASHTO's allowable deflection for a pedestrian bridge.

5.4 CLOSING REMARKS

Bridge A6101, Missouri's first HPS bridge, is a hybrid design that saved 17% in weight over a conventional steel bridge and an estimated savings of 11% in cost. The future of HPS is promising. HPS70W is a superior steel with higher yield strength, improved weldability, greater levels of toughness, and improved weathering resistance that can lead to more economical bridges than conventional 50ksi designs. However, the conservative serviceability procedures used by some states will cause many HPS designs to be controlled by deflection, instead of strength parameters, which negates the benefit of using higher strength materials.

REFERENCES

AASHTO, 1998, *LRFD Bridge Design Specifications*, Second Edition, American Association of State Highway and Transportation Officials, Washington, D.C.

AASHTO, 1996, *Standard Specifications for Highway Bridges*, Sixteenth Edition, American Association of State Highway and Transportation Officials, Washington, D.C.

AISC, 1996, *SIMON Systems User Manual*, Version 8.1, American Institute of Steel Construction.

Barker, Imhoff, McDaniel, Frederick, 1999, *Field Testing and Load Rating Procedures for Steel Girder Bridges*, Missouri Department of Transportation RDT 99-004 Final Report. University of Missouri Columbia, May.

Barker, M.G. and Schrage, S.D. , 2000, *High Performance Steel Bridge Design and Cost Comparison*, Transportation Research Record No. 1740, Transportation Research Board, Washington, D.C., pp 33-39.

Bakht, B. , 1988, *Observed Behavior of a New Medium Span Slab-on-Girder Bridge*, Structural Research Report SRR-88-02, Research and Development Branch, Ministry of Transportation, Downsview, Ontario.

Barth, K.E., Christopher, R.A., 2000, *Live-Load Deflection Criteria for Steel I-Girder Bridges*, Presentation to AISI Bridge Task Force, West Virginia University, August.

Billing, J.R., 1979, *Estimation of the Natural Frequencies of Continuous Multi-Span Bridges*, Ontario Ministry of Transportation and Communications Research and Development Division, January.

Criswell, C. , 1999, *MoDOT Live Load Deflection Survey*.

Davis, J.M., 2003, *Serviceability Field Testing of Hybrid HPS Bridge A6101*, Master's Thesis, University of Missouri, Columbia, July.

Frederick, T.L., 1998, *Experimental Load Rating of a Slab-on-Steel Girder Bridge*, Master's Thesis, University of Missouri, Columbia, July.

Imhoff, C.M. , 1997, *Development of an Electro-Optical Deflection Measurement Device for Use in Bridge Field Testing*, Undergraduate Honors Report, University of Missouri, Columbia, May.

Imhoff, C.M., 1998, *Testing and Modeling of Bridge R-289*, Master's Thesis, University of Missouri, Columbia, July.

LabVIEW, 1997, User's Manual, Version 4.1.

McDaniel, W.T., 1998, *Field Test of Bridge R-289 by Utilizing the University of Missouri Bridge Field Test Unit*, Master's Thesis, University of Missouri, Columbia, July.

MoDOT, 2002, *Bridge Design Manual*, Missouri Department of Transportation Bridge Division, Jefferson City, Missouri.

MoDOT, 2000, *Summary of Design of Bridge A6101 Over Route 13*, Missouri Department of Transportation Bridge Division, Jefferson City, Missouri.

Oesch, E.R. , 2003, *Serviceability and Performance Field Testing of Hybrid HPS Bridge A6101*, Master's Thesis, University of Missouri, Columbia, July.

Ontario Highway Bridge Design Code, 1983, Second Edition, Ontario Ministry of Transportation and Communications Highway Engineering Division, Toronto, Ontario.

Ontario Highway Bridge Design Code Commentary, 1983, Second Edition, Ontario Ministry of Transportation and Communications Highway Engineering Division, Toronto, Ontario

Origin Version 7 Evaluation Software, 2002, OriginLab Corporation, Northampton, Maine.

Schrage, S., 1998, *Laser Referenced Deflection Measuring System for Bridge Field Testing*, Undergraduate Honors Thesis, University of Missouri, Columbia, May.

Wu, Haiyong, 2003, *Improved Live Load Deflection Limits for Steel Bridge Superstructures*, doctoral dissertation, West Virginia University, Morgantown, WV.